

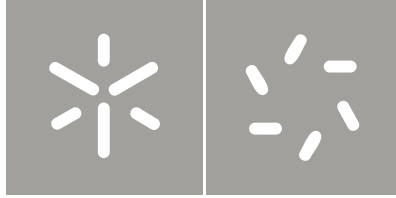


Universidade do Minho
Escola de Ciências

João Pedro Nunes Pereira

Polyvinylidene fluoride based nanocomposites
for the development of energy systems

João Pedro Nunes Pereira Polyvinylidene fluoride based nanocomposites
for the development of energy systems



Universidade do Minho
Escola de Ciências

João Pedro Nunes Pereira

Polyvinylidene fluoride based nanocomposites
for the development of energy systems

Tese de Doutoramento
Física / Ciências

Trabalho efectuado sob a orientação de
Professor Doutor Senentxu Lanceros-Méndez
Professor Doutor José Gerardo Vieira da Rocha

DECLARAÇÃO

Nome:

João Pedro Nunes Pereira

Endereço electrónico: jpereira@fisica.uminho.pt

Telefone: +351966141759

Número do Bilhete de Identidade:

12197835

Título da tese:

Polyvinylidene fluoride based nanocomposites for the development of energy systems

Orientadores:

Senentxu Lanceros-Méndez

José Gerardo Vieira da Rocha

Ano de conclusão: Outubro de 2013

Designação do Ramo de Conhecimento do Doutoramento:

Doutoramento em Ciências

Especialidade em Física

Nos exemplares das teses de doutoramento ou de mestrado ou de outros trabalhos entregues para prestação de provas públicas nas universidades ou outros estabelecimentos de ensino, e dos quais é obrigatoriamente enviado um exemplar para depósito legal na Biblioteca Nacional e, pelo menos outro para a biblioteca da universidade respectiva, deve constar uma das seguintes declarações:

É AUTORIZADA A REPRODUÇÃO INTEGRAL DESTA TESE APENAS PARA EFEITOS DE INVESTIGAÇÃO, MEDIANTE DECLARAÇÃO ESCRITA DO INTERESSADO, QUE A TAL SE COMPROMETE.

Universidade do Minho, 17 /10 /2013

Assinatura: _____

João Pereira

*for my PARENTS,
to whom I fully dedicate this work!*

Acknowledgments

I would like to thank to Portuguese Foundation for Science and Technology – FCT for the financial support (SFRH/BD/66930/2009) and to University of Minho for giving me all the conditions to develop my work.

Being a researcher is a lifestyle which is only possible if one is surrounded by fantastic people helping us to take the right decisions. Belong to the Electroactive Smart Materials group was undoubtedly the key of success of this work... without you my friends, none of this would be possible. Thank you all, especially Carlos and Vítor for having guided me so patiently in my first steps.

Professor Senentxu, I can find no words to express my deep gratitude and admiration for everything you taught me and for every moment I lived with you along this long journey. After all these years I can truly say that you are my "*father in science*" and you will always be a reference to me and an example to follow. THANK YOU!

Professor Gerardo, thank you for all the support and encouragement shown throughout these years and the good advices you always gave me.

Thank you Professor Manuela for all the support and availability that always showed to work with me.

Thank you Professor Darrell for the amazing time I have experienced with your research group at Bath University.

Many thanks Vítor, Susana and Pedro for your friendship and constant presence throughout these years.

Madi, Daniel, Ritinha, Sarinha, Anita, Óscar and Teresinha heartfelt thanks for all the love you put in my life! I am a very happy and lucky guy to have you near me!

And you My Beloved's mom and dad...THANK YOU... for all the love you always gave me since my first day, I owe you everything!

Abstract

The economic and environmental costs of current energy resources created the need to develop new methods to generate and store energy. In this sense, the development of polymer materials led to the emergence of a new generation of porous polymers for energy applications, which are typically described as “energy polymers”.

The specific properties of poly(vinylidene fluoride) (PVDF) and its copolymer poly(vinylidene fluoride-*co*-trifluoroethylene) (P(VDF-TrFE)), such as high dielectric permittivity, high polarity, softness and flexibility, among others, make them excellent choices for energy applications. The incorporation of fillers into these polymeric matrices can also be highly advantageous, since it allows tuning certain properties of the matrices optimizing their characteristics for specific applications.

According this, P(VDF-TrFE) based composite membranes with zeolites (Y zeolite, NaY), clays (montmorillonite, MMT), multiwalled-carbon nanotubes (MWCNT) and barium titanate (BaTiO₃) fillers were prepared by thermally induced phase separation (TIPS) for batteries separator applications. PVDF and P(VDF-TrFE) polymers and composites with BaTiO₃ were also prepared by electrospinning for energy harvesting systems.

P(VDF-TrFE) composite membranes showed suitable morphological, thermal, mechanical and electrochemical properties for the development of lithium ion separator membranes for battery applications.

The developed membranes showed high degrees of porosity, ranging from 70 % for the pristine polymer to a maximum of 83 % for MMT filled membrane, excepting NaY membrane which showed the lowest value of 36 %. The porosity increase is reflected in electrolyte solution uptake, which increases markedly for membranes with higher porosity reaching values above 300 % for BaTiO₃ and MMT filled membranes, whereas for the pristine polymer is ~225 %.

The room temperature ionic conductivity showed a strong increase for all composites, from 5.24×10^{-7} S/cm for the pristine polymer to a maximum of 9.22×10^{-6} S/cm for the BaTiO₃/P(VDF-TrFE) membrane. The ionic conductivity variation with temperature is diminished with the inclusion of fillers, in particular for the MMT and MWCNT filled membranes. The stable operation window is at least 6.0 V for all membranes.

Pristine polymer electrospun fibers of PVDF showed the best energy harvesting performance with generated output powers of 0.02 μW and 25 μW , under low and high mechanical deformation conditions, respectively. Pristine P(VDF-TrFE) and BaTiO₃/P(VDF-TrFE) composites fibers showed lower output powers.

The objectives of the study were successfully achieved, and the overall results are an effective contribute for the development of novel polymer based materials for energy systems applications.

Resumo

Os custos económicos e ambientais das fontes de energia mais usadas na atualidade criaram a necessidade de procurar novos métodos de armazenar e gerar energia. Neste sentido, a disponibilidade de materiais poliméricos possibilitou o aparecimento de uma nova geração de polímeros porosos para aplicações energéticas designados por “polímeros energéticos”.

As propriedades específicas do poli(fluoreto de vinilideno) (PVDF) e do seu copolímero poli(fluoreto de vinilideno-co-trifluoretileno) (P(VDF-TrFE)), tais como elevada constante dielétrica, alta polaridade e flexibilidade, entre outras, fazem deles excelentes escolhas para este tipo de aplicações.

Desta forma prepararam-se membranas poliméricas compósitas baseadas em P(VDF-TrFE) com zeólitos (zeólito Y, NaY), argilas (montmorillonite, MMT), nanotubos de carbono (MWCNT) e titanato de bário (BaTiO₃), pelo método de separação de fase termicamente induzida (TIPS), para aplicações em separadores de baterias, bem como fibras de PVDF, P(VDF-TrFE) e BaTiO₃/P(VDF-TrFE) por *electrospinning* para sistemas de *energy harvesting*.

As membranas compósitas de P(VDF-TrFE) revelaram propriedades morfológicas, térmicas, mecânicas e eletroquímicas adequadas para aplicações em separadores de baterias de lítio.

A maior parte das membranas compósitas apresentaram elevados valores de porosidade, desde 70 % para o polímero simples até 83 % para a membrana com MMT, com a exceção da membrana com zeólitos que apresentou o valor mais baixo de 36 %. Os aumentos da porosidade refletiram-se na absorção de líquido eletrólito, que aumentou de forma mais acentuada nas membranas com maior porosidade atingindo valores superiores a 300 % para as membranas com BaTiO₃ e MMT, quando comparado com os 200 % do polímero puro.

A condutividade iónica à temperatura ambiente apresentou fortes aumentos em todos os compósitos, desde o valor de 5.24×10^{-7} S/cm para o polímero puro até ao máximo de 9.22×10^{-6} S/cm para a membrana de BaTiO₃/P(VDF-TrFE). As variações da condutividade em função da temperatura foram diminuídas nos compósitos, principalmente para as membranas com MMT e MWCNT. A janela estável de operação foi no mínimo de 6.0 V para todas as membranas.

As fibras poliméricas de P(VDF-TrFE) produzidas por *electrospinning* apresentaram o melhor resultado em termos de geração de energia, gerando potências saída de 0.02 μW e 25 μW , em condições de baixa a alta deformação mecânica, respetivamente. O polímero P(VDF-TrFE) e o compósito BaTiO₃/P(VDF-TrFE) apresentaram potências mais baixas.

Os objetivos deste estudo foram alcançados com sucesso e os resultados globais são um contributo efetivo para o desenvolvimento de novos materiais poliméricos para aplicações em sistemas de energia.

Contents

1 - Introduction.....	1
1.1. Polymers and energy systems	3
1.2. Poly(vinylidene) fluoride	4
1.3. Applications	6
1.4. Objectives.....	9
1.5. Thesis structure	10
1.6. References	11
2 - Materials and methods	15
2.1. Materials.....	17
2.2. Sample preparation.....	18
2.2.1. Porous membranes for battery separator applications	18
2.2.2. Electrospun polymer fibers for energy harvesting	19
2.3. Sample characterization	20
2.3.1. Microstructure and polymer phase.....	20
2.3.2. Thermal properties and degree of crystallinity	21
2.3.3. Porosity	21
2.3.4. Electrolyte solution uptake.....	22
2.3.5. Mechanical properties	22
2.3.6. Electrochemical impedance spectroscopy.....	23
2.3.7. Cyclic voltammetry	24
2.3.8. Energy harvesting response.....	24
2.4. References	26
3 - Porous membranes of NaY/P(VDF-TrFE)	27
3.1. Introduction.....	29
3.2. Results and Discussion.....	31

3.2.1. Microstructural characteristics and polymer phase.....	31
3.2.2. Thermal and mechanical properties	34
3.2.3. Electrical properties	38
3.3. Conclusion.....	43
3.4. References	45
4 - Porous membranes of MMT/P(VDF-TrFE)	51
4.1. Introduction	53
4.2. Results and discussion.....	56
4.2.1. Microstructural characteristics and polymer phase.....	56
4.2.2. Porosity, electrolyte uptake and tortuosity.....	59
4.2.3. Thermal and mechanical properties	60
4.2.4. Electrical properties	62
4.3. Conclusion.....	66
4.4. References	68
5 - Porous membranes of CNT/P(VDF-TrFE).....	73
5.1. Introduction	75
5.2. Results and discussion.....	77
5.2.1. MWCNT type and concentration	77
5.2.2. Microstructural characteristics	78
5.2.3. Thermal and mechanical properties	82
5.2.4. Electrical properties	84
5.2.5. MWCNT type comparison.....	90
5.4. Conclusion.....	91
5.5. References	92
6 - Porous membranes of BaTiO ₃ /P(VDF-TrFE).....	97
6.1. Introduction	99
6.2. Results and discussion.....	101

6.2.1. Microstructural characteristics	101
6.2.5. Particles size effect.....	110
6.3. Conclusion.....	113
6.4. References	115
7 - Energy harvesting performance of PVDF based electrospun fibers	121
7.1. Introduction	123
7.2. Results and discussion.....	125
7.2.1. Morphology	125
7.2.2. Polymer phase and crystallinity	129
7.2.3. Energy harvesting response.....	130
7.3. Conclusion.....	135
7.4. References	136
8 - Final remarks, conclusions and future work	139
8.1. Final remarks.....	141
8.2. Conclusions	145
8.3. Future work	146
8.4. References	148

List of figures

Figure 1.1: Schematic representations of PVDF α , β and γ -phases.	5
Figure 1.2: Schematic representation of P(VDF-TrFE).	6
Figure 2.1: Scheme of the procedure for sample preparation.	19
Figure 2.2: Scheme of the procedure for the preparation of the BaTiO ₃ /P(VDF-TrFE) electrospun fibers.....	20
Figure 2.3: a) Scheme of the experimental setup used for the periodic bending tests; b) interdigitated electrode plate with electrospun fibers; c) electromechanical generator during a energy harvesting bending test.	25
Figure 3.1: Cross-section SEM images of the NaY/P(VDF-TrFE) composites with different zeolite contents: a) 0 % (P(VDF-TrFE)); b) 4 %; c) 16 %; d) 32 %.	31
Figure 3.2: a) Influence of the zeolite content in the mean diameter of pores and porosity in the NaY/P(VDF-TrFE) composites and b) 1 M LiClO ₄ .3H ₂ O-PC solution uptake as a function of zeolite content for the NaY/P(VDF-TrFE) composites.	32
Figure 3.3: FTIR spectra for NaY/P(VDF-TrFE) composites for different zeolite contents: a) without electrolyte solution uptake; b) with electrolyte solution uptake. ...	33
Figure 3.4: DSC thermograms of the NaY/P(VDF-TrFE) composites with different zeolite filler contents: a) without electrolyte solution uptake; b) with electrolyte solution uptake.....	35
Figure 3.5: Stress-Strain curves of the NaY/P(VDF-TrFE) composites with different zeolite particles contents: a) without electrolyte solution uptake; b) with electrolyte solution uptake.....	36
Figure 3.6: Stress-Strain curves of the NaY/P(VDF-TrFE) composites for 16 wt% at different temperatures.....	38

Figure 3.7: a) Nyquist plot of the NaY/P(VDF-TrFE) composites for all filler contents at 50 °C; b-c) Bode diagram of the NaY/P(VDF-TrFE) composites for all contents at 50 °C and d) impedance modulus as a function of zeolite content at different temperatures.....	39
Figure 3.8: Log σ_i as function of 1000/T for NaY/P(VDF-TrFE) composites a) without electrolyte solution uptake and b) with electrolyte solution uptake.	41
Figure 3.9: a) Voltammograms of NaY/P(VDF-TrFE) with 16 wt% of zeolites at different scanning rates and b) voltammograms of NaY/P(VDF-TrFE) composites at 0.5 V/s.....	42
Figure 4.1: Cross section SEM images of the MMT/P(VDF-TrFE) composites with different clay content: a) 0 wt%, b) 4 wt%, c) 16 wt% and d) 32 wt%.	57
Figure 4.2: FTIR spectra of the MMT/P(VDF-TrFE) composites with different MMT contents without electrolyte solution uptake.	58
Figure 4.3: a) Porosity as a function of clay content for MMT/P(VDF-TrFE) composites; b) 1 M LiClO ₄ .3H ₂ O-PC solution uptake as a function of clay content for the MMT/P(VDF-TrFE) composites.	59
Figure 4.4: DSC thermograms of the MMT/P(VDF-TrFE) composites for the different clay contents without electrolyte solution uptake.....	60
Figure 4.5: Stress-Strain curves of the MMT/P(VDF-TrFE) composites with different clay contents: a) without electrolyte solution uptake and b) with electrolyte solution uptake.....	61
Figure 4.6: a) Nyquist plot of the MMT/P(VDF-TrFE) composites for all filler contents at 50 °C, b-c) Bode diagram of the MMT/P(VDF-TrFE) composites for all contents at 50 °C and d) impedance modulus as a function of clay content at different temperatures.	63
Figure 4.7: Log σ_i as a function of 1000/T for MMT/P(VDF-TrFE) composites: a) without electrolyte solution uptake and b) with electrolyte solution uptake.....	64

Figure 4.8: a) Voltammogram of MMT/P(VDF-TrFE) composites at 0.5 V/s; b) voltammogram of MMT/P(VDF-TrFE) with 16 wt% of clays at different scanning rates.	66
Figure 5.1: DC conductivity as function of filler amount for the different MWCNT used at room temperature.	77
Figure 5.2: Cross section SEM images and histograms of pore size diameter of the MWCNT/P(VDF-TrFE) composites with different filler content: a) and c) 0.0 wt%, b) and d) 0.5 wt%.	78
Figure 5.3: Porosity and electrolyte uptake as function of MWCNT content for membranes with different content of fillers.	79
Figure 5.4: FTIR spectra of the MWCNT/P(VDF-TrFE) composites with different MWCNT content without electrolyte solution uptake.	80
Figure 5.5: Room temperature ionic conductivity and tortuosity of membranes + 1 M LiClO ₄ .3H ₂ O; σ_0 (S/cm) = 9.8 mS/cm at 25 °C.	81
Figure 5.6: DSC thermograms of the MWCNT/P(VDF-TrFE) composites for the different filler contents without electrolyte solution uptake.	82
Figure 5.7: Stress-strain curves of the MWCNT/P(VDF-TrFE) composites with different filler contents: a) without electrolyte solution uptake; b) with electrolyte solution uptake.	83
Figure 5.8: a) Nyquist plot and b-c) Bode diagram of the MWCNT/P(VDF-TrFE) composites for different filler content at 25 °C.	84
Figure 5.9: Equivalent circuit proposed for the impedance data measured in the different MWCNT/P(VDF-TrFE) membranes at different temperatures.	85
Figure 5.10: Nyquist plot for the experimental data and fitting for the equivalent circuit of figure 5.9 for membrane with 0.2 wt% of MWCNT at 50 °C.	86

Figure 5.11: Log σ_i as a function of $1000/T$ for MWCNT/P(VDF-TrFE) composites: a) without electrolyte solution uptake; b) with electrolyte solution uptake.	87
Figure 5.12: a) Voltammogram of MWCNT/P(VDF-TrFE) composites at 0.1 V/s; b) voltammogram of MWCNT/P(VDF-TrFE) with 0.5 wt% of MWCNT at different scanning rates.	88
Figure 5.13: a) Stress-strain curves of the MWCNT/P(VDF-TrFE) membranes with electrolyte uptake; b) Nyquist plot of the MWCNT/P(VDF-TrFE) composites with electrolyte uptake at 25 °C; c) Log σ_i as a function of $1000/T$ for MWCNT/P(VDF-TrFE) composites with electrolyte uptake; d) Voltammograms of the MWCNT/P(VDF-TrFE) membranes with electrolyte uptake at 0.5 V/s.....	90
Figure 6.1: Cross section SEM images of the BaTiO ₃ /P(VDF-TrFE) composites with different filler contents: a) 0 wt%, b) 4 wt%, c) 16 wt% and d) 32 wt%; e) average pore size distribution and f) electrolyte content as function of time, for membrane with 16 wt% of BaTiO ₃	102
Figure 6.2: a) Average pore size and porosity and b) electrolyte content as function of BaTiO ₃ content for all membrane.....	103
Figure 6.3: a) FTIR spectra of the BaTiO ₃ /P(VDF-TrFE) composites with different filler contents; b) DSC thermogram of membrane composites with different amounts of ceramic particles.	104
Figure 6.4: Stress-strain curves of the BaTiO ₃ /P(VDF-TrFE) composites with different ceramic nanoparticles contents after electrolyte solution uptake.	106
Figure 6.5: a) Nyquist plot for the BaTiO ₃ /P(VDF-TrFE) composites at 25 °C; b) Log σ_i as a function of $1000/T$ for BaTiO ₃ /P(VDF-TrFE) composites with electrolyte solution uptake.....	107
Figure 6.6: a) Voltammogram of BaTiO ₃ /P(VDF-TrFE) composites at 0.1 V/s with different filler contents; b) voltammogram of BaTiO ₃ /P(VDF-TrFE) with 16 wt% of ceramic particles with 100 nm in diameter at different scanning rates.	109

Figure 6.7: Cross section SEM images of BaTiO ₃ /P(VDF-TrFE) composites with 16 wt% of ceramic particles with filler sizes of a) 10 nm and b) 500 nm.....	110
Figure 6.8: a) Average pore size and porosity and b) electrolyte content of membranes with 16 wt% of BaTiO ₃ particles as a function of filler average diameter.....	111
Figure 6.9: a) Tensile stress-strain measurements, b) Nyquist plot at 25 °C, c) Log σ_i as a function of 1000/T and d) cyclic voltammetry, of BaTiO ₃ /P(VDF-TrFE) composites with 16 wt% filler content.	112
Figure 7.1: BaTiO ₃ /P(VDF-TrFE) electrospun membrane obtained at 15/85 polymer/solution and with 5 % BaTiO ₃ nanoparticles with particle size of $\varnothing = 100$ nm: a) 20 kV, b) 35 kV, c) 25 kV and d) backscattering image of sample obtained at 25 kV (image b). Traveling distance of 20 cm, needle inner diameter of 0.5 mm and flow rate of 0.5 mL/h.	126
Figure 7.2: a) Influence of applied electric field on the mean diameter of the electrospun BaTiO ₃ /P(VDF-TrFE) fibers, the flow rate was 0.5 mL/h and needle inner diameter of 0.5 mm; b) Influence of tip inner diameter on the mean diameter of the electrospun BaTiO ₃ /P(VDF-TrFE) fibers, the flow rate was 0.5 mL/h and applied electric field of 1.25 kV/cm; c) Influence of flow rate on the mean diameter of the electrospun BaTiO ₃ /P(VDF-TrFE) fibers, the tip inner diameter was 0.5 mm and the applied electric field of 1.25 kV/cm; d) Influence of BaTiO ₃ content on the fiber mean diameter for the electrospun BaTiO ₃ /P(VDF-TrFE) membrane, the tip inner diameter was 0.5 mm, applied electric field of 1.25 kV/cm and a flow rate of 0.5 mL/h. Average filler size: $\varnothing = 100$ nm; filler concentration in a), b) and c) 5 %.	127
Figure 7.3: Influence of BaTiO ₃ particle average size in the composite fiber diameter: a) 10 nm, b) 500 nm, c) backscattering image of electrospun fibers with 20 % BaTiO ₃ ($\varnothing = 100$ nm) and d) electrospun BaTiO ₃ /P(VDF-TrFE) (20 % BaTiO ₃ and $\varnothing = 100$ nm) membrane obtained at 750 rpm. For all samples, tip inner diameter was 0.5 mm, applied electric field of 1.25 kV/cm and a flow rate of 0.5 mL/h.	128
Figure 7.4: a) Infrared measurements for the PVDF and BaTiO ₃ /P(VDF-TrFE) electrospun membranes with a tip inner diameter of 0.5 mm, applied voltage of 25 kV, distance between tip and collector of 20 cm and a flow rate of 1.0 and 8.0 mL/h; b) DSC	

results for the PVDF and BaTiO₃/P(VDF-TrFE) electrospun membranes with a tip inner diameter of 0.5 mm, applied voltage of 25 kV and a distance between tip and collector of 20 cm and a flow rate of 1.0 and 8.0 mL/h. 129

Figure 7.5: Voltage generated during 6 ms at a frequency of 1 kHz, of an electrospun sample of BaTiO₃/P(VDF-TrFE) with 20 % of ceramic 10 nm; b) maximum voltage generated at different frequencies for all type of samples produced; c) piezopotential obtained at 1 kHz for P(VDF-TrFE) and BaTiO₃/P(VDF-TrFE) with 20 % ceramic filler and d) maximum power generated by the electrospun membranes as a function of frequency. 132

Figure 7.6: a) Diagram of a bending test performed with a finger; b) Positive output voltage generated during a test performed with finger deformation for the PVDF electrospun fibers..... 134

Figure 8.1: Cross section images of: a) pristine P(VDF-TrFE), b) 16 wt% NaY/P(VDF-TrFE), c) 4 wt% MMT/ P(VDF-TrFE), d) 0.1 wt% MWCNT/ P(VDF-TrFE) and e) 16 wt% BaTiO₃/ P(VDF-TrFE) membranes. 141

Figure 8.2: a) Average pore size and b) porosity and uptake for the P(VDF-TrFE), 16 wt% NaY/P(VDF-TrFE), 4 wt% MMT/P(VDF-TrFE), 0.1 wt% MWCNT/P(VDF-TrFE) and 16 wt% BaTiO₃/P(VDF-TrFE) membranes..... 142

Figure 8.3: Room temperature a) ionic conductivity; b) tortuosity and activation energy for the P(VDF-TrFE), 16 wt% NaY/P(VDF-TrFE), 4 wt% MMT/P(VDF-TrFE), 0.1 wt% MWCNT/P(VDF-TrFE) and 16 wt% BaTiO₃/P(VDF-TrFE) membranes. 143

Figure 8.4: Log σ_i as function of 1000/T of (VDF-TrFE), 16 wt% NaY/P(VDF-TrFE), 4 wt% MMT/P(VDF-TrFE), 0.1 wt% MWCNT/P(VDF-TrFE) and 16 wt% BaTiO₃/P(VDF-TrFE) membranes..... 144

List of tables

Table 2.1: Materials, provider and prepared samples in each chapter.....	17
Table 3.1: Ionic conductivity and tortuosity of 1 M LiClO ₄ .3H ₂ O + separator membrane; $\sigma_0 = 9.8$ mS/cm at 25 °C.	34
Table 3.2: Degree of Crystallinity of all samples calculated through equation 2.1 to the melting peak of samples without electrolyte solution uptake.....	35
Table 3.3: Mechanical properties of the composite membranes.	37
Table 3.4: Activation energy for all porous membranes with and without electrolyte solution.	41
Table 3.5: Diffusion coefficient calculated by equation 2.8 for all porous membranes with electrolyte solution.	43
Table 4.1: Room temperature ionic conductivity and tortuosity of 1M LiClO ₄ .3H ₂ O + separator membrane; $\sigma_0 = 9.8$ mS/cm at 25 °C.....	59
Table 4.2: Degree of crystallinity calculated applying equation 2.1 to the melting peak of the samples.	61
Table 4.3: Mechanical properties of the MMT/P(VDF-TrFE) membranes with and without electrolyte solution uptake.....	62
Table 4.4: Activation energy for the different porous membranes with and without electrolyte solution uptake.....	65
Table 5.1: Characteristics of the MWCNT.....	77
Table 5.2: Degree of crystallinity of the membranes calculated by applying equation 2.1 to the melting peak of the samples	82
Table 5.3: Mechanical properties of the MWCNT/P(VDF-TrFE) membranes with and without electrolyte solution uptake.....	83

Table 5.4: Equivalent circuit parameters for MWCNT/P(VDF-TrFE) membranes at 50 °C.	86
Table 5.5: Activation energies for all membranes with and without electrolyte solution uptake.....	88
Table 6.1: Structural properties of the ceramic fillers [35].	101
Table 6.2: Degree of crystallinity of the BaTiO ₃ /P(VDF-TrFE) membranes with different amounts of ceramic fillers.....	105
Table 6.3: Mechanical properties of the membranes with electrolyte solution uptake.	106
Table 6.4: Room temperature ionic conductivity (σ_i) and tortuosity (τ) of the membranes filled with 1 M LiClO ₄ .3H ₂ O electrolyte solution; $\sigma_0 = 9.8$ mS/cm at 25 °C.	107
Table 6.5: Activation energy (E_a) of the composite membranes with electrolyte solution uptake, determined after equation 2.7.	108
Table 7.1: Characteristic physical properties of electroactive PVDF, P(VDF-TrFE) and BaTiO ₃ [26, 31].	133
Table 7.2: Structural properties of the BaTiO ₃ ceramic particles [35].	134
Table 8.1: Average pore size, porosity and electrolyte uptake of the membranes.	142
Table 8.2: Room temperature ionic conductivity (σ_i), tortuosity (τ) and activation energy (E_a) of the membranes filled with 1 M LiClO ₄ .3H ₂ O electrolyte solution; $\sigma_0 = 9.8$ S/cm at 25 °C.	143

List of symbols

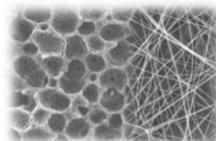
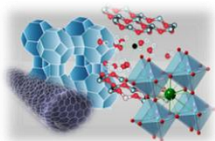
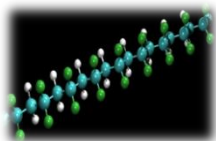
A	Area
C	Capacitor
C_0	Analyte concentration
d	Thickness
D	Diffusion coefficient
d_{3n}	Piezoelectric coefficient
E	Voltage
E_a	Activation energy
E_{content}	Electrolyte content
I	Current intensity
i_p	Oxidative peak current
k_{3n}	Electromechanical coupling coefficient
m_n	Mass
N	Number of electrons
n_n	Parameter n
P_n	Power
Q	Differential heat
R	Ideal gas constant
R_n	Resistance / resistor
T	Temperature
t	Time
T'	Period
T_c	Curie temperature
T_g	Glass transition temperature
T_m	Melting temperature
v	Potential scan rate
V_n	Voltage
W_s	Warburg impedance
$ Z $	Absolute impedance
Z'	Imaginary impedance
Z''	Real impedance

ΔH	Enthalpy
ε	Porosity
ε'	Dielectric constant
σ_n	Conductivity
τ	Tortuosity
\varnothing	Diameter
χ_c	Degree of crystallinity

List of abbreviations

ATR	Attenuated total reflectance
CNT	Carbon nanotubes
CPE	Constant phase element
DMC	Dimethyl carbonate
DMF	N,N-dimethylformamide
DSC	Differential scanning calorimetry
EC	Ethylene carbonate
EIS	Electrochemical impedance spectroscopy
FE	Ferroelectric
FTIR	Fourier transformed infrared spectroscopy
MEK	Methylethylketone
MMT	Montmorillonite
MWCNT	Multiwalled-carbon nanotubes
MWS	Maxwell-Wagner-Sillars
NMP	N-methyl-pyrrolidone
P(VDF-TrFE)	Poly(vinylidene fluoride- <i>co</i> -trifluoroethylene)
PAN	Poly(acrylonitrile)
PC	Propylene carbonate
PE	Paraelectric
PEG	Polyethylene glycol
PEO	Poly(ethylene oxide)
PI	Polyimide
PP	Poly(propylene)
PVA	Polyvinyl alcohol
PVDF	Poly(vinylidene fluoride)
PVDF-HFP	Poly(vinylidene fluoride- <i>co</i> -hexafluoropropene)
PZT	Lead zirconate titanate
SEM	Scanning electron microscope
SPE	Solid polymer electrolyte
TGA	Thermo gravimetric analysis

THF	Tetrahydrofuran
TIPS	Thermally induced phase separation
XRD	X-ray diffraction



1 - Introduction

This chapter introduces the main topics related to the present thesis. A contextualization of the work is provided in accordance to current energy needs. The main characteristics of poly(vinylidene) fluoride (PVDF) and its copolymers are presented, as well as their specific applications in energy systems. Finally the general and specific objectives of the study are defined together with the main structure of the document.

1.1. Polymers and energy systems

For economical and environmental reasons the increasing need of energy by modern societies led to the need to explore clean and renewable energy resources. Fossil fuel resources are getting scarce and expensive and economical activity based on these fuels brought up the carbon dioxide load increase on the atmosphere to values with large impact on global warming. In this sense, new energy generations and storage systems are being explored, some of them based on a new generation of porous polymers for energy applications, which could be described as “energy polymers”. These materials allow new energy related possibilities, with better generation, storage and transportation. Novel polymeric materials for fuel cells membranes, hydrogen and methane storage, nanofoams with high thermal insulation, catalysts, light harvesting, among others, are strongly emerging. Recent advances in the control of polymer molecular structures allow a fine tuning of their properties, which led to increased interest in its use [1-3].

The next generation of energy storage and conservation devices is based on solid polymer electrolytes (SPE), which provides larger operational flexibility and long lifetime for a wide range of applications [4]. Lithium-ion (Li-ion) secondary batteries play a key role in meeting energy demands of current society, mainly in portable electronic devices and in electrical vehicles, since they have high theoretical capacity, improved safety, lower materials cost, simple fabrication and absence of electrolyte leakage. In batteries, electrolyte liquids frequently present numerous disadvantages, such as gas formation during operation, leakage, corrosive reactions, combustible reaction products, difficulty of use in portable devices, among others; these problems led to increased demand for polymer based alternatives [3].

The most widely used polymers in SPE applications are poly(ethylene) (PE), poly(propylene) (PP), poly(ethylene oxide) (PEO), poly(acrylonitrile) (PAN), poly(vinylidene fluoride) (PVDF) and its copolymers [5]. PEO was the first polymer proposed and used in SPE Li-ion rechargeable batteries, however, the electrolyte system exhibited lower room temperature ionic conductivity, due to the crystalline nature of PEO polymer and moderate dielectric constant [3-4]. To overcome this, many studies have focused on composite polymer electrolytes, based on polymers with low glass transition temperature (T_g) with adequate amounts of inert inorganic nanofillers. It is

established that the inclusion of ceramic fillers improves the ionic conductivity of the composite polymer electrolytes [3, 5]. Among fillers, the most commonly used into polymer hosts matrices are the inert oxide ceramics (aluminium oxide – Al_2O_3 , silicon oxide – SiO_2 and titanium dioxide – TiO_2), molecular sieves (zeolites), ferroelectric materials (e.g. BaTiO_3) and carbonaceous fillers [6].

The search for solutions that meet the energy needs of contemporary societies is not restricted to energy storage. New energy generation processes have been studied in order to meet these needs. In this sense, energy harvesting materials and systems have emerged as a prominent research area. Harvesting energy from ambient waste energy for low power electronic applications became a strong ally of wireless devices technologies, since this allows remote electric power sourcing of storage devices, thus extending wireless systems lifespan. This concept has an immediate economic and environmental impact, by reducing chemical waste resulting from the replacement of batteries and maintenance costs. The increasing interest in this area led to many studies, mainly based on the piezoelectric effect of materials to convert environmental vibration into useful electrical energy [7-9].

Among polymers, PVDF is an important case of energy material, its semi-crystalline and high-molecular weight structure, with short and long-term ordering regions, allows obtaining, after poling, a suitable piezoelectric response for these kind of applications. PVDF presents the advantage of being mechanically strong, flexible and resistant to a wide variety of chemicals [7]. Lately, the incorporation of piezoceramics, such as BaTiO_3 and lead zirconate titanate (PZT), into polymeric matrices has raised largest interest and presents itself as a challenge in developing applications [10].

In short, the use of polymers in energy systems is becoming increasingly important. They are easy to process, low cost and the overall mechanical, thermal and electrochemical properties make them excellent choices for the development of new energy systems.

1.2. Poly(vinylidene) fluoride

PVDF is a semi-crystalline polymer with a complex structure which can show five distinct chain conformations. The, designed as all trans (TTT) planar zigzag β -phase,

TGTG (trans-gauche-tans-gauche) α -phase and T₃GT₃G' γ -phase are the most common and used for applications (figure 1.1) [10]. Much of the interest in PVDF for applications is based on its high dipole moment ($5\text{-}8 \times 10^{-30}$ C.m), which is due to the fluorine atoms electronegativity compared to those of hydrogen and carbon [11-12].

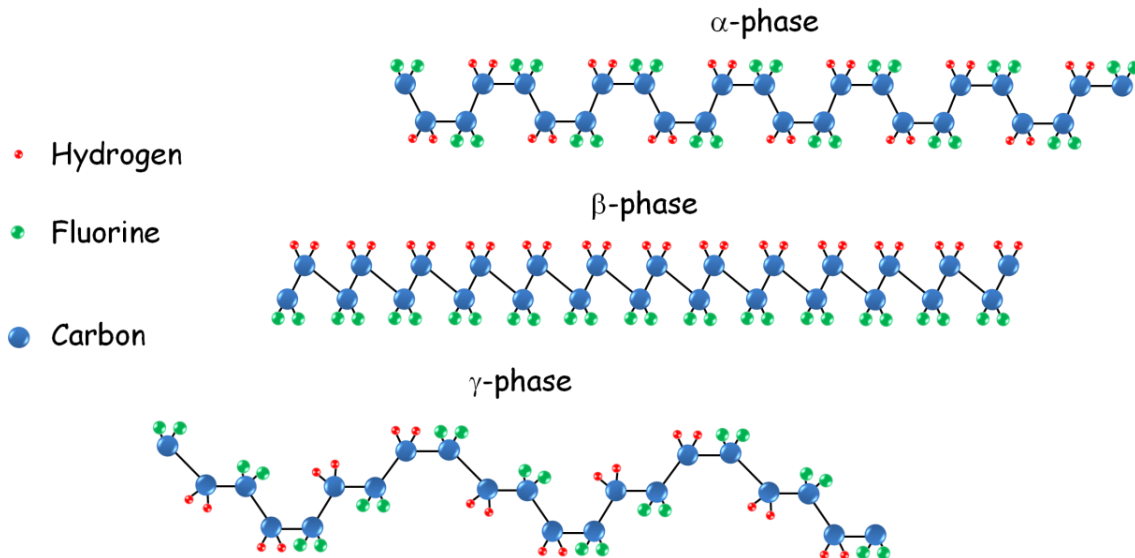


Figure 1.1: Schematic representations of PVDF α , β and γ -phases.

The α -phase is non-polar and is more thermodynamically stable when obtained from the melt or from the solvent evaporated at temperatures above 80 °C [13].

The β -phase is the most interesting for technological applications due to its electroactive properties: piezoelectricity, pyroelectricity and ferroelectricity [14]. It can be obtained in a porous microstructure directly by solution at crystallization temperatures below 70 °C [15], by α -phase stretching at temperature ranging between 70 °C and 100 °C [16], from the melt under specific conditions of pressure [17], external electric field [18] and ultra-fast cooling [19], and by the addition of nucleating fillers, such as BaTiO₃ [20] and clays [21], among others.

The semi-crystalline copolymer poly(vinylidene fluoride-*co*-trifluoroethylene) P(VDF-TrFE) (figure 1.2) always presents a electroactive phase, similar to the one of the β -phase of PVDF, for specific molar ratios of vinylidene fluoride (VDF) and TrFE, independently on the processing method (from the melt or from solution) [22]. The ferroelectric-paraelectric (FE-PE) phase transition of P(VDF-TrFE) occurs at a T_c below the melting temperature (T_m). These temperatures depend on the crystallization conditions and molar ratio of VDF and TrFE [23-25].

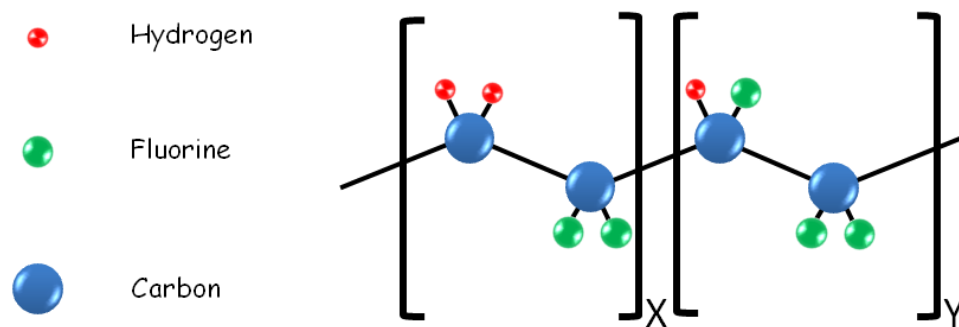


Figure 1.2: Schematic representation of P(VDF-TrFE).

1.3. Applications

PVDF and PVDF based composites have specific properties of high electrical permittivity, low thermal conductivity, softness and flexibility, good impedance matching to air and water and relatively low cost, making them excellent choices for several applications, such as sensors, actuators, vibrations control, ultrasonic transducers, batteries, filters, chemical warfare protection, magnetoelectric materials, and recently in the biological fields [18, 26-28]. Less known are the applications in tactile sensors, ferroelectric devices, energy conservation devices, shock sensors, thermal and optical property measurement devices and pyroelectric infrared arrays, among others [29].

There is a recent increasing interest in developing polymer electrolytes with high ionic conductivity, good mechanical strength and thermal stability for Li-ion batteries, and also other electrochemical devices like supercapacitors and electrochromic devices, which should meet the requirements of safety, energy density and mechanical properties

for these kind of applications [10]. PVDF has high polarity, dielectric permittivity and anodic stability, which provides larger affinity with polar liquid electrolytes and supports ionizations of lithium salts, so that their incorporation into PVDF polymeric matrix lead to high functional polymer electrolytes [5, 10]. PVDF has proven to enhance lithium transport number due to selective interactions with anionic species. The ionic conduction process depends on electrolyte solution uptake, which in turn depends on the porosity and pore size of the polymer matrix [30]. However, the affinity of PVDF with the electrolyte liquid may affect the thermal and mechanical stabilities, if too much solution fills the matrix pores [31]. Costa *et al.* [32] studied the copolymer P(VDF-TrFE) membranes for this purpose and found that best performances were obtained in porous membranes with hydrated lithium salts loaded by uptake technique. The incorporation of lithium triflate salt into poly(vinylidene fluoride-co-hexafluoropropene) copolymer (PVDF-HFP) matrix proved to be a way to increase ionic conductivity by reducing crystallinity of the polymer [33], once the interactions between PVDF and lithium salts mainly occurs in the polymer amorphous area [34].

The major challenge for materials for battery applications is to combine good ionic conductivity and high electrolyte uptake whilst keeping proper mechanical properties (in the temperature range of lithium battery operation).

The use of PVDF and copolymers based composites in Li-ion batteries applications is a promising way for these kinds of applications, namely through the fabrication of polymeric matrices with homogeneous multilayers or hierarchical pore structures in order to enhance the thermal and mechanical stability, electrodes compatibility and ionic conduction, as well as electrochemical performance [5, 10]. The use of several fillers has been reported with profitable results; the incorporation of nano-clays particles into PVDF matrices shows enhanced porosities, electrolyte uptakes, room temperature ionic conductivity and electrodes interfacial resistance [35]; the inclusion of $\text{SiO}_2(\text{Li}^+)$ into PVDF leads to higher electrolyte uptakes and ionic conductivities [36]; TiO_2 in PVDF-HFP helps to improve the mechanical strength, ionic conductivity and electrolyte/electrode interfacial stability [37]. The nature and amount of fillers is crucial in determining the properties of the composite [5].

PVDF has also been widely used as sensor and actuator on the basis of its piezoelectric properties. However, the piezoelectric ceramics/polymers with improved properties, with respect to the polymer matrix, represent the major challenge of this area [38-39]. In this sense, the inclusion of ceramic fillers like BaTiO_3 [36, 40] or lead

zirconate titanate (PZT) [41], carbon nanotubes [41], among others, in PVDF and P(VDF-TrFE) matrices contributes to improve dielectric constant, enabling to tune the piezoelectric response to obtain higher output powers in vibration harvesting structures [10]. The vast majority of recent research in power harvesting with piezoelectric materials has focused on improving the efficiency of piezoelectric power harvesting systems, however, improving the power harvesting circuitry and energy management techniques has also been targeted. The large challenge of this area remains in the gap between energy consumption of electronic devices and the energy generation capabilities of the power harvesting systems [9].

In short, PVDF and its copolymers are the most interesting and promising polymers for the development of energy storage and generation applications, due to their large dielectric constant, piezoelectric, pyroelectric and ferroelectric effects, among others. They offer broad engineering possibilities for materials preparation with tailored microstructure and properties, showing therefore large potential for a new generation of energy related applications. The inclusion of fillers in these systems also represents a real alternative to optimize energy devices based on these materials [5, 10].

1.4. Objectives

Since the improvement of existing energy generation and storage devices represents a part of the solution to meet current energy demands of the modern world, the main objective of the present study is to develop new polymer composite materials, based on PVDF and P(VDF-TrFE), with the requirements for lithium battery separators and vibration energy harvesting applications. To achieve this purpose, the main specific objectives are:

1. Prepare porous P(VDF-TrFE) based composite membranes, by thermally induced phase separation (TIPS), with different filler types, shape and contents: zeolites (Y zeolite, NaY), clays (montmorillonite, MMT), multiwalled-carbon nanotubes (MWCNT) and barium titanate (BaTiO_3) for lithium battery separator applications;
2. Prepare PVDF, P(VDF-TrFE) and $\text{BaTiO}_3/\text{P(VDF-TrFE)}$ fibers, by electrospinning technique, with different amounts of the piezoceramic BaTiO_3 , for energy harvesting systems;
3. Obtain a complete characterization of the morphological, thermal, mechanical and electrochemical properties of the prepared samples, as well as knowing the relationship between these properties and fillers added;
4. Evaluate the performance of the prepared materials for applications.

1.5. Thesis structure

This thesis is divided into eight chapters to provide a logical sequence of the developed work during this investigation. Five of the eight chapters are based on published scientific papers focused on the development of materials for energy systems applications.

The chapter 1 describes a general state of art of materials and systems developed during the study. A specific state of art is provided in each of the following chapters, whenever necessary. The objectives of the study are also presented as well as the structure of the thesis report.

The chapter 2 provides a description of the experimental procedures, including used materials and preparation methods of respective samples, the experimental techniques carried out to characterize morphological, thermal, mechanical and electrochemical properties of the samples, as well as the procedures used to test the performance of the materials for the intended applications.

The chapters 3, 4, 5 and 6 report the study of the influence of NaY, MMT, MWCNT and BaTiO₃ fillers, respectively, in the morphological, thermal, mechanical and electrochemical properties of the P(VDF-TrFE) composite membranes for lithium battery applications. All these chapters are based on published scientific papers.

Chapter 7 describes the preparation and testing of a energy harvesting device based on PVDF, P(VDF-TrFE) and P(VDF-TrFE) with BaTiO₃ ceramic particles. This chapter is based on a published scientific paper.

The chapter 8 provides some final remarks by comparing the main characteristics of the membranes presented in chapters 3, 4, 5 and 6 for battery applications, the general conclusions of the study as well as the future work perspectives.

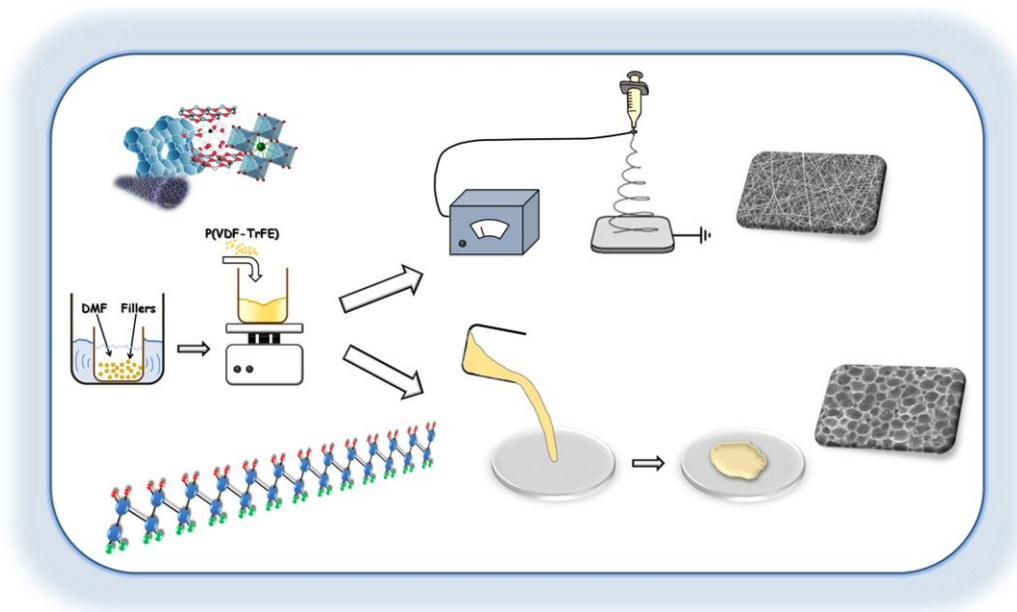
1.6. References

1. Thomas, A., P. Kuhn, J. Weber, M.-M. Titirici, and M. Antonietti. *Porous Polymers: Enabling Solutions for Energy Applications*. Macromolecular Rapid Communications, 2009. **30**(4-5): p. 221-236.
2. Vilela, F., K. Zhang, and M. Antonietti. *Conjugated porous polymers for energy applications*. Energy & Environmental Science, 2012. **5**(7): p. 7819-7832.
3. Mittal, V. *Polymers for energy storage and conversion*. 2013, New Jersey: John Wiley & Sons.
4. Hickner, M.A. and J.E. McGrath. 10.32 - *Polymers in Energy Applications*, in *Polymer Science: A Comprehensive Reference*, M. Editors-in-Chief: Krzysztof and M. Martin, Editors. 2012, Elsevier: Amsterdam. p. 597-600.
5. Costa, C.M., M.M. Silva, and S. Lancers-Mendez. *Battery separators based on vinylidene fluoride (VDF) polymers and copolymers for lithium ion battery applications*. RSC Advances, 2013. **3**(29): p. 11404-11417.
6. Costa, C.M., J. Nunes-Pereira, L.C. Rodrigues, M.M. Silva, J.L.G. Ribelles, and S. Lancers-Méndez. *Novel poly(vinylidene fluoride-trifluoroethylene)/poly(ethylene oxide) blends for battery separators in lithium-ion applications*. Electrochimica Acta, 2013. **88**(0): p. 473-476.
7. Erturk, A. and D.J. Inman. *Piezoelectric Energy Harvesting*. 2011: Wiley.
8. Priya, S. and D.J. Inman. *Energy Harvesting Technologies*. 2008: Springer.
9. Anton, S.R. and H.A. Sodano. *A review of power harvesting using piezoelectric materials (2003–2006)*. Smart Materials and Structures, 2007. **16**(3): p. R1.
10. Martins, P., A.C. Lopes, and S. Lancers-Mendez *Electroactive phases of poly(vinylidene fluoride): Determination, processing and applications*. Progress in Polymer Science, DOI: <http://dx.doi.org/10.1016/j.progpolymsci.2013.07.006>.
11. Salimi, A. and A.A. Yousefi. *Analysis Method: FTIR studies of β -phase crystal formation in stretched PVDF films*. Polymer Testing, 2003. **22**(6): p. 699-704.
12. Giannetti, E. *Semi-crystalline fluorinated polymers*. Polymer International, 2001. **50**(1): p. 10-26.
13. Gregorio, J.R. and M. Cestari. *Effect of crystallization temperature on the crystalline phase content and morphology of poly(vinylidene fluoride)*. Journal of Polymer Science Part B: Polymer Physics, 1994. **32**(5): p. 859-870.
14. Silva, M.P., C.M. Costa, V. Sencadas, A.J. Paleo, and S. Lancers-Méndez. *Degradation of the dielectric and piezoelectric response of β -poly(vinylidene*

- fluoride) after temperature annealing*. Journal of Polymer Research, 2011. **18**(6): p. 1451-1457.
15. Magalhães, R., N. Durães, M. Silva, J. Silva, V. Sencadas, G. Botelho, J.L. Gómez Ribelles, and S. Lanceros-Méndez. *The Role of Solvent Evaporation in the Microstructure of Electroactive β -Poly(Vinylidene Fluoride) Membranes Obtained by Isothermal Crystallization*. Soft Materials, 2010. **9**(1): p. 1-14.
 16. Sencadas, V., R. Gregorio, and S. Lanceros-Méndez. *α to β Phase Transformation and Microstructural Changes of PVDF Films Induced by Uniaxial Stretch*. Journal of Macromolecular Science, Part B, 2009. **48**(3): p. 514-525.
 17. Hattori, T., M. Kanaoka, and H. Ohigashi. *Improved piezoelectricity in thick lamellar beta-form crystals of poly(vinylidene fluoride) crystallized under high pressure*. Journal of Applied Physics, 1996. **79**(4): p. 2016-2022.
 18. Ribeiro, C., V. Sencadas, J.L.G. Ribelles, and S. Lanceros-Méndez. *Influence of Processing Conditions on Polymorphism and Nanofiber Morphology of Electroactive Poly(vinylidene fluoride) Electrospun Membranes*. Soft Materials, 2010. **8**(3): p. 274-287.
 19. Yang, D. and Y. Chen. *β -phase formation of poly(vinylidene fluoride) from the melt induced by quenching*. Journal of Materials Science Letters, 1987. **6**(5): p. 599-603.
 20. Mendes, S.F., C.M. Costa, C. Caparros, V. Sencadas, and S. Lanceros-Méndez. *Effect of filler size and concentration on the structure and properties of poly(vinylidene fluoride)/BaTiO₃ nanocomposites*. Journal of Materials Science, 2012. **47**(3): p. 1378-1388.
 21. Patro, T.U., M.V. Mhalgi, D.V. Khakhar, and A. Misra. *Studies on poly(vinylidene fluoride)-clay nanocomposites: Effect of different clay modifiers*. Polymer, 2008. **49**(16): p. 3486-3499.
 22. Nalwa, H.S. *Ferroelectric polymers : chemistry, physics, and applications*. 1995, New York: Dekker.
 23. Lovinger, A.J., T. Furukawa, G.T. Davis, and M.G. Broadhurst. *Crystallographic changes characterizing the Curie transition in three ferroelectric copolymers of vinylidene fluoride and trifluoroethylene: 2. Oriented or poled samples*. Polymer, 1983. **24**(10): p. 1233-1239.
 24. Furukawa, T., G.E. Johnson, H.E. Bair, Y. Tajitsu, A. Chiba, and E. Fukada. *Ferroelectric phase transition in a copolymer of vinylidene fluoride and trifluoroethylene*. Ferroelectrics, 1981. **32**(1): p. 61-67.
 25. Li, W., Y. Zhu, D. Hua, P. Wang, X. Chen, and J. Shen. *Crystalline morphologies of P(VDF-TrFE) (70/30) copolymer films above melting point*. Applied Surface Science, 2008. **254**(22): p. 7321-7325.

26. Martins, P., J.S. Nunes, G. Hungerford, D. Miranda, A. Ferreira, V. Sencadas, and S. Lanceros-Méndez. *Local variation of the dielectric properties of poly(vinylidene fluoride) during the α - to β -phase transformation*. Physics Letters A, 2009. **373**(2): p. 177-180.
27. Martins, P., C. Caparros, R. Gonçalves, P.M. Martins, M. Benelmekki, G. Botelho, and S. Lanceros-Mendez. *Role of Nanoparticle Surface Charge on the Nucleation of the Electroactive β -Poly(vinylidene fluoride) Nanocomposites for Sensor and Actuator Applications*. The Journal of Physical Chemistry C, 2012. **116**(29): p. 15790-15794.
28. Sencadas, V., R. Gregorio Filho, and S. Lanceros-Mendez. *Processing and characterization of a novel nonporous poly(vinylidene fluoride) films in the β phase*. Journal of Non-Crystalline Solids, 2006. **352**(21–22): p. 2226-2229.
29. Lang, S.B. and S. Muensit. *Review of some lesser-known applications of piezoelectric and pyroelectric polymers*. Applied Physics A, 2006. **85**(2): p. 125-134.
30. Saito, Y., H. Kataoka, E. Quartarone, and P. Mustarelli. *Carrier Migration Mechanism of Physically Cross-Linked Polymer Gel Electrolytes Based on PVDF Membranes*. The Journal of Physical Chemistry B, 2002. **106**(29): p. 7200-7204.
31. Saunier, J., F. Alloin, J.Y. Sanchez, and L. Maniguet. *Plasticized microporous poly(vinylidene fluoride) separators for lithium-ion batteries. III. Gel properties and irreversible modifications of poly(vinylidene fluoride) membranes under swelling in liquid electrolytes*. Journal of Polymer Science Part B: Polymer Physics, 2004. **42**(12): p. 2308-2317.
32. Costa, C.M., V. Sencadas, J.G. Rocha, M.M. Silva, and S. Lanceros-Méndez. *Evaluation of the main processing parameters influencing the performance of poly(vinylidene fluoride-trifluoroethylene) lithium-ion battery separators*. Journal of Solid State Electrochemistry, 2013. **17**(3): p. 861-870.
33. Ramesh, S. and S.-C. Lu. *Effect of lithium salt concentration on crystallinity of poly(vinylidene fluoride-co-hexafluoropropylene)-based solid polymer electrolytes*. Journal of Molecular Structure, 2011. **994**(1–3): p. 403-409.
34. Tian, L.-y., X.-b. Huang, and X.-z. Tang. *Study on morphology behavior of PVDF-based electrolytes*. Journal of Applied Polymer Science, 2004. **92**(6): p. 3839-3842.
35. Prasanth, R., N. Shubha, H.H. Hng, and M. Srinivasan. *Effect of nano-clay on ionic conductivity and electrochemical properties of poly(vinylidene fluoride) based nanocomposite porous polymer membranes and their application as polymer electrolyte in lithium ion batteries*. European Polymer Journal, 2013. **49**(2): p. 307-318.

36. Ye, H.-J., W.-Z. Shao, and L. Zhen. *Crystallization kinetics and phase transformation of poly(vinylidene fluoride) films incorporated with functionalized baTiO₃ nanoparticles*. Journal of Applied Polymer Science, 2013. **129**(5): p. 2940-2949.
37. Miao, R., B. Liu, Z. Zhu, Y. Liu, J. Li, X. Wang, and Q. Li. *PVDF-HFP-based porous polymer electrolyte membranes for lithium-ion batteries*. Journal of Power Sources, 2008. **184**(2): p. 420-426.
38. Cui, C., R.H. Baughman, Z. Iqbal, T.R. Kazmar, and D.K. Dahlstrom. *Improved piezoelectric s for hydrophone applications based on calcium-modified lead titanate/poly(vinylidene fluoride) composites*. Sensors and Actuators A: Physical, 1998. **65**(1): p. 76-85.
39. Safari, A. *Development of piezoelectric composites for transducers*. Journal de physique. III, 1994. **4**(7): p. 1129-1149.
40. Nunes-Pereira, J., V. Sencadas, V. Correia, J.G. Rocha, and S. Lanceros-Méndez. *Energy harvesting performance of piezoelectric electrospun polymer fibers and polymer/ceramic composites*. Sensors and Actuators A: Physical, 2013. **196**(0): p. 55-62.
41. Guan, X., Y. Zhang, H. Li, and J. Ou. *PZT/PVDF composites doped with carbon nanotubes*. Sensors and Actuators A: Physical, 2013. **194**(0): p. 228-231.



2 - Materials and methods

This chapter provides a description of the materials used in this investigation, as well as the experimental details on sample preparation. The experimental conditions for the characterization of the morphological, thermal, mechanical and electrochemical or electromechanical properties of the prepared samples are also presented.

2.1. Materials

The materials used in the present study are shown in table 2.1, together with the provider as well as the reference to the prepared sample, and the chapter in which the results are presented.

Table 2.1: Materials, provider and prepared samples in each chapter.

Chapter	Material	Provider	Sample
3	Poly(vinylidene fluoride-co-trifluoroethylene) (70/30) (P(VDF-TrFE))	Solvay	P(VDF-TrFE)/DMF (15/85) (w/w)
	N,N-dimethylformamide (DMF)	Merck	
	Y zeolite (NaY)	Zeolyst International	4, 16 and 32 wt% NaY/P(VDF-TrFE)
	Propylene carbonate (PC)	Merck	Electrolyte uptake in 1 M LiClO ₄ ·3H ₂ O-PC for all samples
	Lithium perchlorate trihydrate (LiClO ₄ ·3H ₂ O)	Merck	
4	Poly(vinylidene fluoride-co-trifluoroethylene) (70/30) (P(VDF-TrFE))	Solvay	P(VDF-TrFE)/DMF (15/85) (w/w)
	N,N-dimethylformamide (DMF)	Merck	
	Montmorillonite K10 (MMT)	Sigma Aldrich	4, 16 and 32 wt% MMT/P(VDF-TrFE)
	Propylene carbonate (PC)	Merck	Electrolyte uptake in 1 M LiClO ₄ ·3H ₂ O-PC for all samples
	Lithium perchlorate trihydrate (LiClO ₄ ·3H ₂ O)	Merck	
5	Poly(vinylidene fluoride-co-trifluoroethylene) (70/30) (P(VDF-TrFE))	Solvay	P(VDF-TrFE)/DMF (15/85) (w/w)
	N,N-dimethylformamide (DMF)	Merck	
	Multiwalled-carbon nanotubes C 150P (MWCNT_B)	Baytubes [®]	0.1, 0.2 and 0.5 wt% MWCNT/P(VDF-TrFE)
	Multiwalled-carbon nanotubes NC3100 (MWCNT_N)	Nanocyl [™]	
	Propylene carbonate (PC)	Merck	Electrolyte uptake in 1 M LiClO ₄ ·3H ₂ O-PC for all samples
	Lithium perchlorate trihydrate (LiClO ₄ ·3H ₂ O)	Merck	

6	Poly(vinylidene fluoride-co-trifluoroethylene) (70/30) (P(VDF-TrFE))	Solvay	P(VDF-TrFE)/DMF (15/85) (w/w)
	N,N-dimethylformamide (DMF)	Merck	
	Barium titanate particles (BaTiO ₃) Ø = 10, 100 and 500 nm	Nanoamor	4, 16 and 32 wt% BaTiO ₃ /P(VDF-TrFE)
	Propylene carbonate (PC)	Merck	Electrolyte uptake in 1 M LiClO ₄ ·3H ₂ O-PC for all samples
	Lithium perchlorate trihydrate (LiClO ₄ ·3H ₂ O)	Merck	
7	Poly(vinylidene) fluoride (PVDF) Solef 1010	Solvay	PVDF/DMF/MEK (15/68/17) (w/w) and P(VDF-TrFE)/DMF/MEK (15/68/17) (w/w)
	Poly(vinylidene fluoride-co-trifluoroethylene) (70/30) (P(VDF-TrFE))	Solvay	
	N,N-dimethylformamide (DMF)	Merck	
	Methylethylketone (7.0/3.0, v/v) (MEK)	Panreac	
	Barium titanate particles (BaTiO ₃) Ø = 10, 100 and 500 nm	Nanoamor	5, 10 and 20 wt% BaTiO ₃ /P(VDF-TrFE)

2.2. Sample preparation

2.2.1. Porous membranes for battery separator applications

NaY/P(VDF-TrFE), MMT/P(VDF-TrFE), MWCNT/P(VDF-TrFE) and BaTiO₃/P(VDF-TrFE) porous membranes were prepared by thermally induced phase separation (figure 2.1). The fillers were dispersed in a DMF solution during 4 hours. P(VDF-TrFE) powder was added to the fillers to achieve a concentration of 15 % (w/w) of the two components in solution. The fillers to polymer relative concentration ranged from 0 up to 32 % for NaY, MMT and BaTiO₃ particles and 0.1 up to 0.5 % for MWCNT (as it should be below the percolation threshold for both MWCNT types to be suitable for the intended purpose [1]). The solution was prepared at room temperature under constant magnetic stirring until complete polymer dissolution, i.e., until a homogeneous solution was obtained (~2 hours). In order to prevent the formation of

aggregates and to improve polymer dissolution, the solution temperature was increased 5 °C above room temperature during the first 15 min. Finally, the mixture was placed in a glass Petri dish allowing completely DMF solvent evaporation at room temperature during 15 days in a gas extraction chamber.

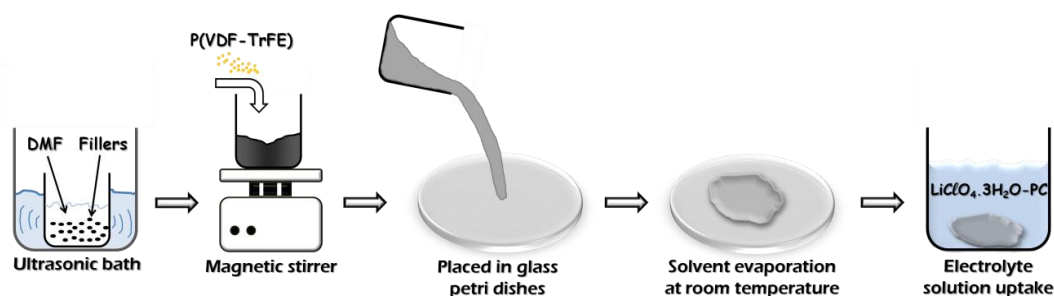


Figure 2.1: Scheme of the procedure for sample preparation.

2.2.2. Electrospun polymer fibers for energy harvesting

PVDF, P(VDF-TrFE) and BaTiO₃/P(VDF-TrFE) electrospun fiber samples were prepared by dispersing the ceramic powder in a solution of DMF and MEK, from Panreac to obtain a total concentration of 15 % (w/w) of polymer plus ceramic present in the solution. The ceramic to polymer relative concentration ranged from 0 up to 20 % ceramic content (w/w). The final solution was dissolved at room temperature under constant magnetic stirring until complete polymer dissolution, i.e., until a homogeneous solution was obtained (~2 hours) (figure 2.2).

The polymer solution was placed in a commercial plastic syringe (10 mL) fitted with a steel needle with inner diameter ranging from 0.5 to 1.7 mm. Electrospinning was conducted in a range between 20 and 35 kV with a high voltage power supply from Glassman (model PS/FC30P04). A syringe pump (from Syringepump) was used to feed the polymer solutions into the needle tip at rate between 0.5 and 8 mL/h.

The electrospun fibers were collected in a grounded collecting plate (random fibers) or in a rotating drum (oriented fibers), placed at a distance between 10 and 30 cm from the needle (figure 2.2), and in interdigitated electrode plates (figure 2.3b).

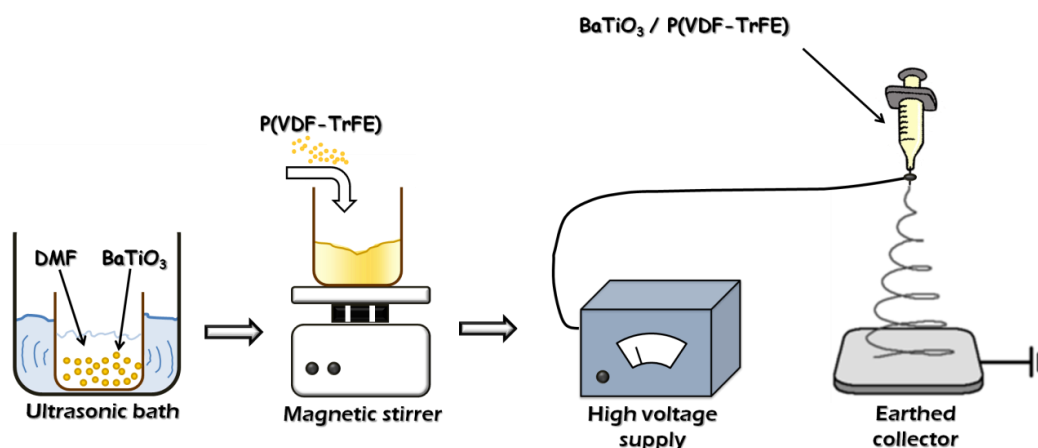


Figure 2.2: Scheme of the procedure for the preparation of the BaTiO₃/P(VDF-TrFE) electrospun fibers.

2.3. Sample characterization

The common techniques for porous membrane and electrospun fiber characterization (scanning electron microscopy (SEM), Fourier transformed infrared spectroscopy (FTIR) and differential scanning calorimetry (DSC)) are presented first, followed by the specific techniques used for porous membrane characterization (porosity, electrolyte solution uptake, stress strain measurements, electrochemical impedance spectroscopy (EIS) and cyclic voltammetry) and for electrospun fiber characterization (periodic bending tests).

2.3.1. Microstructure and polymer phase

Samples were coated with a thin gold layer using a sputter coating (Polaron, model SC502 sputter coater) and the morphology analyzed using a scanning electron microscope (Leica Cambridge apparatus at room temperature) with an accelerating voltage of 15 kV. The membrane average pore diameter and the electrospun fiber diameter were determined on the basis of the diameter of 40 pores and fibers, respectively, using the SEM images at 200x magnification and the Image J software.

Polymer phase of the porous membranes and electrospun fibers were assessed by FTIR performed at room temperature with a Jasco FTIR-4100. FTIR spectra were collected in attenuated total reflectance mode (ATR) from 4000 to 600 cm^{-1} after 32 scans with a resolution of 4 cm^{-1} .

2.3.2. Thermal properties and degree of crystallinity

The thermal properties of the porous membranes and electrospun fibers were determined by DSC with a Mettler Toledo 821^e apparatus. The samples were cut from the central region of the samples, placed in 50 μL crucibles and heated from 50 to 200 $^{\circ}\text{C}$ at a rate of 10 $^{\circ}\text{C}/\text{min}$, under an argon atmosphere. The degree of crystallinity (χ_c) was calculated (equation 2.1) from the melting/crystallization enthalpy (ΔH_f) based on the enthalpy of a 100 % crystalline sample (P(VDF-TrFE): $\Delta H_{100} = 103.4 \text{ J/g}$) [2]:

$$\chi_c = \frac{\Delta H_f}{\Delta H_{100}} \times 100 \quad (2.1)$$

2.3.3. Porosity

The porosity of the membranes (ϵ) was measured with a pycnometer by the following procedure: the pycnometer was filled with ethanol and the mass was measured (m_1); the mass of the sample was measured (m_0) and then immersed in ethanol; after the sample being completely soaked in ethanol, more ethanol was added to fill completely the pycnometer, and the mass of the assembly (sample + pycnometer) was measured (m_2); finally, the sample was removed from the pycnometer and the residual weight of the pycnometer with ethanol was measured (m_3). Ethanol was used because of its low density and easy soaking within the sample.

The porosity of the membrane was calculated according to [3]:

$$\epsilon = \frac{m_2 - m_3 - m_0}{m_1 - m_3} \quad (2.2)$$

The mean porosity of each membrane was obtained as the average of the values determined in six measurements.

2.3.4. Electrolyte solution uptake

The porous membranes were immersed in an electrolyte solution of 1 M LiClO₄·3H₂O in PC during 24 hours (figure 2.1) and the **uptake** was evaluated according to:

$$\text{Uptake} = \frac{m - m_0}{m_0} \times 100 \quad (2.3)$$

where **m₀** is the mass of the membrane and **m_E** is the mass of the membrane after immersion in the electrolyte solution.

The electrolyte content (**E_{content}**) was evaluated according to:

$$E_{\text{content}} = 1 - \frac{m_0}{m_E} \times 100 \quad (2.4)$$

where **m₀** is the mass of the dry membrane and **m_E** is the mass of the membrane filled with electrolyte solution.

LiClO₄·3H₂O was chosen for the electrolyte solution as it improves the conductivity of the composite as compared to LiClO₄, as reported in other works [4-6]. This salt is widely used in electrolyte solutions due to its excellent solubility and high anodic stability, as well as high decomposition temperature in solution (above 100 °C) [6].

2.3.5. Mechanical properties

The mechanical properties of the porous membranes (~1.0×2.5 cm) were evaluated by stress strain measurements carried out in a TST350 Linkam Scientific Instruments set up at a strain rate of 15 μm/s.

2.3.6. Electrochemical impedance spectroscopy

The ionic conductivity of the porous membranes was evaluated by an Autolab PGSTAT-12 (Eco Chemie) set-up in a frequency range from 500 mHz to 65 kHz. The samples were placed in a constant volume support equipped with gold blocking electrodes located within a Buchi TO 50 oven. The temperature, measured by a type K thermocouple, was varied between 20 and 120 °C. The ionic conductivity (σ_i) was calculated for each heating cycle according to:

$$\sigma_i = \frac{d}{R_b A} \quad (2.5)$$

where R_b is the bulk resistance, d is the thickness and A is the area of the sample.

The tortuosity (τ), the ratio between the effective capillarity and thickness of the sample was determined by [7]:

$$\tau = \sqrt{\frac{\sigma_0 \varepsilon}{\sigma_i}} \quad (2.6)$$

where σ_0 is the conductivity of the liquid electrolyte, σ_i is the conductivity of the membrane and the electrolyte set at room temperature and ε is the porosity of the membrane.

The ionic conductivity (σ_i) temperature dependence follows the Arrhenius equation:

$$\sigma_i = \sigma_0 \exp\left(\frac{-E_a}{RT}\right) \quad (2.7)$$

where σ_0 , is the pre-exponential factor, E_a is the apparent activation energy for ion transport, R is the gas constant (8.314 J/mol.K) and T is the temperature.

2.3.7. Cyclic voltammetry

Cyclic voltammetry was performed within a glove box with argon atmosphere using a two electrode configuration and a gold microelectrode as working electrode. The 25 μm diameter gold microelectrodes were previously polished, washed with tetrahydrofuran (THF) and dried in hot air. The cell assembly was performed within the glove box by placing a lithium disk (10 mm diameter, 1 mm thick, Aldrich, 99.9% purity) as a counter electrode on a stainless steel current collector. Then the porous membrane sample was centred over the counter electrode and the gold microelectrode was centred over the sample. The assembly was firmly attached by a clamp, placed inside a Faraday cage and connected to an Autolab PGSTAT-12 (Eco Chemie) that records the voltammograms at a scan rate from 0.05 to 1 mV/s. From the voltammograms, the diffusion coefficient (D) of the electroactive species was calculated according to the Randles-Sevcik equation [8]:

$$i_p = (2.69 \times 10^5) n^{3/2} A D^{1/2} \nu^{1/2} C_0 \quad (2.8)$$

where i_p is the oxidative peak current in A, n is the number of electrons transferred in the redox reaction, A is the electrode area in cm^2 , ν is the potential scan rate in V/s and C_0 is the analyte concentration in mol/cm^3 .

2.3.8. Energy harvesting response

Energy harvesting performance of the electrospun samples was evaluated by periodic bending tests (low deformation) in an electromechanical generator (Frederiksen 2185.00) excited from 1 Hz to 1 kHz using a signal generator (Circuitmate GF2) with an internal resistance of 1 M Ω (figure 2.3a). The maximum vertical displacement of the samples was ~ 7 mm measured from the initial position at 1 Hz (figure 2.3c). The voltage output was performed using an oscilloscope (Axo 4005) and the data collected

with the Picoscope software. The maximum average power was calculated from the first 100 ms of vibration trough:

$$P_L = \frac{1}{T'} \int \frac{V_0(t)^2}{R_L} dt \quad (2.9)$$

where $V_0(t)$ is the real time voltage, R_L is the load resistance and T' is the period of load application.

Samples were also submitted to bending tests with high deformation, where the mechanical stress was applied by a finger, following the procedure applied by [9].

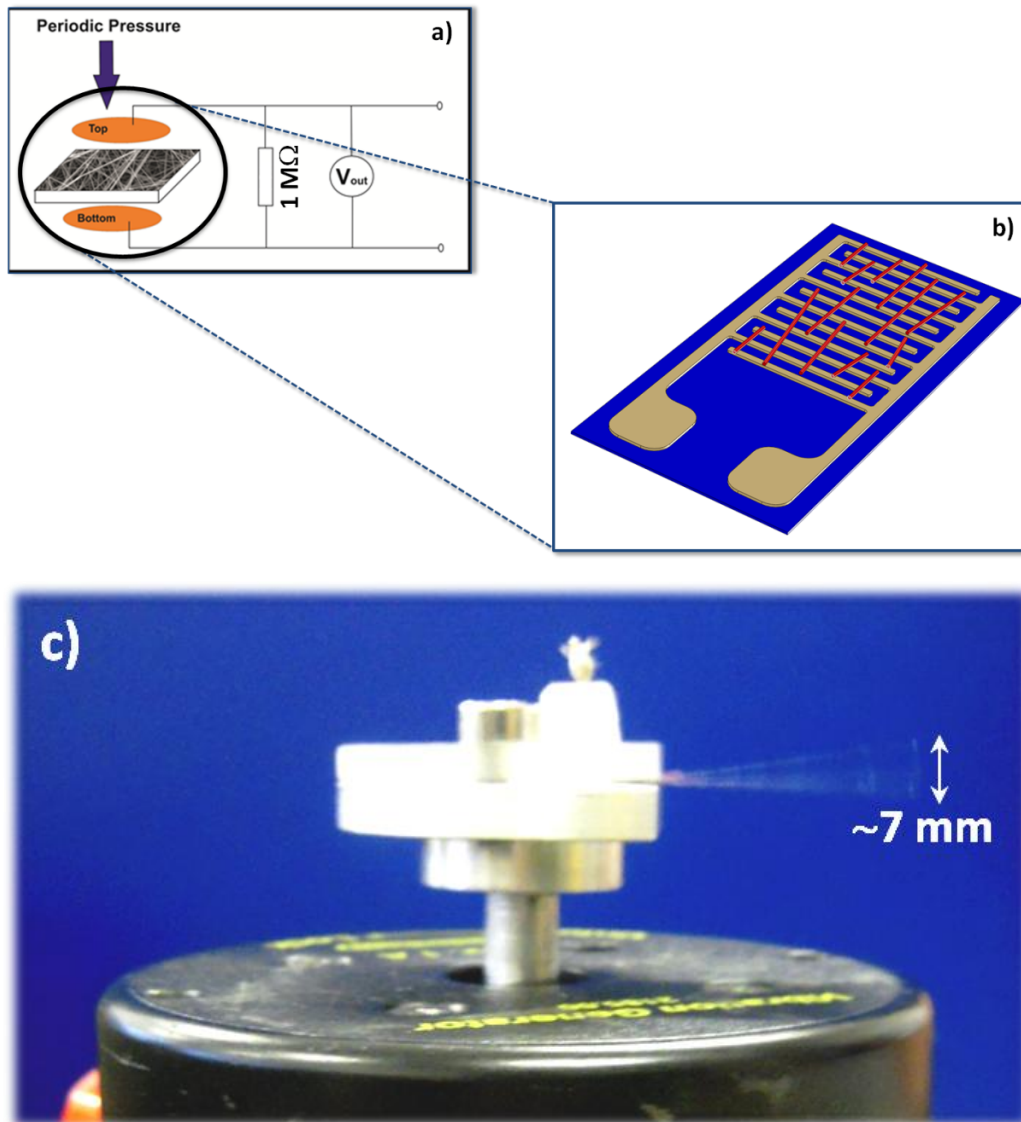
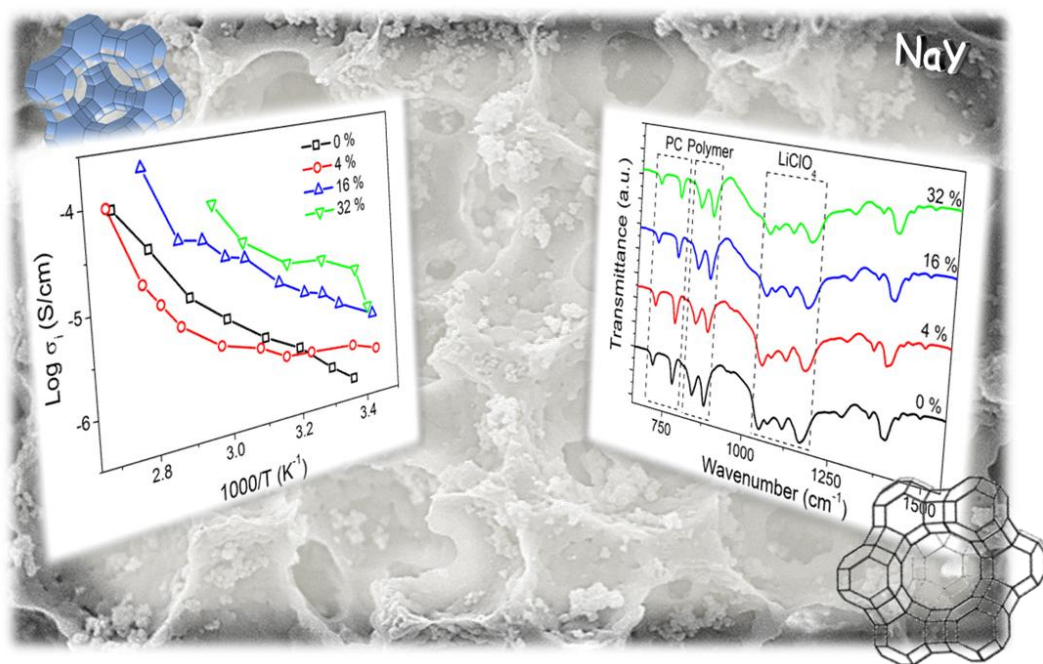


Figure 2.3: a) Scheme of the experimental setup used for the periodic bending tests; b) interdigitated electrode plate with electrospun fibers; c) electromechanical generator during a energy harvesting bending test.

2.4. References

1. Carabineiro, S.A.C., M.F.R. Pereira, J. Nunes-Pereira, J. Silva, C. Caparros, V. Sencadas, and S. Lanceros-Méndez. *The effect of nanotube surface oxidation on the electrical properties of multiwall carbon nanotube/poly(vinylidene fluoride) composites*. Journal of Materials Science, 2012. **47**(23): p. 8103-8111.
2. Bassett, D.C. *Developments in Crystalline Polymers*. 1982, London: Applied Science Publishers.
3. California, A., V.F. Cardoso, C.M. Costa, V. Sencadas, G. Botelho, J.L. Gómez-Ribelles, and S. Lanceros-Mendez. *Tailoring porous structure of ferroelectric poly(vinylidene fluoride-trifluoroethylene) by controlling solvent/polymer ratio and solvent evaporation rate*. European Polymer Journal, 2011. **47**(12): p. 2442-2450.
4. Costa, C.M., V. Sencadas, J.G. Rocha, M.M. Silva, and S. Lanceros-Méndez. *Evaluation of the main processing parameters influencing the performance of poly(vinylidene fluoride-trifluoroethylene) lithium-ion battery separators*. Journal of Solid State Electrochemistry, 2013. **17**(3): p. 861-870.
5. Nunes, S.C., V. de Zea Bermudez, D. Ostrovskii, P.B. Tavares, P.C. Barbosa, M.M. Silva, and M.J. Smith. *Spectroscopic and structural studies of di-ureasils doped with lithium perchlorate*. Electrochimica Acta, 2007. **53**(4): p. 1466-1475.
6. Xu, K. *Nonaqueous Liquid Electrolytes for Lithium-Based Rechargeable Batteries*. Chemical Reviews, 2004. **104**(10): p. 4303-4418.
7. Karabelli, D., J.C. Leprêtre, F. Alloin, and J.Y. Sanchez. *Poly(vinylidene fluoride)-based macroporous separators for supercapacitors*. Electrochimica Acta, 2011. **57**(0): p. 98-103.
8. Bard, A.J. and L.R. Faulkner. *Electrochemical Methods: Fundamentals and Applications*. 2000, New York; Chichester: John Wiley.
9. Chen, X., S. Xu, N. Yao, and Y. Shi. *1.6 V Nanogenerator for Mechanical Energy Harvesting Using PZT Nanofibers*. Nano Letters, 2010. **10**(6): p. 2133-2137.



3 - Porous membranes of NaY/P(VDF-TrFE)

This chapter is based on the following publication:

Nunes-Pereira, J., A.C. Lopes, C.M. Costa, L.C. Rodrigues, M.M. Silva, and S. Lanceros-Méndez. *Microporous membranes of NaY zeolite/poly(vinylidene fluoride-trifluoroethylene) for Li-ion battery separators*. *Journal of Electroanalytical Chemistry*, 2013. **689**: p. 223-232.

3.1. Introduction

The increasing use of handheld devices has driven the technological advances in rechargeable solid-state batteries. Lithium-ion batteries are the systems of choice, offering high energy density, flexible and lightweight design and longer lifespan than comparable battery technologies [1].

The lithium battery industry is rapidly expanding and already represents the largest segment of the industry of portable batteries for computers, cell phones and cameras. However these batteries still have some aspects to improve [2], in particular related to the high reactivity of the lithium with the components of the electrolyte. One solution to this problem could be the use of polymer electrolytes. Primary lithium batteries are now stated as a mature technology, future major developments must be focused on secondary cells [3].

A battery is a transducer that converts chemical energy into electrical energy. The principal constituents are the anode, cathode and separator membrane (SPE). In the case of lithium batteries the anode is the source of lithium ions, the cathode is the sink for the lithium ions and the electrolyte provides the separation for ionic and electronic transport [2]. Generally, the solid polymer electrolyte (SPE) is a porous membrane placed between the electrodes of opposite polarity, permeable to ionic flow but preventing electric contact of electrodes. It play a key role in all batteries, keeping the positive and negative electrodes separated, avoiding short circuits and allowing rapid transport of ionic charge carriers [4-5]. The main parameters determining the performance of SPE are thickness, permeability, porosity/pore size, wettability, electrolyte absorption and retention, chemical, dimensional and thermal stability [4, 6]. For the SPE, the lithium salt is placed in the membrane through incorporation of an electrolyte solution or directly in the membrane in the form of composite [7-8]. The most used polymer matrixes for SPE applications are poly(ethylene oxide) (PEO) [9-12], poly(acrylonitrile) (PAN) [13-14], poly(vinylidene fluoride) (PVDF) and its copolymers [15-18].

PVDF and its copolymer poly(vinylidene fluoride-*co*-trifluoroethylene) P(VDF-TrFE) are used for SPE due to their good mechanical properties, wettability by organic solvents, chemically inertness, good contact between electrode and electrolyte and being stable in cathodic environment [18-19]. The main difference between P(VDF-TrFE) and PVDF is that the copolymer exhibit the ferroelectric to paraelectric transition (FE-PE) at

a Curie temperature (T_c) below melting temperature (T_m), and crystallizes both from the melt or by solution casting in a polar ferroelectric transplanar chain configuration [20-22]. P(VDF-TrFE) membranes for lithium ion battery have been prepared by different processing techniques. The porous membranes were produced by solvent casting with varying porosity in which lithium ions were introduced by uptake; composite separators were also prepared with the lithium salts introduced within the polymer matrix [18, 23-24]. The results showed that the ionic conductivity of the membrane depends on the porosity and the pore size, which is related to the ability to uptake. Large advances in SPE technologies are produced by the incorporation of suitable fillers into the host polymer for improving mechanical strength, thermal stability and ionic conductivities [25-26]. Among these fillers are oxide ceramic, zeolites, carbon nanotubes, etc. [26].

Zeolites are hydrated aluminosilicates with a crystalline structure where SiO_4^{4-} and AlO_4^{5-} tetrahedral units are linked by common oxygen atoms, forming channels and cavities with regular dimensions. For each AlO_4^{5-} unit present a framework of negative charge is created that can be balanced by protons or metal cations [27-28]. The presence of these exchangeable cations makes zeolite to have a high electric conductivity when compared with other ionic crystalline solids [29].

Due to their properties, zeolite fillers are used in composite materials for application as fuel cells and lithium-ion batteries [30-33]. Porous membranes with zeolite nanofillers are suitable for high-performance lithium-ion batteries as they can provide composites with higher ionic conductivity with respect to the pure polymers and also provide mechanical strength [30].

Due to the promising results of P(VDF-TrFE) separators for battery applications, the main goal of this work consist on the preparation of polar zeolite/P(VDF-TrFE) porous membranes by solvent evaporation with different contents of zeolite nanoparticles for improving electrical and mechanical properties. In this study the Y zeolite (faujasite structure) on the sodium form (NaY) has been used, with a Si/Al ratio of 2.83 as it has been proven to provide increased dielectric constant and conductivity to poly(vinylidene fluoride) thin films [34].

The influence of the zeolite content in the performance of the battery separator membranes, with and without electrolyte solution (1 M $\text{LiClO}_4 \cdot 3\text{H}_2\text{O}$ -PC), was evaluated through the study of the morphological, thermal, mechanical and electrical properties.

3.2. Results and Discussion

3.2.1. Microstructural characteristics and polymer phase

Figure 3.1 shows a cross-section scanning electron microscopy (SEM) images of the NaY/P(VDF-TrFE) composites with different zeolites contents.

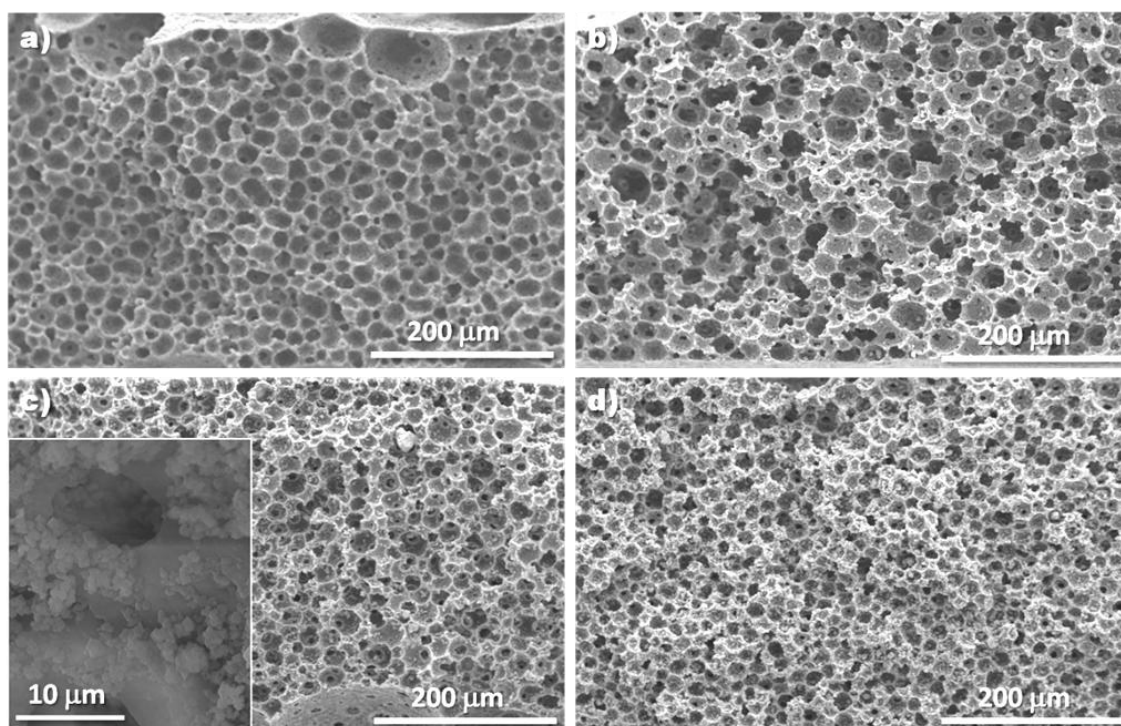


Figure 3.1: Cross-section SEM images of the NaY/P(VDF-TrFE) composites with different zeolite contents: a) 0 % (P(VDF-TrFE)); b) 4 %; c) 16 %; d) 32 %.

The samples are characterized by a uniform distribution of micropores, independently of the zeolite content. Therefore, the microstructure is independent of the zeolite content and similar to the one obtained for the pure copolymer [18]. The mechanism of polymer/solvent evaporation for P(VDF-TrFE)/DMF without fillers does not seem to be affected by the presence of the zeolite fillers, and it is explained as a liquid/liquid spinodal decomposition followed by polymer crystallization, depending mainly on the evaporation rate of the solvent and the crystallization temperature [35-36]. Due to their porous structure, the zeolite particles absorb solvent during sample preparation, shifting to the solvent-rich areas during the liquid-liquid phase separation. In this way, zeolites are not incorporated into the polymer microstructure during crystallization, remaining decorating the internal walls of the polymer pores for all zeolite contents (detail in figure 3.1c).

Thus, was observed that the inclusion of zeolites does not affect the pore distribution of the membrane but can modify the average pore size.

Figure 3.2 shows the dependence of the average pore size, porosity and electrolyte uptake of NaY/P(VDF-TrFE) membranes with different zeolite contents.

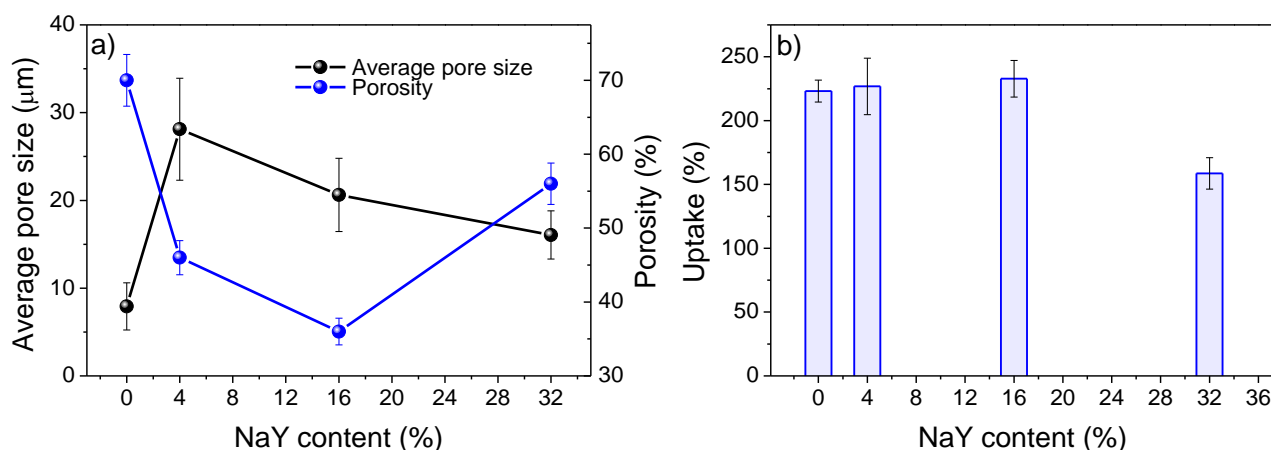


Figure 3.2: a) Influence of the zeolite content in the mean diameter of pores and porosity in the NaY/P(VDF-TrFE) composites and b) 1 M LiClO₄·3H₂O-PC solution uptake as a function of zeolite content for the NaY/P(VDF-TrFE) composites.

It is shown that the pore size increases three times and the porosity decreases by introducing zeolites in the membranes due to modification in the phase separation and solvent evaporation kinetics [35-36]. Similar behaviour was observed for PEO-PVDF-HFP-Al₂O₃/PP [37]. On the other hand, increasing NaY content reduces pore size due to filler accumulation on the pore walls. Only for the sample with 32 wt% zeolite content the porosity increases. In this case, the porosity due to the higher amounts of zeolite cavities counteracts the decrease of the porosity of the polymer due to the zeolite placement on the sidewalls of pores. Regarding the electrolyte uptake, the combination of increased pore size and decreasing porosity for filled samples, compared to pristine polymer, leads to similar uptake except for the 32 wt% zeolite content sample, in which the large amount of zeolites on sidewalls of the pores reduces electrolyte uptake. This fact is attributed to the considerable contribution of zeolite cavities to the porosity, being these pores not able to absorb Li salts. In this way, the filler concentration of 32 wt% sets the limit for improved performance for the NaY/P(VDF-TrFE) composites for Li-ion battery applications.

The large degree of porosity associated to the electrolyte uptake facilitates the transfer of lithium ions because increases the number of transport channels [38].

For electroactive polymers of PVDF and copolymer it is possible to determine the polymer crystalline phase accurately, both through X-ray diffraction (XRD) and Fourier transformed infrared spectroscopy (FTIR) [39]. PVDF-TrFE at this co-polymer concentration always crystallizes in the polar phase. In this case, FTIR was also used for to evaluate the interactions between polymer matrix and zeolites, as well as the effect of electrolyte solution introduction in membrane structure (figure 3.3).

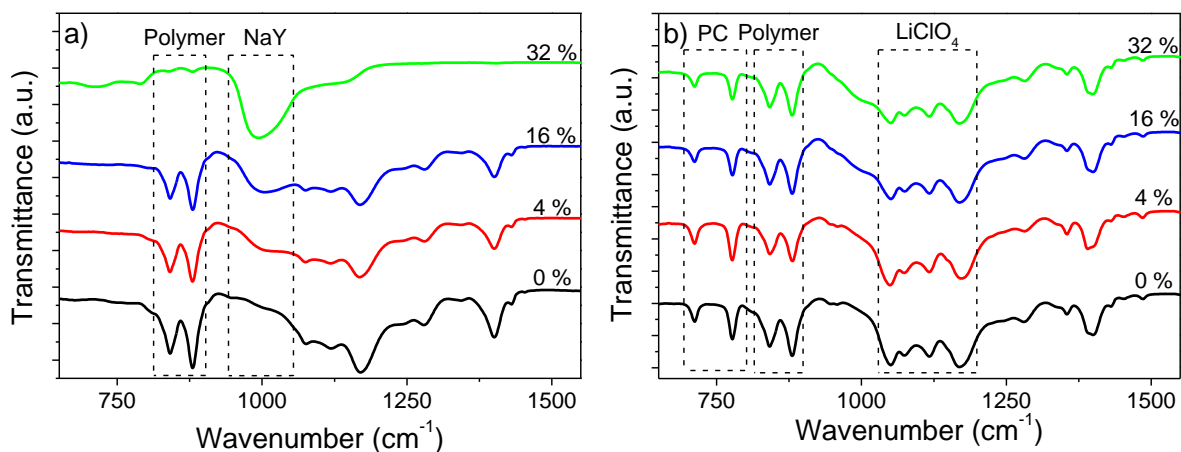


Figure 3.3: FTIR spectra for NaY/P(VDF-TrFE) composites for different zeolite contents: a) without electrolyte solution uptake; b) with electrolyte solution uptake.

Figure 3.3a shows the FTIR spectra for the samples without electrolyte solution uptake, and the characteristic vibration modes (851 cm^{-1} , 886 cm^{-1} and 1402 cm^{-1}) of the polymer all-trans conformation [40] are observed for all zeolite contents. The band increasing with increasing zeolite content around $900\text{--}1100\text{ cm}^{-1}$ corresponds to the stretching vibration of the Si-O bond in the SiO_4 tetrahedrons and reflects the presence the zeolites in the membranes [41]. For the membrane with 32 wt% zeolite content, the characteristic bands of the zeolite superimpose the polymer ones.

Regarding vibration modes of samples with electrolyte solution (figure 3.3 b), the two strong bands related to the presence of propylene carbonate (712 cm^{-1} and 777 cm^{-1}), as well as the two vibration modes at 933 cm^{-1} and 1150 cm^{-1} , identified by symmetric stretching band and asymmetric bending band, respectively of ClO_4^- [42], are detected. Further, the characteristic bands of the polymer and zeolites are unaffected by the presence of electrolyte, maintaining the membrane physico-chemical characteristics.

Table 3.1 presents the room temperature ionic conductivity (equation 2.5) and tortuosity (equation 2.6) for all samples after electrolyte uptake.

Table 3.1: Ionic conductivity and tortuosity of 1 M LiClO₄·3H₂O + separator membrane; $\sigma_0 = 9.8$ mS/cm at 25 °C.

Sample	σ_i (S/cm)	τ
0 %	5.24×10^{-7}	115
4 %	3.54×10^{-7}	113
16 %	2.33×10^{-6}	39
32 %	2.87×10^{-6}	43

The ionic conductivity of porous membranes increases with increasing zeolite content due to the large surface area of the zeolites, that reduces the growth rate of the resistive layer on the electrode surface and aids to trap residual traces of impurities, such as water and oxygen, leading to an improvement of the compatibility between membranes and the electrodes, resulting in increased ionic conductivity [43-44].

The tortuosity describes the average pore connectivity of the solid and is related with the ionic transport, providing information about the effect of the pore blockage. The tortuosity decreases with increasing zeolite content until the filler concentration of 32 wt%. The membranes without zeolites and the one with 4 wt% show high tortuosity values due to poor pore connectivity which hinders the ionic transport. For higher zeolite contents the tortuosity decreases as the ionic transport is now supported by the higher conductivity of the zeolite fillers in the sidewalls of the pores, leading to better pore connectivity [45].

3.2.2. Thermal and mechanical properties

The characterization of the porous membrane by thermal (differential scanning calorimetry measurements – DSC) and mechanical (stress-strain curves) techniques is crucial to evaluate the performance of membranes for battery applications and to determine the influence of zeolite content in the polymeric matrix.

DSC thermograms for NaY/P(VDF-TrFE) membranes without and with electrolyte solution are depicted in figures 3.4 a) and b), respectively.

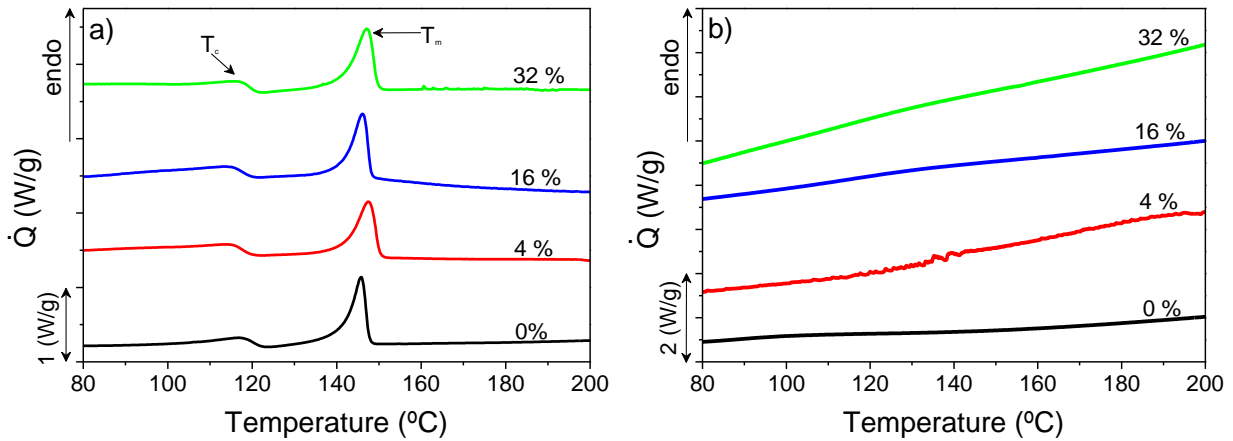


Figure 3.4: DSC thermograms of the NaY/P(VDF-TrFE) composites with different zeolite filler contents: a) without electrolyte solution uptake; b) with electrolyte solution uptake.

In DSC thermograms for NaY/P(VDF-TrFE) membranes without electrolyte solution (figure 3.4a) two endothermic peaks are observed, representing the ferroelectric-paraelectric phase transition (lower temperature peak, T_c) at 117 °C and melting temperature of the polymer matrix (higher temperature peak, T_m) at 146 °C [46]. These peaks does not depend on zeolite content present in the polymeric matrix, indicating that fillers inclusion does not significantly influence the polymer ferroelectric phase, degree of crystallinity and thermal stability, because fillers are mainly placed on the outside walls of the polymer.

This fact is demonstrated in table 3.2 where the degree of crystallinity, calculated by equation 2.1, is shown for NaY/P(VDF-TrFE) membranes without electrolyte solution uptake.

Table 3.2: Degree of Crystallinity of all samples calculated through equation 2.1 to the melting peak of samples without electrolyte solution uptake.

Sample	$\chi_c \pm 2$ (%)
0 %	28
4 %	26
16 %	23
32 %	20

The degree of crystallinity shows a small decrease by increasing filler content, due to the defective induced crystallization in the polymer structure in the places where

it interacts with the zeolites. Nucleation and growth kinetics of the polymer is changed due to the large zeolite contents (above 4 wt%) [47].

In the DSC thermograms for samples with electrolyte solution (figure 3.4b) the two endothermic peaks characteristics of the polymeric matrix are not detected for all filler contents due to the high absorption of the electrolyte solution by the composite membranes. It is reported that the PC present in the electrolyte solution leads to the collapse of some crystallites of P(VDF-TrFE), increasing the amorphous content within the polymer matrix [48]. Nevertheless, membranes stability is demonstrated up to the ferroelectric-paraelectric phase transition temperature, around 120 °C, in which the polarity and electrical characteristics of the membrane changes.

The mechanical properties of the separator membranes for lithium ion batteries are essential for performance, integrity and safety of the batteries [49-50]. The mechanical properties of porous materials depend on porosity, pore size, distribution and geometry [51], and represent one of the main drawbacks of polymer porous membranes that can be solved by suitable selection of reinforcing fillers.

The stress-strain curves of NaY/P(VDF-TrFE) composites with different zeolite nanoparticle contents are represented in figure 3.5 without electrolyte solution (figure 3.5a) and with electrolyte solution (figure 3.5b). In table 3.3 the mechanical parameters (elastic modulus, stress at break and strain at break) obtained from figure 3.5 are shown.

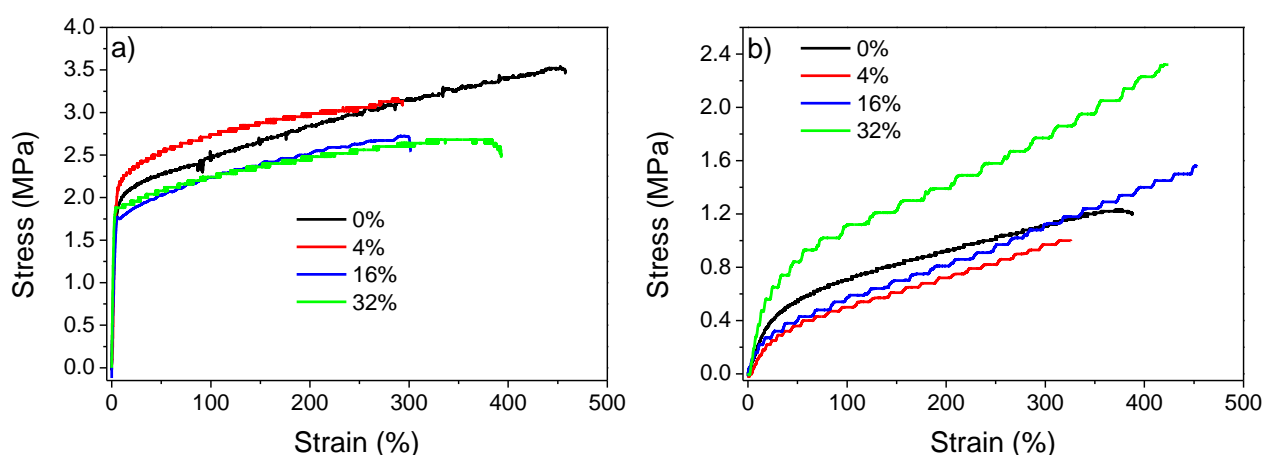


Figure 3.5: Stress-Strain curves of the NaY/P(VDF-TrFE) composites with different zeolite particles contents: a) without electrolyte solution uptake; b) with electrolyte solution uptake.

Table 3.3: Mechanical properties of the composite membranes.

Sample	Without Uptake				With Uptake			
	0 %	4 %	16 %	32 %	0 %	4 %	16 %	32 %
Stretching strain at break (%)	455	293	299	383	392	326	455	426
Stress at break (MPa)	3.5	3.1	2.7	2.7	1.2	1	1.55	2.3
Elastic Modulus (MPa)	40	51	62	76	1.9	1.4	1.7	3.8

Figure 3.5a shows that addition of zeolites up to 4 wt% improves the mechanical properties (yielding stress) of the membrane separator in comparison with zeolites free membranes. This phenomenon is attributed to the Lewis acid-base interactions between the polymer matrix and the Lewis acid sites on the surface of the zeolite particles [52].

For zeolite contents above 4 wt%, the mechanical stress at yielding of the membranes decreases due to aggregate formation at the membrane surface.

The elastic modulus (table 3.3) increases with increasing filler content, indicating the reinforcing effect of the zeolites. This behaviour can be explained by a folding effect of the polymer chains within the zeolite particles at the filler-polymer contact points. The mechanical properties (elastic modulus, stress at break and strain at break) of the samples with electrolyte solution decrease, compared to the ones without electrolyte, due to large uptakes. The effect of electrolyte uptake in the mechanical properties is similar for all zeolite concentrations, nevertheless, the elastic modulus and the stretching at break are higher for samples with larger zeolite content. It is interesting to observe that the stress-strain curves with electrolyte solution have the form of steps resulting from the collapse of the pores in membrane structure.

The determination of the mechanical properties as function of temperature is crucial to set limits of applicability of the porous membranes to different environments. Figure 3.6 shows the mechanical behaviour of the NaY/P(VDF-TrFE) composites for 16% wt at different temperatures.

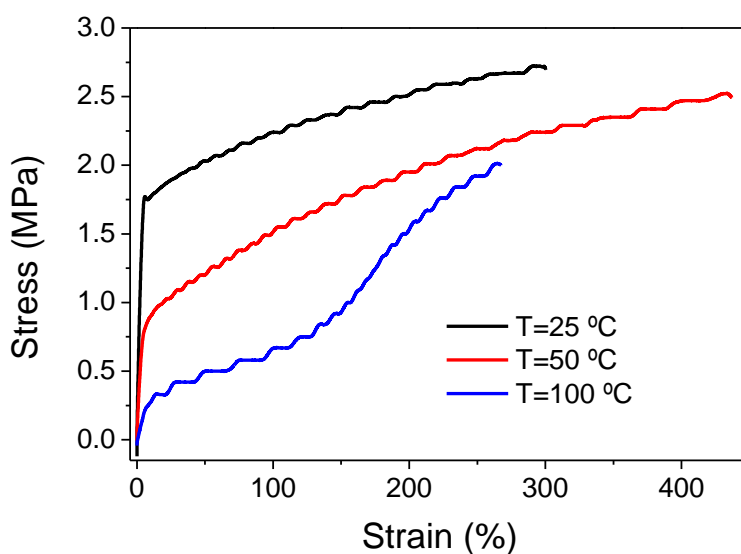


Figure 3.6: Stress-Strain curves of the NaY/P(VDF-TrFE) composites for 16 wt% at different temperatures.

The mechanical response (figure 3.6) determined through the different parameters (elastic modulus, stress at break and strain at break) decreases with increasing temperature.

Increasing temperature induces larger polymer chain mobility within the crystalline and amorphous phases, particularly at temperatures higher than the α_c -relaxation temperature of the polymer around 60 °C, resulting in the decrease of mechanical properties [53]. This behaviour was observed for all samples independently of the zeolite content.

3.2.3. Electrical properties

The electrochemical properties of all samples with and without electrolyte solution were determined by electrochemical impedance spectroscopy (EIS) and are represented through Nyquist plots (imaginary impedance Z'' versus real impedance Z'), Bode plots (absolute impedance $|Z|$ and phase angle versus frequency) and ionic conductivity versus temperature. For all samples with electrolyte solution the Nyquist

plots at 50 °C are presented in figure 3.7a) and the Bode diagram in figure 3.7b) and c). Figure 3.7d shows the impedance modulus as a function of zeolite content for the different samples at different temperatures and at a frequency of 1 kHz.

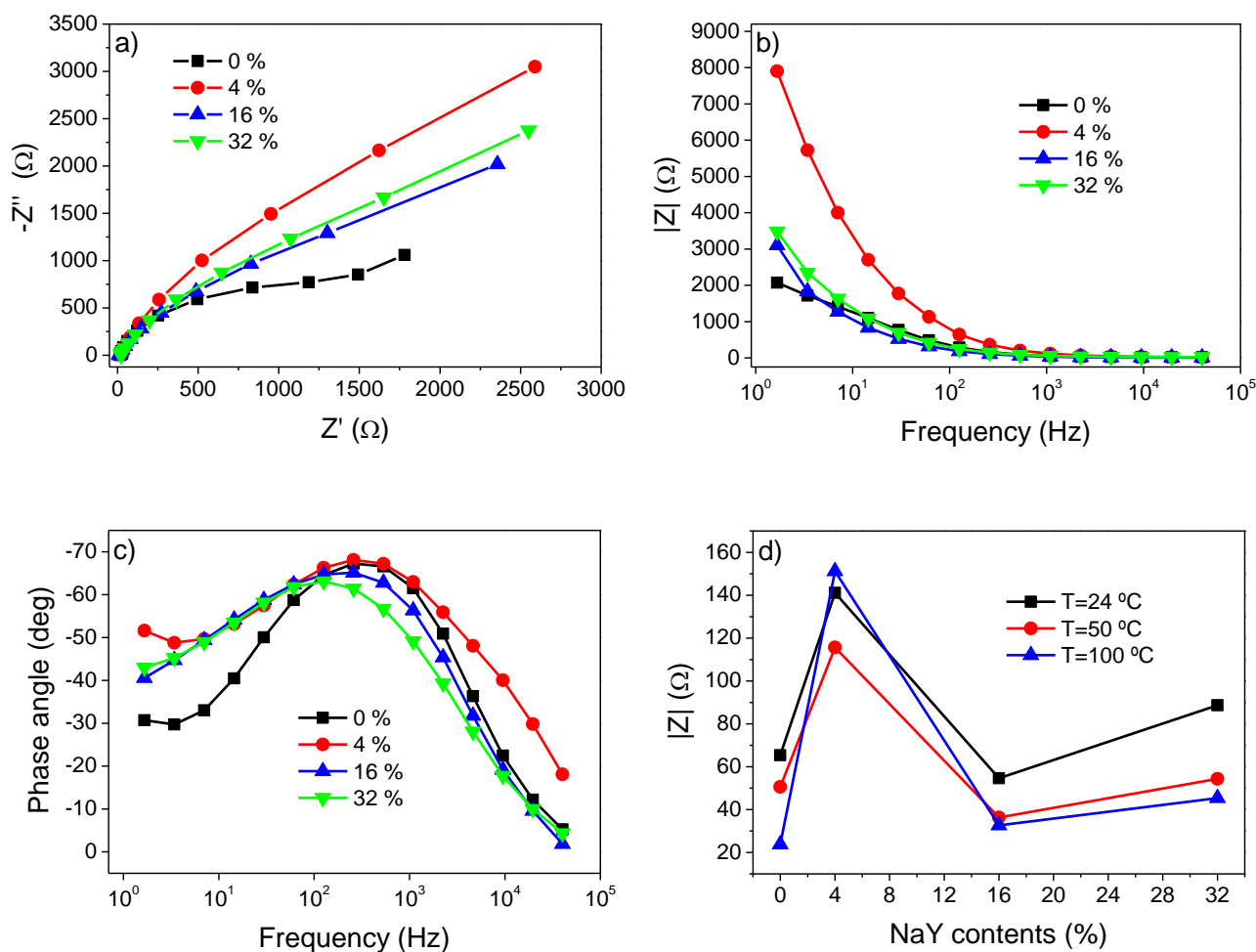


Figure 3.7: a) Nyquist plot of the NaY/P(VDF-TrFE) composites for all filler contents at 50 °C; b-c) Bode diagram of the NaY/P(VDF-TrFE) composites for all contents at 50 °C and d) impedance modulus as a function of zeolite content at different temperatures.

Usually, Nyquist plot is characterized by three distinct parts: a semicircle located at the high-frequency range that corresponds to the charge transfer process, a straight line for lower frequency related to the diffusion process and the transition between these phenomena [54-55].

In figure 3.7a, the semi-circle at higher frequencies is observed for the pristine polymer membrane. This semicircle is not clearly identified in the composite membranes as the inclusion of zeolites improves the charge transfer process. The larger pore size and the high value of the tortuosity can be the reasons for the high value of the Nyquist curve in the membrane with 4 wt% of zeolites.

The impedance modulus as a function of frequency for all samples at 50 °C is represented in figure 3.7b. For all membranes, the impedance modulus decreases with increasing frequency, being this decrease more significant for lower frequencies up to 1 kHz. This behaviour indicates the restricted dynamics of ion mobility within the porous membranes.

The phase angle as function of frequency for all membranes at 50 °C is shown in figure 3.7c. The maximum phase angle occurs at -70 °, independently of the zeolite content. For an ideal resistor and capacitor in series, the maximum phase angle should be -90 °. In this case, as the maximum phase angle is lower than -90 °, the behaviour is better represented by a constant phase element (CPE) [56], which can be modelled as a capacitor with a distribution of relaxation times [57-58].

The influence of zeolites in the electric conduction behaviour is due to their intrinsic conductivity and to their effect in the polymer matrix. With respect the later, zeolite fillers show strong Lewis acid centres in their frameworks and inside the channels, which contribute to the reduction of the crystallinity of the polymer host, thus resulting in a higher conductivity and Li^+ transference number. The conductivity behaviour in the separator membrane is also influenced by the zeolite contents; for small contents of zeolites, and despite the higher diameter of zeolite cavity (13 Å) compared to lithium ions, the uptake occurs mainly in the polymer matrix. Further, the zeolite content is not enough to establish channels networks of conduction. For higher zeolite contents, the channel conduction networks are created, resulting in an increase of porous membrane ionic conductivity.

Figure 3.7d shows the impedance modulus as a function of zeolite content at different temperatures at 1 kHz. For all membranes, the impedance modulus decreases with increasing temperature due to the release of trapped ionic charges followed by their accumulation in the polymer matrix and in the interfaces between zeolites and polymer. On the other hand, the zeolite filler increases the ac conductivity and is an evidence of the Maxwell-Wagner-Sillars (MWS) contribution [59]. It has been shown that applying a power law fit for 4 wt% composite the exponent number of Jonscher law is 1 [59]. Further, electrode polarization contributions are presented, for temperatures below 60 °C, in the frequency region between 10^0 at 10^2 Hz.

Regardless the temperature, the impedance modulus increases with increasing zeolite content up to 4 wt% and decreases for larger filler contents. This results from the

large pore size and still low zeolite content to create a conductivity network in the 4 wt% sample.

Figure 3.8 shows the temperature dependence of ionic conductivity of composite all membranes without (figure 3.8a) and with (figure 3.8b) electrolyte solution uptake.

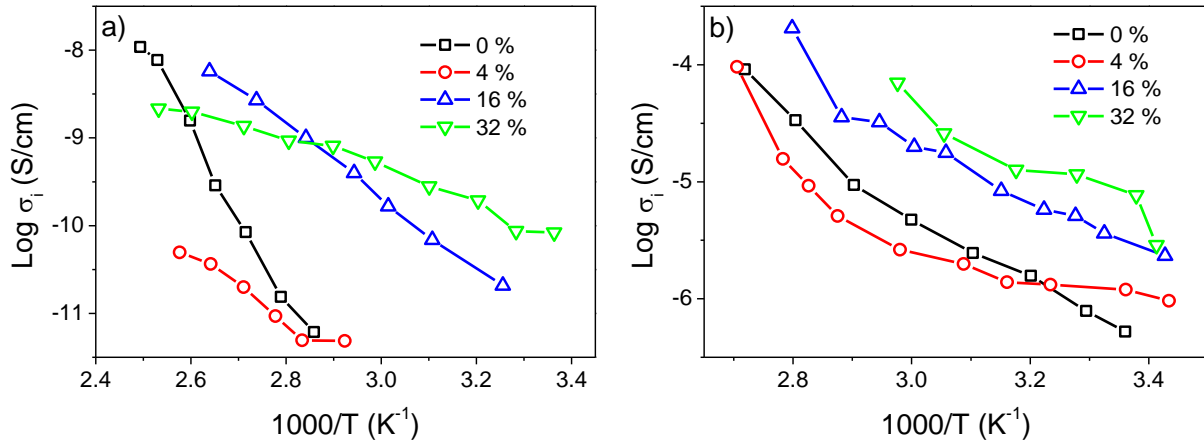


Figure 3.8: Log σ_i as function of $1000/T$ for NaY/P(VDF-TrFE) composites a) without electrolyte solution uptake and b) with electrolyte solution uptake.

Regardless the electrolyte uptake, ionic conductivity increases with increasing temperature, as the polymer tends to expand leading to higher free volume. Further, polymer segmental and charge nobilities are also enhanced [60].

The inclusion of zeolites increases the ionic conductivity of the membrane, by increasing pore size and by the zeolites two-dimensional interconnected channels. The electrolyte solution absorbed in the zeolites structure may form a conducting pathway in the porous membrane when its content is high enough, as shown in figure 3.8 [30, 52]. In the table 3.4 it is presented the activation energy, E_a , for ion transport for all samples calculated from the Arrhenius equation (equation 2.7) applied to the data of figure 3.8.

Table 3.4: Activation energy for all porous membranes with and without electrolyte solution.

Samples	Without electrolyte solution (kJ/mol)	With electrolyte solution (kJ/mol)
0 %	181	64
4 %	76	43
16 %	78	44
32 %	34	42

The activation energy values show dependence on filler content and electrolyte solution uptake, which improves the mobility and ionic charge carriers in the porous

membranes [61]. Significant differences in the activation energy value are observed between membranes with and without fillers, due to the charge and conductive pathways introduced by zeolites particles. Increasing filler content decreases the ion transport energy barrier, leading to a decrease in the activation energy [62]. The electrochemical stability and the diffusion coefficient of the membranes were measured by microelectrode cyclic voltammetry over the potential range -2.0 V to 6.0 V with electrolyte solution (figure 3.9).

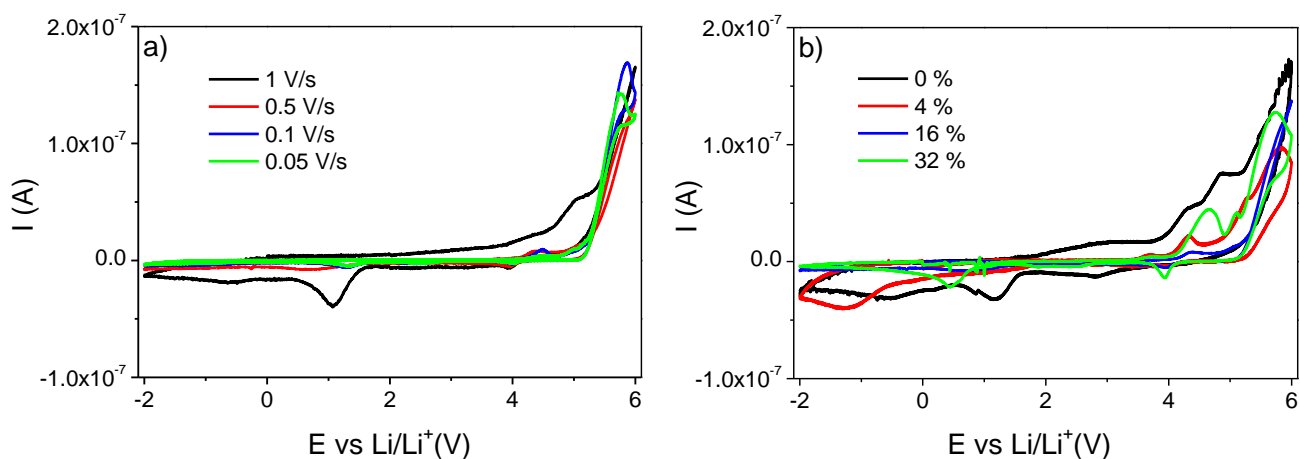


Figure 3.9: a) Voltammograms of NaY/P(VDF-TrFE) with 16 wt% of zeolites at different scanning rates and b) voltammograms of NaY/P(VDF-TrFE) composites at 0.5 V/s.

The voltammogram of the membrane with 16 wt% of zeolite (figure 3.9a) exhibits good electrochemical stability independently of scanning rate, with anodic potentials higher than 5.5 V *versus* Li/Li⁺ and oxidation peak around 1.0 V. The anodic current onset may be associated with the decomposition of the polymer electrolyte. Increasing potential sweeping rate shifts the cathodic peak potential in the negative direction. The small peak around 1.0 V has been ascribed to reduction of water present in PE or oxygen impurities. Similar behaviour has been observed for other systems based on PEO and lithium salt [63].

For the same scanning rate (0.5 V/s) multiples anodic potentials higher than 4 V were obtained for high zeolite contents, the oxidation peak also depending on the zeolite content present in the polymeric matrix.

The diffusion coefficients calculated by equation 2.8 for all porous membranes are shown in table 3.5. The diffusion coefficient of PVDF is $1.98 \times 10^{-6} \text{ cm}^2/\text{s}$.

Table 3.5: Diffusion coefficient calculated by equation 2.8 for all porous membranes with electrolyte solution.

Samples	Diffusion coefficient (cm^2/s)
0 %	3.45×10^{-5}
4 %	2.58×10^{-5}
16 %	4.09×10^{-5}
32 %	3.29×10^{-5}

The diffusion coefficient does not show strong dependence on zeolite content, presenting the maximum value of $4.09 \times 10^{-5} \text{ cm}^2/\text{s}$ for membrane with 16 wt% of zeolites. The diffusion coefficient of the copolymer is higher than the one of PVDF, due to copolymerization with TrFE.

3.3. Conclusion

NaY zeolite/PVDF-TrFE porous membranes with different zeolite contents were prepared for lithium ion battery applications by thermally induced phase separation (TIPS). The electrolyte solution was 1 M $\text{LiClO}_4 \cdot 3\text{H}_2\text{O}$ -PC. The zeolite inclusion changes the pore size, porosity and uptake of membranes. The polymer phase is not affected by the inclusion of the zeolites. The tortuosity decreases with increasing zeolite content, indicating that ionic transport is now supported by a better pore connectivity. The membranes are thermally stable above 100 °C and the inclusion of fillers improves the mechanical strength of the membranes.

The ionic conductivity is influenced by the filler content and a maximum value $2.33 \times 10^{-6} \text{ S/cm}$ is obtained at room temperature for the P(VDF-TrFE) membrane with 16 wt% zeolite content. The zeolite particles form a conducting pathway in the polymeric matrix for high zeolite contents, improving the ionic conductivity. The overall stability of the porous membrane, determined by cyclic voltammetry, is appropriate for the intended applications with no electrochemical oxidation occurring at potentials lower than 3.0 V. These results shows that the NaY/P(VDF-TrFE) porous

membranes have adequate electrochemical stability, thermal, mechanical and electrical properties for being used as battery separators in lithium ion batteries.

3.4. References

1. Tarascon, J.M. and M. Armand. *Issues and challenges facing rechargeable lithium batteries*. Nature, 2001. **414**(6861): p. 359-367.
2. Whittingham, M.S. *Lithium Batteries and Cathode Materials*. Chemical Reviews, 2004. **104**(10): p. 4271-4302.
3. Vincent, C.A. *Lithium batteries: a 50-year perspective, 1959–2009*. Solid State Ionics, 2000. **134**(1–2): p. 159-167.
4. Arora, P. and Z. Zhang. *Battery Separators*. Chemical Reviews, 2004. **104**(10): p. 4419-4462.
5. Besenhard, J.O. *Handbook of battery materials*. 1999, Weinheim; New York: Wiley-VCH.
6. Xu, K. *Nonaqueous Liquid Electrolytes for Lithium-Based Rechargeable Batteries*. Chemical Reviews, 2004. **104**(10): p. 4303-4418.
7. Manuel Stephan, A. *Review on gel polymer electrolytes for lithium batteries*. European Polymer Journal, 2006. **42**(1): p. 21-42.
8. Barbosa, P.C., M.M. Silva, M.J. Smith, A. Gonçalves, and E. Fortunato. *Studies of solid-state electrochromic devices based on PEO/siliceous hybrids doped with lithium perchlorate*. Electrochimica Acta, 2007. **52**(8): p. 2938-2943.
9. Persi, L., F. Croce, B. Scrosati, E. Plichta, and M.A. Hendrickson. *Poly(ethylene oxide)-Based, Nanocomposite Electrolytes as Improved Separators for Rechargeable Lithium Polymer Batteries*. Journal of The Electrochemical Society, 2002. **149**(2): p. A212-A216.
10. Kim, D.-W., J.-M. Ko, J.-H. Chun, S.-H. Kim, and J.-K. Park. *Electrochemical performances of lithium-ion cells prepared with polyethylene oxide-coated separators*. Electrochemistry Communications, 2001. **3**(10): p. 535-538.
11. Wang, C., Y. Wei, G.R. Ferment, W. Li, and T. Li. *Poly(ethylene oxide)–silica hybrid materials for lithium battery application*. Materials Letters, 1999. **39**(4): p. 206-210.
12. Li, H., X.-T. Ma, J.-L. Shi, Z.-K. Yao, B.-K. Zhu, and L.-P. Zhu. *Preparation and properties of poly(ethylene oxide) gel filled polypropylene separators and their corresponding gel polymer electrolytes for Li-ion batteries*. Electrochimica Acta, 2011. **56**(6): p. 2641-2647.
13. Cho, T.H., T. Sakai, S. Tanase, K. Kimura, Y. Kondo, T. Terao, and M. Tanaka. *Electrochemical Performances of Polyacrylonitrile Nanofiber-Based Nonwoven Separator for Lithium-Ion Battery*. Electrochemical and Solid-State Letters, 2007. **10**(7): p. A159-A162.

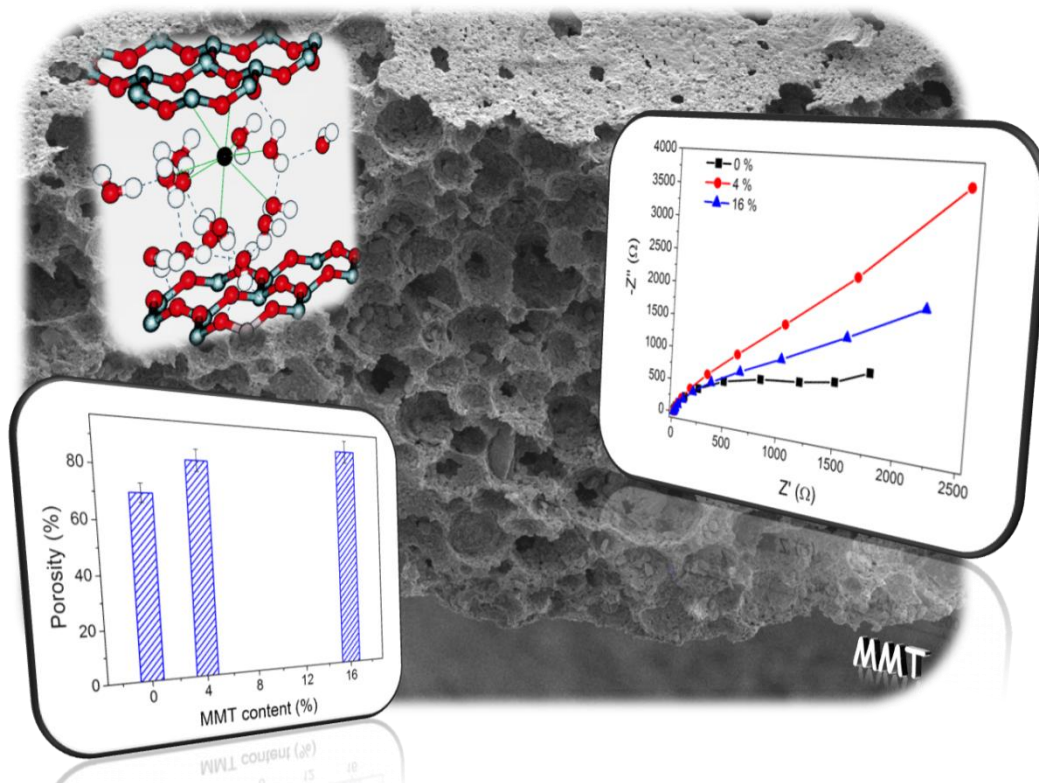
14. Huai, Y., J. Gao, Z. Deng, and J. Suo. *Preparation and characterization of a special structural poly(acrylonitrile)-based microporous membrane for lithium-ion batteries*. *Ionics*, 2010. **16**(7): p. 603-611.
15. Cheng, C.L., C.C. Wan, and Y.Y. Wang. *Preparation of porous, chemically cross-linked, PVdF-based gel polymer electrolytes for rechargeable lithium batteries*. *Journal of Power Sources*, 2004. **134**(2): p. 202-210.
16. Wachtler, M., D. Ostrovskii, P. Jacobsson, and B. Scrosati. *A study on PVdF-based SiO₂-containing composite gel-type polymer electrolytes for lithium batteries*. *Electrochimica Acta*, 2004. **50**(2-3): p. 357-361.
17. Stephan, A.M., K.S. Nahm, M. Anbu Kulandainathan, G. Ravi, and J. Wilson. *Poly(vinylidene fluoride-hexafluoropropylene) (PVdF-HFP) based composite electrolytes for lithium batteries*. *European Polymer Journal*, 2006. **42**(8): p. 1728-1734.
18. Costa, C.M., L.C. Rodrigues, V. Sencadas, M.M. Silva, J.G. Rocha, and S. Lanceros-Méndez. *Effect of degree of porosity on the properties of poly(vinylidene fluoride-trifluoroethylene) for Li-ion battery separators*. *Journal of Membrane Science*, 2012. **407-408**(0): p. 193-201.
19. Djian, D., F. Alloin, S. Martinet, and H. Lignier. *Macroporous poly(vinylidene fluoride) membrane as a separator for lithium-ion batteries with high charge rate capacity*. *Journal of Power Sources*, 2009. **187**(2): p. 575-580.
20. Nalwa, H.S. *Ferroelectric polymers : chemistry, physics, and applications*. 1995, New York: Dekker.
21. Lovinger, A.J., T. Furukawa, G.T. Davis, and M.G. Broadhurst. *Crystallographic changes characterizing the Curie transition in three ferroelectric copolymers of vinylidene fluoride and trifluoroethylene: 2. Oriented or poled samples*. *Polymer*, 1983. **24**(10): p. 1233-1239.
22. Furukawa, T., G.E. Johnson, H.E. Bair, Y. Tajitsu, A. Chiba, and E. Fukada. *Ferroelectric phase transition in a copolymer of vinylidene fluoride and trifluoroethylene*. *Ferroelectrics*, 1981. **32**(1): p. 61-67.
23. Costa, C.M., A. California, V.F. Cardoso, V. Sencadas, L.C. Rodrigues, M.M. Silva, and S. Lanceros-Méndez. *Electroactive Poly(Vinylidene Fluoride-Trifluoroethylene) (PVDF-TrFE) Microporous Membranes for Lithium-Ion Battery Applications*. *Ferroelectrics*, 2012. **430**(1): p. 103-107.
24. Costa, C.M., L.C. Rodrigues, V. Sencadas, M.M. Silva, and S. Lanceros-Méndez. *Effect of the microstructure and lithium-ion content in poly[(vinylidene fluoride)-co-trifluoroethylene]/lithium perchlorate trihydrate composite membranes for battery applications*. *Solid State Ionics*, 2012. **217**(0): p. 19-26.

25. Weston, J.E. and B.C.H. Steele. *Effects of inert fillers on the mechanical and electrochemical properties of lithium salt-poly(ethylene oxide) polymer electrolytes*. Solid State Ionics, 1982. **7**(1): p. 75-79.
26. Srun Jung, Dae Won Kim, Sang Deuk Lee, Minserk Cheong, Dinh Quan Nguyen, Byung Won Cho, and H.S. Kim. *Fillers for Solid-State Polymer Electrolytes: Highlight*. Bull. Korean Chem. Soc, 2009. **30**(10).
27. Martínez, C. and A. Corma. *Inorganic molecular sieves: Preparation, modification and industrial application in catalytic processes*. Coordination Chemistry Reviews, 2011. **255**(13–14): p. 1558-1580.
28. Hersh, C.K. *Molecular sieves*. 1961, New York: Reinhold Publishing Corporation.
29. Abdoulaye, A., J.V. Zanchetta, F. Di Renzo, J.C. Giuntini, J. Vanderschueren, and G. Chabanis. *Dielectric properties of faujasites: comparison between types X and Y during dehydration*. Microporous and Mesoporous Materials, 2000. **34**(3): p. 317-325.
30. Xi, J., X. Qiu, and L. Chen. *PVDF-PEO/ZSM-5 based composite microporous polymer electrolyte with novel pore configuration and ionic conductivity*. Solid State Ionics, 2006. **177**(7–8): p. 709-713.
31. Piao, J., S. Liao, and Z. Liang. *A novel cesium hydrogen sulfate-zeolite inorganic composite electrolyte membrane for polymer electrolyte membrane fuel cell application*. Journal of Power Sources, 2009. **193**(2): p. 483-487.
32. Wang, J., X. Zheng, H. Wu, B. Zheng, Z. Jiang, X. Hao, and B. Wang. *Effect of zeolites on chitosan/zeolite hybrid membranes for direct methanol fuel cell*. Journal of Power Sources, 2008. **178**(1): p. 9-19.
33. Sancho, T., J. Soler, and M.P. Pina. *Conductivity in zeolite-polymer composite membranes for PEMFCs*. Journal of Power Sources, 2007. **169**(1): p. 92-97.
34. Lopes, A.C., R. Gonçalves, C.M. Costa, A.M. Fonseca, G. Botelho, I.C. Neves, and S. Lanceros-Mendez. *Effect of Zeolite Content in the Electrical, Mechanical and Thermal Degradation Response of Poly(vinylidene fluoride)/NaY Zeolite Composites*. Journal of Nanoscience and Nanotechnology, 2012. **12**(8): p. 6804-6810.
35. California, A., V.F. Cardoso, C.M. Costa, V. Sencadas, G. Botelho, J.L. Gómez-Ribelles, and S. Lanceros-Mendez. *Tailoring porous structure of ferroelectric poly(vinylidene fluoride-trifluoroethylene) by controlling solvent/polymer ratio and solvent evaporation rate*. European Polymer Journal, 2011. **47**(12): p. 2442-2450.
36. Ferreira, A., J. Silva, V. Sencadas, J.L.G. Ribelles, and S. Lanceros-Méndez. *Poly[(vinylidene fluoride)-co-trifluoroethylene] Membranes Obtained by*

- Isothermal Crystallization from Solution*. Macromolecular Materials and Engineering, 2010. **295**(6): p. 523-528.
37. Liao, Y.H., X.P. Li, C.H. Fu, R. Xu, L. Zhou, C.L. Tan, S.J. Hu, and W.S. Li. *Polypropylene-supported and nano-Al₂O₃ doped poly(ethylene oxide)–poly(vinylidene fluoride-hexafluoropropylene)-based gel electrolyte for lithium ion batteries*. Journal of Power Sources, 2011. **196**(4): p. 2115-2121.
 38. Zhang, P., H.P. Zhang, G.C. Li, Z.H. Li, and Y.P. Wu. *A novel process to prepare porous membranes comprising SnO₂ nanoparticles and P(MMA-AN) as polymer electrolyte*. Electrochemistry Communications, 2008. **10**(7): p. 1052-1055.
 39. Lanceros-Méndez, S., J.F. Mano, A.M. Costa, and V.H. Schmidt. *FTIR AND DSC STUDIES OF MECHANICALLY DEFORMED β-PVDF FILMS*. Journal of Macromolecular Science, Part B, 2001. **40**(3-4): p. 517-527.
 40. Prabu, A.A., J.S. Lee, K.J. Kim, and H.S. Lee. *Infrared spectroscopic studies on crystallization and Curie transition behavior of ultrathin films of P(VDF/TrFE) (72/28)*. Vibrational Spectroscopy, 2006. **41**(1): p. 1-13.
 41. Shikunov, B.I., L.I. Lafer, V.I. Yakerson, I.V. Mishin, and A.M. Rubinshtein. *Infrared spectra of synthetic zeolites*. Russian Chemical Bulletin, 1972. **21**(1): p. 201-203.
 42. Chen, Y., Y.-H. Zhang, and L.-J. Zhao. *ATR-FTIR spectroscopic studies on aqueous LiClO₄, NaClO₄, and Mg(ClO₄)₂ solutions*. Physical Chemistry Chemical Physics, 2004. **6**(3): p. 537-542.
 43. Gentili, V., S. Panero, P. Reale, and B. Scrosati. *Composite gel-type polymer electrolytes for advanced, rechargeable lithium batteries*. Journal of Power Sources, 2007. **170**(1): p. 185-190.
 44. Jiang, Y.-X., Z.-F. Chen, Q.-C. Zhuang, J.-M. Xu, Q.-F. Dong, L. Huang, and S.-G. Sun. *A novel composite microporous polymer electrolyte prepared with molecule sieves for Li-ion batteries*. Journal of Power Sources, 2006. **160**(2): p. 1320-1328.
 45. Quartarone, E., P. Mustarelli, and A. Magistris. *Transport Properties of Porous PVDF Membranes*. The Journal of Physical Chemistry B, 2002. **106**(42): p. 10828-10833.
 46. Sencadas, V., S. Lanceros-Méndez, and J.F. Mano. *Thermal characterization of a vinylidene fluoride-trifluorethylene (75–25) (%mol) copolymer film*. Journal of Non-Crystalline Solids, 2006. **352**(50–51): p. 5376-5381.
 47. Costa, C.M., S. Firmino Mendes, V. Sencadas, A. Ferreira, R. Gregorio Jr, J.L. Gómez Ribelles, and S. Lanceros-Méndez. *Influence of processing parameters on the polymer phase, microstructure and macroscopic properties of*

- poly(vinylidene fluoride)/Pb(Zr_{0.53}Ti_{0.47})O₃ composites*. Journal of Non-Crystalline Solids, 2010. **356**(41–42): p. 2127-2133.
48. Tian, L.-y., X.-b. Huang, and X.-z. Tang. *Study on morphology behavior of PVDF-based electrolytes*. Journal of Applied Polymer Science, 2004. **92**(6): p. 3839-3842.
49. Tian, Z., X. He, W. Pu, C. Wan, and C. Jiang. *Preparation of poly(acrylonitrile–butyl acrylate) gel electrolyte for lithium-ion batteries*. Electrochimica Acta, 2006. **52**(2): p. 688-693.
50. Sheidaei, A., X. Xiao, X. Huang, and J. Hitt. *Mechanical behavior of a battery separator in electrolyte solutions*. Journal of Power Sources, 2011. **196**(20): p. 8728-8734.
51. Lu, G., G.Q. Lu, and Z.M. Xiao. *Mechanical Properties of Porous Materials*. Journal of Porous Materials, 1999. **6**(4): p. 359-368.
52. Xi, J., S. Miao, and X. Tang. *Selective Transporting of Lithium Ion by Shape Selective Molecular Sieves ZSM-5 in PEO-Based Composite Polymer Electrolyte*. Macromolecules, 2004. **37**(23): p. 8592-8598.
53. Costa, C.M., V. Sencadas, I. Pelicano, F. Martins, J.G. Rocha, and S. Lanceros-Mendez. *Microscopic origin of the high-strain mechanical response of poled and non-poled poly(vinylidene fluoride) in the β -phase*. Journal of Non-Crystalline Solids, 2008. **354**(32): p. 3871-3876.
54. Chang, B.-Y. and S.-M. Park. *Electrochemical Impedance Spectroscopy*. Annual Review of Analytical Chemistry, 2010. **3**(1): p. 207-229.
55. Park, M., X. Zhang, M. Chung, G.B. Less, and A.M. Sastry. *A review of conduction phenomena in Li-ion batteries*. Journal of Power Sources, 2010. **195**(24): p. 7904-7929.
56. Zelinka, S.L., L. Ortiz-Candelaria, D.S. Stone, and D.R. Rammer. *Electrochemical impedance spectroscopy (EIS) as a tool for measuring corrosion of polymer-coated fasteners used in treated wood*. Forest products journal, 2009. **59**(1-2): p. 77-82.
57. Cole, K. *Dispersion and Absorption in Dielectrics I. Alternating Current Characteristics*. J. Chem. Phys., 1941. **9**(4): p. 341.
58. Raistrick, I.D. *Application of Impedance Spectroscopy to Materials Science*. Annual Review of Materials Science, 1986. **16**(1): p. 343-370.
59. Lopes, A.C., C.M. Costa, R.S.i. Serra, I.C. Neves, J.L.G. Ribelles, and S. Lanceros-Méndez. *Dielectric relaxation, ac conductivity and electric modulus in poly(vinylidene fluoride)/NaY zeolite composites*. Solid State Ionics, 2013. **235**(0): p. 42-50.

60. Karabelli, D., J.C. Leprêtre, F. Alloin, and J.Y. Sanchez. *Poly(vinylidene fluoride)-based macroporous separators for supercapacitors*. *Electrochimica Acta*, 2011. **57**(1): p. 98-103.
61. Every, H.A., F. Zhou, M. Forsyth, and D.R. MacFarlane. *Lithium ion mobility in poly(vinyl alcohol) based polymer electrolytes as determined by ⁷Li NMR spectroscopy*. *Electrochimica Acta*, 1998. **43**(10–11): p. 1465-1469.
62. Gray, F.M. *Solid polymer electrolytes : fundamentals and technological applications*. 1991, New York, NY: VCH.
63. Aurbach, D., M. Daroux, P. Faguy, and E. Yeager. *The electrochemistry of noble metal electrodes in aprotic organic solvents containing lithium salts*. *Journal of Electroanalytical Chemistry and Interfacial Electrochemistry*, 1991. **297**(1): p. 225-244.



4 - Porous membranes of MMT/P(VDF-TrFE)

This chapter is based on the following publication:

Nunes-Pereira, J., A.C. Lopes, C.M. Costa, R. Leones, M.M. Silva, and S. Lanceros-Méndez. *Porous Membranes of Montmorillonite/Poly(vinylidene fluoride-trifluoroethylene) for Li-Ion Battery Separators*. *Electroanalysis*, 2012. **24**(11): p. 2147-156.

4.1. Introduction

The battery industry has experienced a strong growth over the past few years in the area of portable and rechargeable battery packs, due to the widespread use of cell phones, PDA's, laptop computers, cameras and other wireless electronics as well as due to the demand for power hybrid electric vehicles, full electric vehicles and by the need of energy storage related to renewable energies [1-3]. Lithium ion batteries are most often the systems of choice for portable applications, offering high energy density, flexible and lightweight design, and longer lifespan than competing battery technologies. At present, it is the largest sector representative in batteries for portable systems and shows the best performance mainly due to its high energy density (210 W.h/kg) [3-4].

Nevertheless, the actual secondary battery systems use expensive materials, which act as an obstacle to the sustained growth of this industry. In addition, the safety of these devices is still questioned [2]. The use of lithium in secondary cells is difficult due to its high reactivity with the electrolyte components. One solution to this problem can be the use of polymer electrolytes. In this way, future developments in secondary cells will focus mainly on two areas: improving cells safety, energy density and electrochemical characteristics and provide larger systems for electric vehicles and dispersed energy storage systems [5].

A battery is a transducer that converts chemical into electrical energy and its main constituents are the cathode, the anode and the membrane separator (e.g. solid polymer electrolyte – SPE). In lithium ion batteries the anode serves as the source of ions, the cathode provides the function of collecting the ions and the electrolyte ensures the separation for ionic and electronic transport [2]. The separator is a porous membrane between the electrodes of opposite polarity, permeable to ionic flow but preventing electric contact between electrodes [6-8].

The SPE performance is determined by parameters like thickness, permeability, porosity/pore size, wettability, electrolyte absorption and retention, chemical, dimensional and thermal stability [6, 9]. In a SPE the lithium salt is incorporated into the membrane through an electrolyte solution or directly in the form of composite [10-11]. The polymer matrix most often used in SPE are poly(ethylene oxide) (PEO) [12-

15], poly(acrylonitrile) (PAN) [16-17] and poly(vinylidene fluoride) (PVDF) and its copolymers [18-21].

PVDF and poly(vinylidene fluoride-*co*-trifluoroethylene) (P(VDF-TrFE)) copolymers have attracted scientific and technological interest as SPE due to their good mechanical properties, wettability by organic solvents, chemical inertness, good contact between electrode and electrolyte and stability in cathodic environment [21-22].

P(VDF-TrFE) has a ferroelectric to paraelectric (FE-PE) phase transition at a Curie temperature (T_c) that occurs below the melting temperature (T_m), and crystallizes from the melt or by solution casting in a polar ferroelectric chain conformation [23]. SPE based on P(VDF-TrFE) for lithium ion batteries have been studied from different approaches: porous membranes were prepared by solvent casting with varying porosity and the lithium ions were introduced by uptake or the polymer composites were prepared with lithium salts introduced within the polymer matrix [21, 24-25]. The results were better for porous membranes and lithium ion uptake, the ionic conductivity depending on membrane porosity and pore size, which are related to the ability for uptake.

The incorporation of suitable fillers into host polymers, such as carbon nanotubes, zeolites, inert oxide ceramics, rare-earth ceramics and others, has proved to be a viable solution for improving mechanical properties, thermal and chemical stability and ionic conductivity of polymer membranes for SPE [26-27]. Among these fillers, ceramics and clays are the ones with the largest application potential [26]. Studies of PVDF reinforced with nanoclays show that the presence of nanoparticles improves the mechanical strength of the materials [28-29]. Clays are, compositionally, similar to zeolites since both are aluminosilicates. However, the rigid 3-dimensional and crystalline structure characteristic of the zeolites, forming channels and cavities with regular dimensions [30], are replaced by a layered crystalline structure in the clays. These thin layers are formed by tetrahedral and octahedral sheets of silicon and alumina, surrounded by oxygen atoms [31]. The combination of these sheets can create a 1:1 or 2:1 layered structure. In particular, montmorillonite (MMT) clay presents a 2:1 layered structure, each layer consisting on two-dimensional silicon sheets bonded to a central alumina sheet by shared oxygen ions. The stacking of these layers gives origin to van der Waals gaps where cations (typically Na^+ and/or Ca^{2+}) are located which are responsible for the balancing of deficiency charge created by the isomorphous substitution within the layers of tetrahedral Si^{4+} by Al^{3+} or octahedral Al^{3+} by Mg^{2+} [31-

32]. The presence of ions leads to water absorption by clays, resulting in the interlayer expansion of MMT resulting therefore in shrinking and swelling as water is absorbed and removed between the layers [33]. On the other hand, in 1:1 layered structures a tetrahedral sheet is fused with an octahedral sheet, whereby the oxygen atoms are shared [34]. Contrary to 2:1 structure, this structure is not able to absorb water. This 1:1 clay structure usually presents a lower amount of cations when compared with the 2:1 layered structure, facts that make the 2:1 layered structure of MMT clays the choice for membrane production.

Some works have already been presented exploring clays/polymer composites for battery applications. Electrical and electrochemical properties of nanocomposite polymer electrolytes based on intercalation of PVDF into organically modified MMT clays were investigated; the results show that the addition of clay enhances the electrolyte uptake due to the affinity between clays and electrolyte molecules. The ionic conductivity increases with increasing clay content to a maximum value of 2.3×10^{-3} S/cm at room temperature for a 4 wt% of clay content. The presence of fillers also provides a better electrochemical stability [35].

Composites of organoclay ALA-MMT (12-aminododecanoic acid - ALA), PAN and LiClO_4 were tested as electrolytes for lithium batteries; the presence of clays improving the electrolyte performance. The ionic conductivity reached the maximum value around 2.44×10^{-4} S/cm at 30 °C for the composites with 7 wt% fillers content. Electrochemical stability and cyclability is confirmed between 0 and 4 V [36].

Montmorillonite/polyvinyl alcohol (MMT/PVA) composites polymer membranes showed ionic conductivity of 3.68×10^{-2} S/cm for composites with 10 wt% of MMT. The stability window was about 2 V [37].

Gel polymer electrolytes based on montmorillonite/poly(vinylidene fluoride-co-hexafluoropropene) (MMT/PVDF-HFP) composites showed ionic conductivity in the range of $1\text{-}2.5 \times 10^{-1}$ mS/cm [38]. Additionally, polymer composite electrolyte based on PVDF, polyethylene glycol (PEG) and functionalized clays showed maximum conductivity of 7.77 mS/cm for 6 wt% of clays. The membrane porosity decreases with increasing filler content from 0 to 10 wt% [39].

Previous reported results as well as the properties of polymeric separators materials based on P(VDF-TrFE) for lithium batteries applications with zeolites [40], support the main objective of this work, which consists in the preparation of

clay/P(VDF-TrFE) porous membranes with different MMT clay contents in order to improve both the electrical and mechanical properties of SPE. The influence of MMT content in the performance of the battery separator membranes, with and without electrolyte solution (1 M LiClO₄·3H₂O-PC), was evaluated through the morphological, thermal, mechanical and electrical properties.

4.2. Results and discussion

4.2.1. Microstructural characteristics and polymer phase

It has been shown [21] that pristine PVDF-TrFE membranes produced under suitable solvent evaporation conditions lead to porosity and pore configuration suitable for lithium ion battery applications. Those conditions were applied for the production of the composite samples.

Figure 4.1 shows surface and cross-section images of the MMT/P(VDF-TrFE) membranes with different clay contents and histograms of the pore diameter distribution determined from the same scanning electron microscopy (SEM) images.

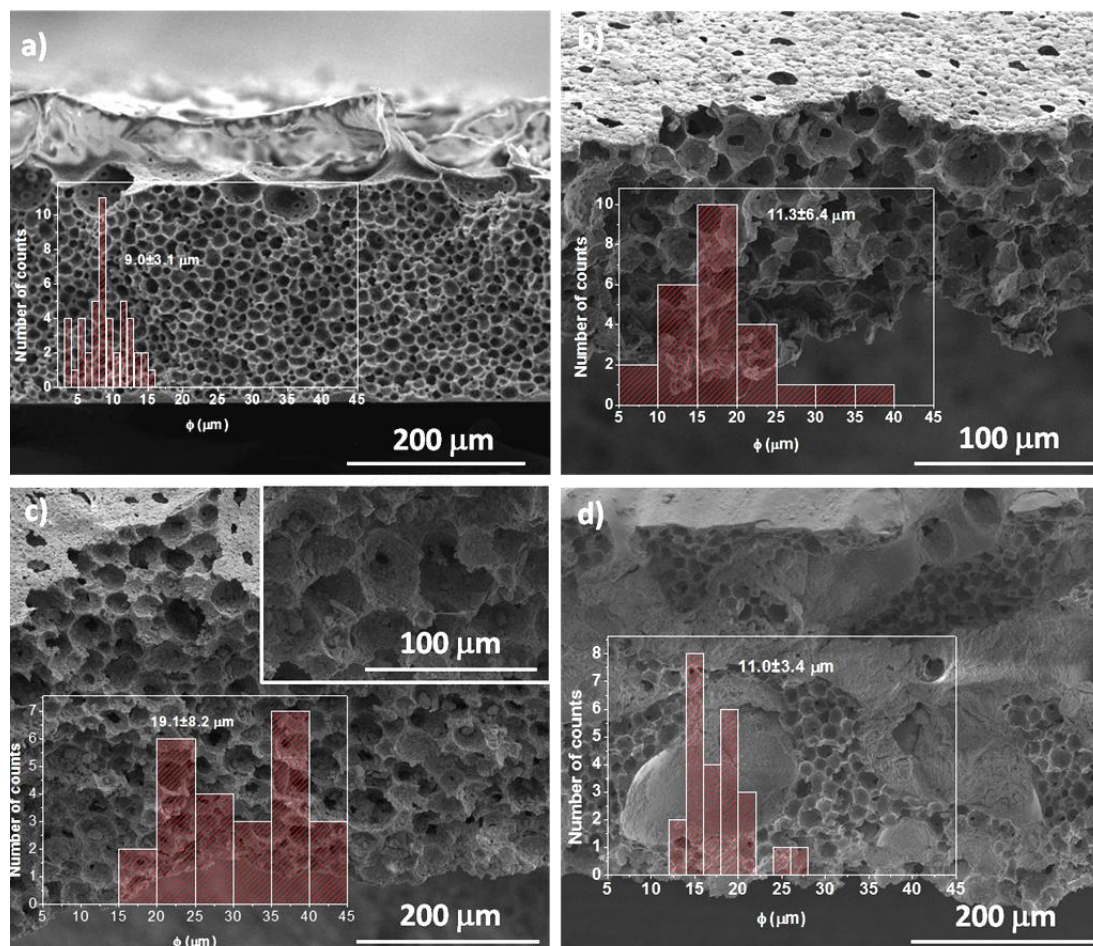


Figure 4.1: Cross section SEM images of the MMT/P(VDF-TrFE) composites with different clay content: a) 0 wt%, b) 4 wt%, c) 16 wt% and d) 32 wt%.

A uniform distribution of pores can be observed independently of clay content for the samples with 4 and 16 wt%. These samples show a structure similar to the one obtained for the pure copolymer when crystallized under the same conditions [41]. In this way, the crystallization mechanism is not affected by the presence of the fillers. The formation of the porous structure is therefore explained by a liquid/liquid spinodal decomposition followed by polymer crystallization depending mainly on the evaporation rate of the solvent and the crystallization temperature [41-42]. The sample with 32 wt% MMT content shows a very distinct microstructure, different from the lower clay concentrations and pristine polymer: the clay particles aggregate in certain areas of the polymer hindering partially the formation of the porous microstructure necessary for the intended application as battery separator membrane [40].

As the formation of the porous structure is strongly affected by the liquid/liquid spinodal decomposition and solvent evaporation rate [41-42], these factors are affected by the presence of the clays, resulting in a tendency to increase the average pore size with increasing MMT content.

Figure 4.2 shows the Fourier transformed infrared spectroscopy (FTIR) spectra for the membranes without electrolyte solution uptake.

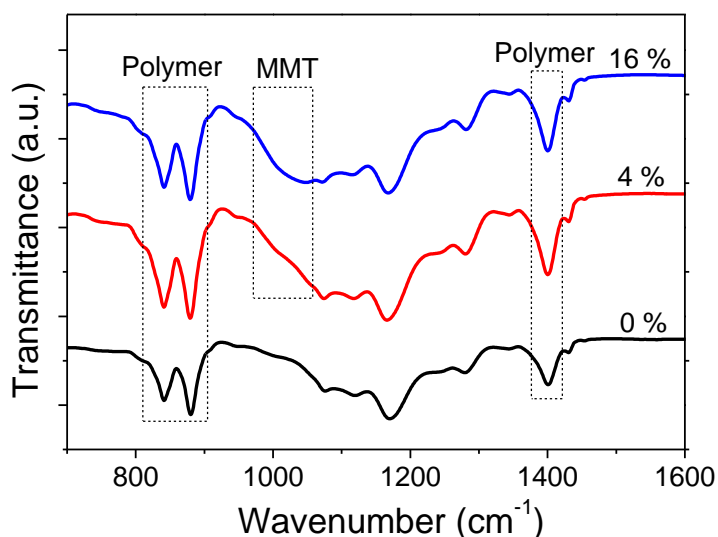


Figure 4.2: FTIR spectra of the MMT/P(VDF-TrFE) composites with different MMT contents without electrolyte solution uptake.

The FTIR spectra (figure 4.2) shows the characteristic vibration modes (851 cm^{-1} , 886 cm^{-1} and 1402 cm^{-1}) of the polymer all-trans configuration [43] for all clay contents. The polymer characteristic bands are unaffected by the presence of MMT particles. These bands area also unaffected by the presence of the electrolyte solution [40].

For the membranes with 4 and 16 wt% MMT content it is notorious the presence of the characteristic band of MMT around 1084 cm^{-1} corresponding to the stretching vibration modes of Si-O-Si [44].

4.2.2. Porosity, electrolyte uptake and tortuosity

Figure 4.3 shows the electrolyte solution uptake as function of clay content for the samples up to MMT content of 16 wt%, as the samples with higher clay content does not show the necessary porous microstructure (figure 4.1).

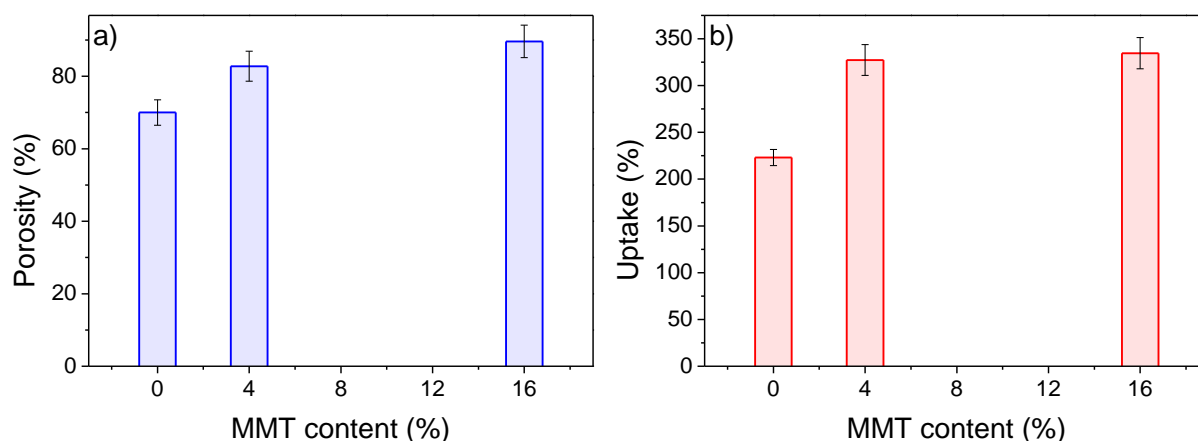


Figure 4.3: a) Porosity as a function of clay content for MMT/P(VDF-TrFE) composites; b) 1 M $\text{LiClO}_4 \cdot 3\text{H}_2\text{O}$ -PC solution uptake as a function of clay content for the MMT/P(VDF-TrFE) composites.

Figure 4.3 shows an increase of the membrane porosity and electrolyte uptake with the presence of MMT. Clay inclusion in the polymeric matrix results in an increase of the porosity, which in turn leads to increased uptake capacity. The increase of uptake (figure 4.3b) is a result of the excellent affinity of MMT particles towards polar PC molecules, the solvent in the electrolyte solution.

Table 4.1 shows the room temperature ionic conductivity and the tortuosity calculated by equation 2.5 and 2.6 respectively.

Table 4.1: Room temperature ionic conductivity and tortuosity of 1M $\text{LiClO}_4 \cdot 3\text{H}_2\text{O}$ + separator membrane; $\sigma_0 = 9.8 \text{ mS/cm}$ at 25 °C.

Sample	$\sigma_i \text{ (S/cm)}$	τ
0 %	5.24×10^{-7}	115
4 %	5.98×10^{-7}	117
16 %	8.11×10^{-7}	104

It is shown that ionic conductivity of the membranes increases slightly with increasing clay content. The inclusion of fillers increases the number of ions within the samples, which leads to a higher conductivity values.

The tortuosity, known as the ratio of the mean capillary length to membrane thickness, describes the average pore connectivity and gives information about the pore blockage. An ideal porous body present a tortuosity of 1, in this case the values indicate a hindered system [6]. However, it is observed a slight decrease of the tortuosity with increasing filler content. The presence of clays increases the connectivity between the pores leading to decrease of pore blockage.

4.2.3. Thermal and mechanical properties

Figure 4.4 shows the differential scanning calorimetry (DSC) thermograms for the MMT/P(VDF-TrFE) membranes.

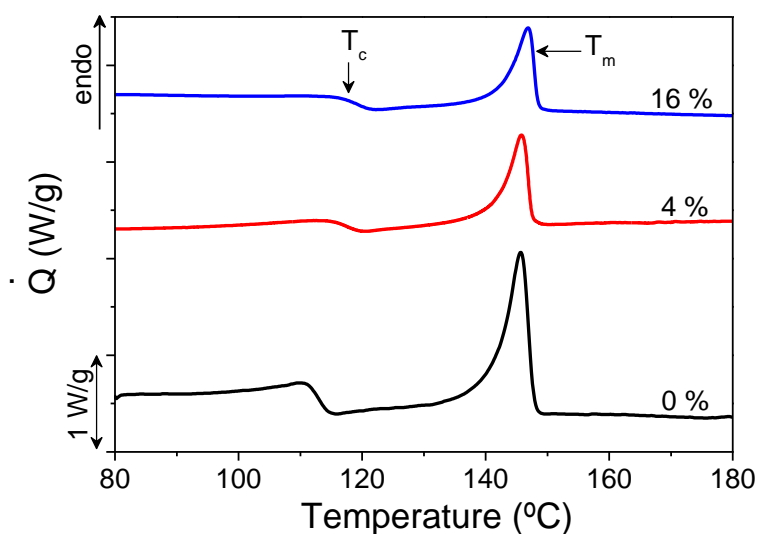


Figure 4.4: DSC thermograms of the MMT/P(VDF-TrFE) composites for the different clay contents without electrolyte solution uptake.

The DSC thermograms show two endothermic peaks corresponding to the ferroelectric-paraelectric phase transition (lower temperature peak, T_c) around 117 °C and the melting temperature of the polymer (higher temperature peak, T_m) around 146 °C [45]. The thermogram shows that the clays content does not affect significantly the polymer ferroelectric phase, its degree of crystallinity and thermal stability. These parameters are also not affected by the presence of the electrolyte solution as shown in [40] for different fillers.

The table 4.2 shows the degree of crystallinity for the MMT/P(VDF-TrFE) membranes as a function of filler content.

Table 4.2: Degree of crystallinity calculated applying equation 2.1 to the melting peak of the samples.

Sample	$\chi_c \pm 2$ (%)
0 %	28
4 %	27
16 %	23

The results show a small decrease in the degree of crystallinity with increasing filler content due to defective crystallization of the polymer structure in the places around the clays particles, due to changes in the nucleation and growth kinetics of the polymer [46].

The performance, integrity and safety of a battery are extremely dependent on the mechanical properties of the membrane separator [47-48], which in turn depend on porosity, pore size and distribution [49]. Mechanical characteristics are among the main drawbacks of polymer porous membranes that can be solved with suitable reinforcing fillers.

Figure 4.5 show the stress-strain curves of the MMT/P(VDF-TrFE) membranes with different filler contents without (figure 4.5a) and with electrolyte solution (figure 4.5b).

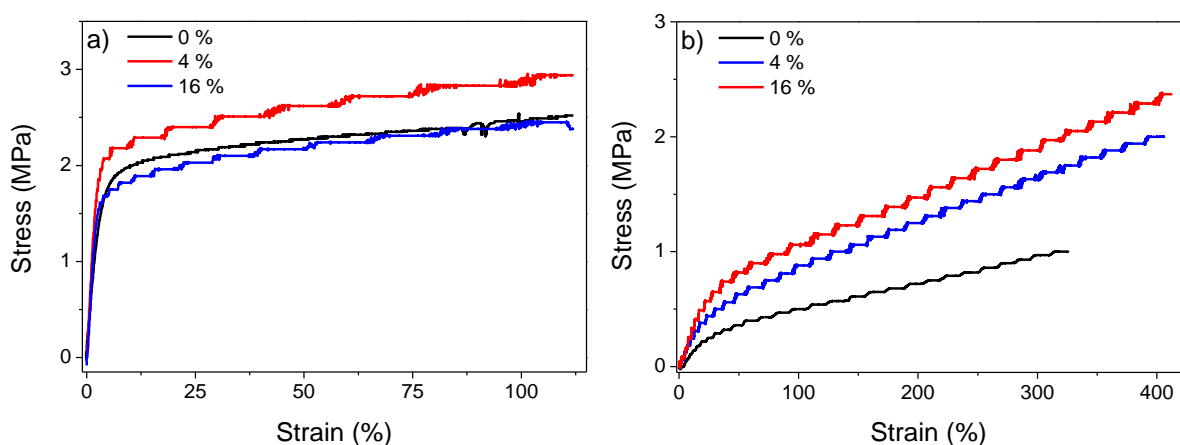


Figure 4.5: Stress-Strain curves of the MMT/P(VDF-TrFE) composites with different clay contents: a) without electrolyte solution uptake and b) with electrolyte solution uptake.

Table 4.3 shows the mechanical properties of the composites with and without electrolyte solution uptake.

Table 4.3: Mechanical properties of the MMT/P(VDF-TrFE) membranes with and without electrolyte solution uptake.

Sample	Without uptake			With uptake		
	0 %	4 %	16 %	0 %	4 %	16 %
Yielding stress (MPa)	2.1	2.6	2.0	0.3	0.6	0.7
Elastic modulus (MPa)	40	81.4	71.7	1.9	2.0	2.7

Figure 4.5a and table 4.3 shows that addition of MMT up to 4 wt% improves the yielding stress and elastic modulus of the membranes previous to uptake, but for 16 wt% these mechanical parameters decrease. The reason for 4 wt% be attributed to the reinforcement effect of the MMT particles caused by its intercalation through the polymer matrix, and for 16 wt%, the layers occupy the full volume suggesting that percolation is achieved [50]. As regard to membranes with electrolyte solution uptake (figure 4.5b), the samples with clays also show better mechanical properties than the pristine polymer. However, a decrease in yielding stress and elastic modulus can be observed in comparison with the membranes without electrolyte solution, attributed to the high electrolyte solution uptake and swelling for all samples.

4.2.4. Electrical properties

The electrochemical properties of the samples, with electrolyte solution uptake, were evaluated by electrochemical impedance spectroscopy (EIS), through the Nyquist plots (imaginary impedance Z'' as function of real impedance Z'), Bode plots (impedance modulus $|Z|$ as function of frequency and phase angle) and ionic conductivity as function of temperature. Figure 4.6 presents the Nyquist plots for all samples with electrolyte uptake at 50 °C (figure 4.6a), the Bode plots (figure 4.6b and 4.6c) and the impedance modulus as function of clays content at 1 kHz and different temperatures (figure 4.6d).

The Nyquist plot is characterized by three distinct zones: a semicircle located at the high frequency range which corresponds to the charge transfer process, a straight

line for lower frequency range which is related to the diffusion process and the transition between these phenomena [51-52].

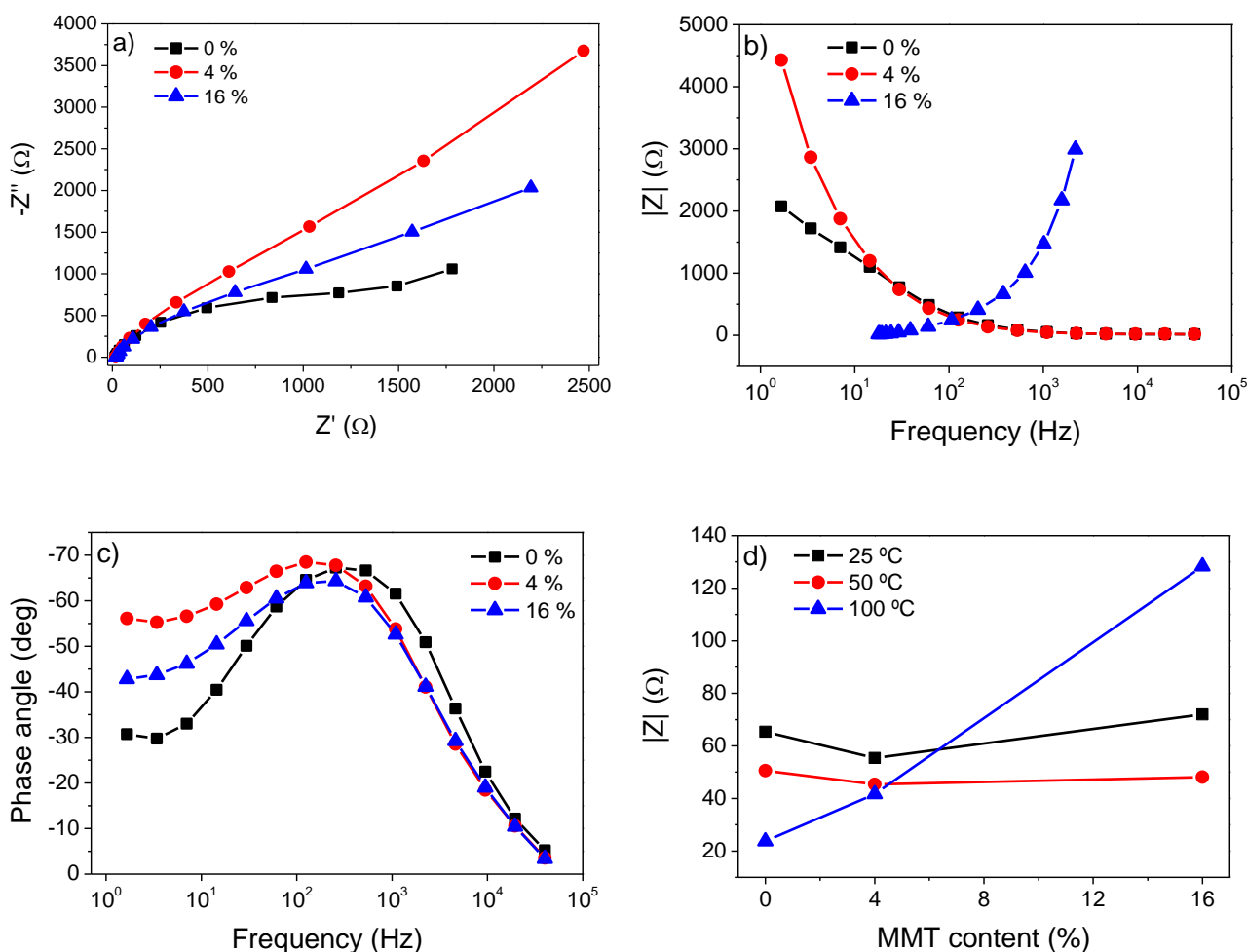


Figure 4.6: a) Nyquist plot of the MMT/P(VDF-TrFE) composites for all filler contents at 50 °C, b-c) Bode diagram of the MMT/P(VDF-TrFE) composites for all contents at 50 °C and d) impedance modulus as a function of clay content at different temperatures.

Figure 4.6a presents the semicircle at higher frequencies for the membrane without fillers, whereas for the samples with fillers it is just slightly noted, showing that the inclusion of clays particles improves the charge transfer process, which suggests the enhancement in number of free ions and their mobility in the increased spacing of intercalated clay galleries.

In figure 4.6b is shown that impedance decrease with increasing frequency for the pure polymer and for sample with 4 wt% of clays particles, due to the contribution of the electrode polarization and Maxwell-Wagner-Sillars (MWS) interfacial polarization. This behaviour is typical for the polymer separator indicating restricted ion mobility within the porous membrane. For the membrane with 16 wt% of fillers the impedance

increases with increasing frequency and is observed two saturation region in the low and high frequency assisted by ion-migration and dipolar relaxation respectively. This amount of fillers is near to the percolation limit and enters a regime dominated by clays and in the case of MWS phenomena, the free charges build up at the interfacing boundaries of the clay fillers.

The Bode diagram of the phase angle as function of frequency (figure 4.6c) shows a maximum phase angle between -60 and -70 °C for all membranes. In an ideal resistor and capacitor in series, the maximum phase angle should be at -90 °C. In this case the behaviour is near a constant phase element (CPE) [53], which can be modelled as a capacitor with a distribution of a relaxation times [54-55].

Figure 4.6d illustrates the impedance modulus as function of clays content for a given frequency of 1 kHz and for different temperatures. The impedance does not show a strong dependence with the clay content for lower temperatures, increasing strongly with clay content at 100 °C. Further, it is observed a decrease in the impedance with increasing temperature, except for the 16 wt% MMT sample which the opposite behaviour is observed for the highest temperature. This behaviour suggests that clay interaction with P(VDF-TrFE) matrix reduce relaxation time of the ionic species thereby assisting ion-transport in the lower temperatures and lower concentration ranges. At high concentrations and temperatures ionic mobility is hindered due to strong interface charge accumulation leading to increased impedance modulus.

Figure 4.7 shows the behaviour of the ionic conductivity with temperature for the polymer composite membranes with and without electrolyte solution uptake.

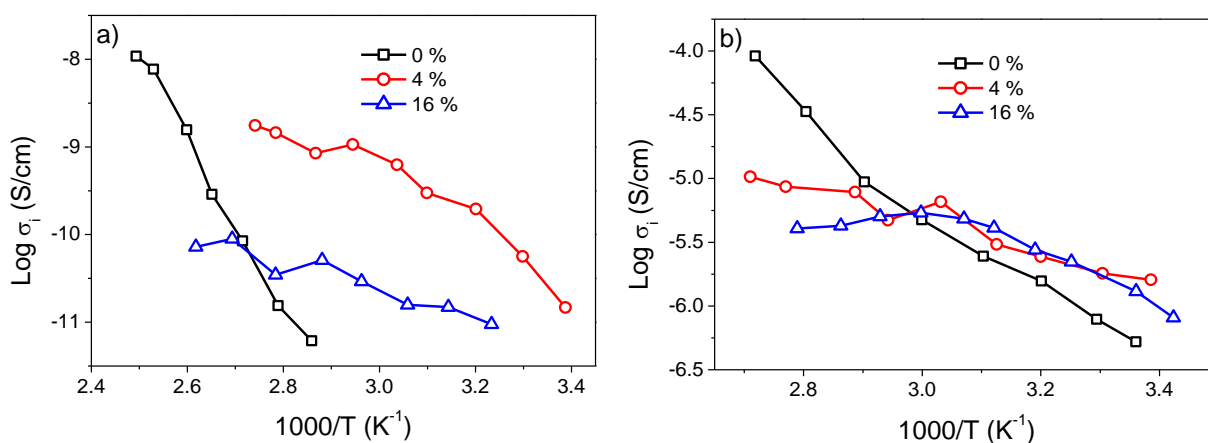


Figure 4.7: $\text{Log } \sigma_1$ as a function of $1000/T$ for MMT/P(VDF-TrFE) composites: a) without electrolyte solution uptake and b) with electrolyte solution uptake.

The ionic conductivity increases slightly with increasing filler content (figure 4.7a). On the one hand the MMT particles increase the free anion content resulting in a larger number of charge carriers [36], on the other hand, it decreases slightly the degree of crystallinity and tortuosity, which in turn leads to an increase of the ionic conductivity [56].

Without electrolyte solution uptake (figure 4.7a) the ionic conductivity is higher for the membrane with lower filler content, due to a higher ionic mobility for the sample with 4 wt% of MMT. In the membrane with 16 wt% of MMT the conductivity decreases due to interface effects caused by the increase in filler inducing defects in the membrane structure.

In the membranes with electrolyte uptake (figure 4.7b) the ionic conductivity increases by about 4 orders of magnitude. Moreover, the thermal stability of the electrical conductivity increases significantly for the membranes with MMT content. The pure polymer presents a conductivity higher than that of the composites but very unstable with temperature. The obtained results of the overall conductivity of the composites are lower than others achieved by clay composites (e.g. [35]) as the present approach does not use organically modified clays, leading to a lower level of exfoliation.

Table 4.4 shows the activation energy (E_a) for ion transport, calculated by the application of Arrhenius equation (equation 2.7) to the data of figure 4.7

Table 4.4: Activation energy for the different porous membranes with and without electrolyte solution uptake.

Samples	E_a without electrolyte solution (kJ/mol)	E_a with electrolyte solution (kJ/mol)
0 %	181	64
4 %	25	10
16 %	16	15

The E_a shows a strong dependence with MMT filler content and with electrolyte solution uptake. The E_a decreases with increasing MMT content and with the presence of electrolyte solution. The electrolyte solution strongly improves the mobility and ionic charge carriers in the porous membranes [57].

The electrochemical stability and the diffusion coefficient of the composites were evaluated by cyclic voltammetry over the potential range -2.0 to 6.0 V (figure 4.8).

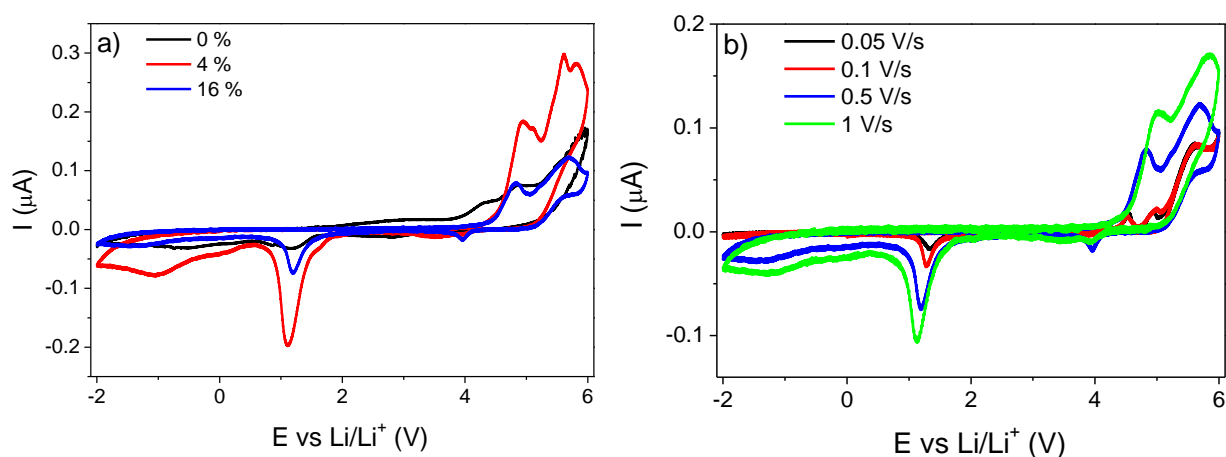


Figure 4.8: a) Voltammogram of MMT/P(VDF-TrFE) composites at 0.5 V/s; b) voltammogram of MMT/P(VDF-TrFE) with 16 wt% of clays at different scanning rates.

The voltammogram of figure 4.8a shows that the anodic and cathodic peaks increase with the addition of clays. Both peaks are more intense for the membrane with 4 wt% filler content. All membranes present a stable operation window between 0.5 and 4.0 V, *versus* Li/Li⁺. It is noted that a reduction peak around 1.0 - 1.5 V appeared for the electrolytes films. Previously, the peak in this region had been ascribed to the reduction of low level of water present or oxygen impurities. Similar behaviour has been observed for other systems based on PEO and lithium salt [58].

Figure 4.8b shows that the increase of the scanning rate affects the electrochemical stability of the membrane. From these data, the diffusion coefficients of all membranes, calculated by equation 2.8, are in the order of $3.50 \times 10^{-5} \text{ cm}^2/\text{s}$ for pure polymer and 16 wt% composite and $5.16 \times 10^{-5} \text{ cm}^2/\text{s}$ for the 4 wt% MMT composite. Therefore, the diffusion coefficient does not depend on filler content.

4.3. Conclusion

MMT/P(VDF-TrFE) porous membranes with different contents of MMT were prepared by thermally induced phase separation (TIPS) for lithium ion battery applications. The electrolyte solution was 1 M LiClO₄·3H₂O-PC. The clay inclusion increases the average pore size, the porosity and electrolyte solution uptake of the

membranes. No variation of the polymer phase is observed due to the inclusion of MMT in the composite. The degree of crystallinity and the tortuosity slightly decrease with increasing filler content, suggesting the later a decrease in the pore blockage. The membranes are thermally stable up to ~100 °C and the inclusion of the fillers enhances its mechanical properties. The ionic conductivity is slightly improved and its temperature stability strongly improved by the presence of clays. The electrochemical stability evaluated by cyclic voltammetry reveals a stable window operation up to 5.0 V, *versus* Li/Li⁺. The overall performance is optimised for the membrane with 4 % filler content.

These results show that MMT/P(VDF-TrFE) porous membranes with 4 % filler content have adequate electrochemical stability, thermal, mechanical and electrical properties for being used as battery separators in lithium ion batteries.

4.4. References

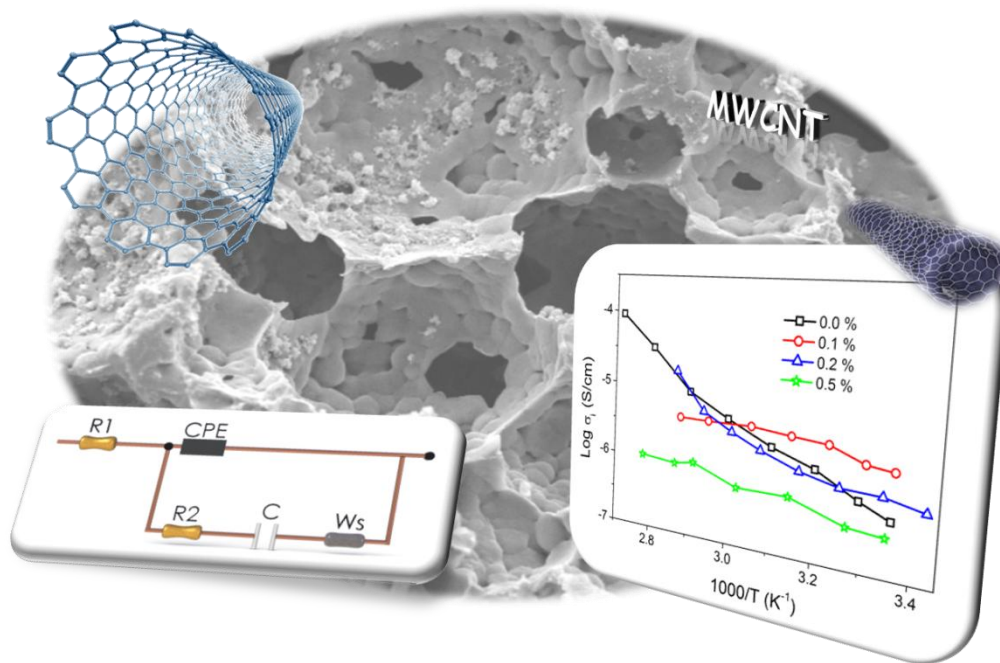
1. Brodd, R.J., K.R. Bullock, R.A. Leising, R.L. Midaugh, J.R. Miller, and E. Takeuchi. *Batteries, 1977 to 2002*. Journal of The Electrochemical Society, 2004. **151**(3): p. K1-K11.
2. Whittingham, M.S. *Lithium Batteries and Cathode Materials*. Chemical Reviews, 2004. **104**(10): p. 4271-4302.
3. Tarascon, J.-M. *Key challenges in future Li-battery research*. Philosophical Transactions of the Royal Society A: Mathematical, Physical and Engineering Sciences, 2010. **368**(1923): p. 3227-3241.
4. Tarascon, J.M. and M. Armand. *Issues and challenges facing rechargeable lithium batteries*. Nature, 2001. **414**(6861): p. 359-367.
5. Vincent, C.A. *Lithium batteries: a 50-year perspective, 1959–2009*. Solid State Ionics, 2000. **134**(1–2): p. 159-167.
6. Arora, P. and Z. Zhang. *Battery Separators*. Chemical Reviews, 2004. **35**(50): p. 4419-4462.
7. Linden, D. and T.B. Reddy. *Linden's handbook of batteries*. 2001, New York: McGraw-Hill.
8. Daniel, C. and J.O. Besenhard. *Handbook of battery materials*. 2011, Weinheim: Wiley-VCH Verlag.
9. Xu, K. *Nonaqueous Liquid Electrolytes for Lithium-Based Rechargeable Batteries*. Chemical Reviews, 2004. **104**(10): p. 4303-4418.
10. Manuel Stephan, A. *Review on gel polymer electrolytes for lithium batteries*. European Polymer Journal, 2006. **42**(1): p. 21-42.
11. Barbosa, P.C., M.M. Silva, M.J. Smith, A. Gonçalves, and E. Fortunato. *Studies of solid-state electrochromic devices based on PEO/siliceous hybrids doped with lithium perchlorate*. Electrochimica Acta, 2007. **52**(8): p. 2938-2943.
12. Persi, L., F. Croce, B. Scrosati, E. Plichta, and M.A. Hendrickson. *Poly(ethylene oxide)-Based, Nanocomposite Electrolytes as Improved Separators for Rechargeable Lithium Polymer Batteries*. Journal of The Electrochemical Society, 2002. **149**(2): p. A212-A216.
13. Kim, D.-W., J.-M. Ko, J.-H. Chun, S.-H. Kim, and J.-K. Park. *Electrochemical performances of lithium-ion cells prepared with polyethylene oxide-coated separators*. Electrochemistry Communications, 2001. **3**(10): p. 535-538.

14. Wang, C., Y. Wei, G.R. Ferment, W. Li, and T. Li. *Poly(ethylene oxide)–silica hybrid materials for lithium battery application*. Materials Letters, 1999. **39**(4): p. 206-210.
15. Li, H., X.-T. Ma, J.-L. Shi, Z.-K. Yao, B.-K. Zhu, and L.-P. Zhu. *Preparation and properties of poly(ethylene oxide) gel filled polypropylene separators and their corresponding gel polymer electrolytes for Li-ion batteries*. Electrochimica Acta, 2011. **56**(6): p. 2641-2647.
16. Cho, T.H., T. Sakai, S. Tanase, K. Kimura, Y. Kondo, T. Tarao, and M. Tanaka. *Electrochemical performances of polyacrylonitrile nanofiber-based nonwoven separator for lithium-ion battery*. Electrochemical and Solid State Letters, 2007. **10**(7): p. A159-A162.
17. Huai, Y., J. Gao, Z. Deng, and J. Suo. *Preparation and characterization of a special structural poly(acrylonitrile)-based microporous membrane for lithium-ion batteries*. Ionics, 2010. **16**(7): p. 603-611.
18. Cheng, C.L., C.C. Wan, and Y.Y. Wang. *Preparation of porous, chemically cross-linked, PVdF-based gel polymer electrolytes for rechargeable lithium batteries*. Journal of Power Sources, 2004. **134**(2): p. 202-210.
19. Stephan, A.M., K.S. Nahm, M. Anbu Kulandainathan, G. Ravi, and J. Wilson. *Poly(vinylidene fluoride-hexafluoropropylene) (PVdF-HFP) based composite electrolytes for lithium batteries*. European Polymer Journal, 2006. **42**(8): p. 1728-1734.
20. Wachtler, M., D. Ostrovskii, P. Jacobsson, and B. Scrosati. *A study on PVdF-based SiO₂-containing composite gel-type polymer electrolytes for lithium batteries*. Electrochimica Acta, 2004. **50**(2–3): p. 357-361.
21. Costa, C.M., L.C. Rodrigues, V. Sencadas, M.M. Silva, J.G. Rocha, and S. Lanceros-Méndez. *Effect of degree of porosity on the properties of poly(vinylidene fluoride–trifluoroethylene) for Li-ion battery separators*. Journal of Membrane Science, 2012. **407–408**(0): p. 193-201.
22. Djian, D., F. Alloin, S. Martinet, and H. Lignier. *Macroporous poly(vinylidene fluoride) membrane as a separator for lithium-ion batteries with high charge rate capacity*. Journal of Power Sources, 2009. **187**(2): p. 575-580.
23. Nalwa, H.S. *Ferroelectric polymers : chemistry, physics, and applications*. 1995, New York: Dekker.
24. Costa, C.M., A. California, V.F. Cardoso, V. Sencadas, L.C. Rodrigues, M.M. Silva, and S. Lanceros-Méndez. *Electroactive Poly(Vinylidene Fluoride-Trifluoroethylene) (PVDF-TrFE) Microporous Membranes for Lithium-Ion Battery Applications*. Ferroelectrics, 2012. **430**(1): p. 103-107.
25. Costa, C.M., L.C. Rodrigues, V. Sencadas, M.M. Silva, and S. Lanceros-Méndez. *Effect of the microstructure and lithium-ion content in*

- poly[(vinylidene fluoride)-co-trifluoroethylene]/lithium perchlorate trihydrate composite membranes for battery applications. Solid State Ionics, 2012. 217(0): p. 19-26.*
26. Jung, S., D. Kim, S. Lee, M. Cheong, D. Nguyen, B. Cho, and H. Kim. *{Fillers for Solid-State Polymer Electrolytes : Highlight}*. Polymer, 2009. **30**(10): p. 2355-2361.
27. Weston, J.E. and B.C.H. Steele. *Effects of inert fillers on the mechanical and electrochemical properties of lithium salt-poly(ethylene oxide) polymer electrolytes. Solid State Ionics, 1982. 7(1): p. 75-79.*
28. Hwang, H.-Y., D.-J. Kim, H.-J. Kim, Y.-T. Hong, and S.-Y. Nam. *Effect of nanoclay on properties of porous PVdF membranes. Transactions of Nonferrous Metals Society of China, 2011. 21, Supplement 1(0): p. s141-s147.*
29. Koh, M.J., H.Y. Hwang, D.J. Kim, H.J. Kim, Y.T. Hong, and S.Y. Nam. *Preparation and Characterization of Porous PVdF-HFP/clay Nanocomposite Membranes. Journal of Materials Science & Technology, 2010. 26(7): p. 633-638.*
30. Corma, A. *Inorganic Solid Acids and Their Use in Acid-Catalyzed Hydrocarbon Reactions. Chemical Reviews, 1995. 95(3): p. 559-614.*
31. Pavlidou, S. and C.D. Papaspyrides. *A review on polymer-layered silicate nanocomposites. Progress in Polymer Science, 2008. 33(12): p. 1119-1198.*
32. Xie, W., Z.M. Gao, K.L. Liu, W.P. Pan, R. Vaia, D. Hunter, and A. Singh. *Thermal characterization of organically modified montmorillonite. Thermochemica Acta, 2001. 367: p. 339-350.*
33. Norrish, K. *The swelling of montmorillonite. Discussions of the Faraday Society, 1954. 18(0): p. 120-134.*
34. Ma, C. and R.A. Eggleton. *Cation exchange capacity of kaolinite. Clays and Clay Minerals, 1999. 47(2): p. 174-180.*
35. Deka, M. and A. Kumar. *Electrical and electrochemical studies of poly(vinylidene fluoride)-clay nanocomposite gel polymer electrolytes for Li-ion batteries. Journal of Power Sources, 2011. 196(3): p. 1358-1364.*
36. Chen, H.-W., T.-P. Lin, and F.-C. Chang. *Ionic conductivity enhancement of the plasticized PMMA/LiClO₄ polymer nanocomposite electrolyte containing clay. Polymer, 2002. 43(19): p. 5281-5288.*
37. Yang, C.-C., Y.-J. Lee, and J.M. Yang. *Direct methanol fuel cell (DMFC) based on PVA/MMT composite polymer membranes. Journal of Power Sources, 2009. 188(1): p. 30-37.*

38. Wang, M. and S. Dong. *Enhanced electrochemical properties of nanocomposite polymer electrolyte based on copolymer with exfoliated clays*. Journal of Power Sources, 2007. **170**(2): p. 425-432.
39. Wang, Y.-P., X.-H. Gao, R.-M. Wang, H.-G. Liu, C. Yang, and Y.-B. Xiong. *Effect of functionalized montmorillonite addition on the thermal properties and ionic conductivity of PVDF-PEG polymer electrolyte*. Reactive and Functional Polymers, 2008. **68**(7): p. 1170-1177.
40. Nunes-Pereira, J., A.C. Lopes, C.M. Costa, L.C. Rodrigues, M.M. Silva, and S. Lanceros-Méndez. *Microporous membranes of NaY zeolite/poly(vinylidene fluoride-trifluoroethylene) for Li-ion battery separators*. Journal of Electroanalytical Chemistry, 2013. **689**(0): p. 223-232.
41. California, A., V.F. Cardoso, C.M. Costa, V. Sencadas, G. Botelho, J.L. Gómez-Ribelles, and S. Lanceros-Mendez. *Tailoring porous structure of ferroelectric poly(vinylidene fluoride-trifluoroethylene) by controlling solvent/polymer ratio and solvent evaporation rate*. European Polymer Journal, 2011. **47**(12): p. 2442-2450.
42. Ferreira, A., J. Silva, V. Sencadas, J.L.G. Ribelles, and S. Lanceros-Méndez. *Poly[(vinylidene fluoride)-co-trifluoroethylene] Membranes Obtained by Isothermal Crystallization from Solution*. Macromolecular Materials and Engineering, 2010. **295**(6): p. 523-528.
43. Prabu, A.A., J.S. Lee, K.J. Kim, and H.S. Lee. *Infrared spectroscopic studies on crystallization and Curie transition behavior of ultrathin films of P(VDF/TrFE) (72/28)*. Vibrational Spectroscopy, 2006. **41**(1): p. 1-13.
44. Lopez-Estopier, R., M. Aceves-Mijares, and C. Falcony. *Photoluminescence of Silicon Rich Oxide films with different silicon excess and nitrogen content*. Electrical and Electronics Engineering, 2006 3rd International Conference on, 2006: p. 1-4.
45. Sencadas, V., S. Lanceros-Méndez, and J.F. Mano. *Thermal characterization of a vinylidene fluoride-trifluoroethylene (75-25) (%mol) copolymer film*. Journal of Non-Crystalline Solids, 2006. **352**(50-51): p. 5376-5381.
46. Costa, C.M., S. Firmino Mendes, V. Sencadas, A. Ferreira, R. Gregorio Jr, J.L. Gómez Ribelles, and S. Lanceros-Méndez. *Influence of processing parameters on the polymer phase, microstructure and macroscopic properties of poly(vinylidene fluoride)/Pb(Zr_{0.53}Ti_{0.47})O₃ composites*. Journal of Non-Crystalline Solids, 2010. **356**(41-42): p. 2127-2133.
47. Sheidaei, A., X. Xiao, X. Huang, and J. Hitt. *Mechanical behavior of a battery separator in electrolyte solutions*. Journal of Power Sources, 2011. **196**(20): p. 8728-8734.

48. Tian, Z., X. He, W. Pu, C. Wan, and C. Jiang. *Preparation of poly(acrylonitrile–butyl acrylate) gel electrolyte for lithium-ion batteries*. *Electrochimica Acta*, 2006. **52**(2): p. 688-693.
49. Lu, G., G.Q. Lu, and Z.M. Xiao. *Mechanical Properties of Porous Materials*. *Journal of Porous Materials*, 1999. **6**(4): p. 359-368.
50. Madaleno, L., J. Schjødt-Thomsen, and J.C. Pinto. *Morphology, thermal and mechanical properties of PVC/MMT nanocomposites prepared by solution blending and solution blending + melt compounding*. *Composites Science and Technology*, 2010. **70**(5): p. 804-814.
51. Chang, B.-Y. and S.-M. Park. *Electrochemical Impedance Spectroscopy*. *Annual Review of Analytical Chemistry*, 2010. **3**(1): p. 207-229.
52. Park, M., X. Zhang, M. Chung, G.B. Less, and A.M. Sastry. *A review of conduction phenomena in Li-ion batteries*. *Journal of Power Sources*, 2010. **195**(24): p. 7904-7929.
53. Zelinka, S.L., L. Ortiz-Candelaria, D.S. Stone, and D.R. Rammer. *Electrochemical impedance spectroscopy (EIS) as a tool for measuring corrosion of polymer-coated fasteners used in treated wood*. *Forest products journal*, 2009. **59**(1-2): p. 77-82.
54. Cole, K. *Dispersion and Absorption in Dielectrics I. Alternating Current Characteristics*. *J. Chem. Phys.*, 1941. **9**(4): p. 341.
55. Raistrick, I.D. *Application of Impedance Spectroscopy to Materials Science*. *Annual Review of Materials Science*, 1986. **16**(1): p. 343-370.
56. Kim, S., E.-J. Hwang, Y. Jung, M. Han, and S.-J. Park. *Ionic conductivity of polymeric nanocomposite electrolytes based on poly(ethylene oxide) and organo-clay materials*. *Colloids and Surfaces A: Physicochemical and Engineering Aspects*, 2008. **313–314**(0): p. 216-219.
57. Every, H.A., F. Zhou, M. Forsyth, and D.R. MacFarlane. *Lithium ion mobility in poly(vinyl alcohol) based polymer electrolytes as determined by ⁷Li NMR spectroscopy*. *Electrochimica Acta*, 1998. **43**(10–11): p. 1465-1469.
58. Aurbach, D., M. Daroux, P. Faguy, and E. Yeager. *The electrochemistry of noble metal electrodes in aprotic organic solvents containing lithium salts*. *Journal of Electroanalytical Chemistry and Interfacial Electrochemistry*, 1991. **297**(1): p. 225-244.



5 - Porous membranes of CNT/P(VDF-TrFE)

This chapter is based on the following publication:

Nunes-Pereira, J., C.M. Costa, R. Leones, M.M. Silva, and S. Lanceros-Méndez. *Li-ion battery separator membranes based on poly(vinylidene fluoride-trifluoroethylene)/carbon nanotube composites*. *Solid State Ionics*, 2013. **249–250**: p. 63-71.

5.1. Introduction

Lithium-ion rechargeable battery technology has conquered the market for handheld devices such as laptop computers, cell phones, cameras and other wireless electronics and still presents an increasing market growth [1-3]. Lithium ion batteries provide high energy density (210 Wh/kg; 650 Wh/l), show flexible and lightweight design and longer lifespan when compared to other competing systems such as the ones based on lead-acid, nickel-cadmium (Ni-Cd) or nickel-metal hydride (Ni-MH) [4]. However, their performance is still not enough for the needs of the automobile industry market, their safety and efficiency should be improved for large scale productions, the systems degrade over time and lose efficiency and some components are still expensive [1, 3, 5]. Furthermore, using lithium as the negative metal in secondary cells can be a problem due to the reactivity with the electrolyte components. Two solutions have been proposed for this issue: the use of polymer electrolytes and the use of graphitic carbon electrodes [6].

The main constituents of a lithium ion battery are the anode – the source of lithium ions, the cathode – the sink of lithium ions and the electrolyte/separator – often in the form of a porous membrane (solid polymer electrolyte – SPE) that provides the separation between the electrodes and a path for ionic conduction [2-3, 7]. The role of the separator is extremely important in the operation of a battery by separating the two electrodes and thus avoiding short circuits. Moreover it allows the flow of ions during operation of the cell [2]. A SPE must meet certain requirements such as being an electronic insulator, ionic conductor, mechanically strong, dimensionally stable, readily wetted by the electrolyte and chemically resistant to electrolyte and impurity degradation, among others [2, 7]. Polymers can meet these demands and the matrices most often used as SPE are poly(ethylene oxide) (PEO) [8-11], poly(acrylonitrile) (PAN) [12-13] and poly(vinylidene fluoride) (PVDF) and its copolymers [14-17].

PVDF and poly(vinylidene fluoride-*co*-trifluoroethylene) (P(VDF-TrFE)) copolymers have been investigated as SPE due to their high polarity, controllable porosity, good mechanical properties, wettability by organic solvents, chemical inertness, good contact with the electrodes and electrolyte stability in cathodic environment [15, 18-20].

P(VDF-TrFE) is highly polar with a ferroelectric to paraelectric (FE-PE) transition which occurs at a Curie temperature (T_c) below the melting temperature (T_m)

and crystallizes in the polar phase, which strongly improves electrolyte uptake and ionic conduction of the polymer, when the polymer is prepared from the melt or by solution casting [21]. SPE based on P(VDF-TrFE) have been studied from different approaches: porous membranes prepared by solvent casting with Li ions introduced by uptake and composites prepared with Li salts introduced within polymer matrix [15, 22]. Results show that ionic conductivity is closely related to the porosity and pore size, which in turn is related to the electrolyte uptake ability.

The incorporation of suitable fillers in polymer matrixes, such as carbon nanotubes (CNT) [23], zeolites [20], ceramics and clays [19, 24-25], among others, has been shown to be an interesting approach to improve the mechanical, thermal and chemical stability and electrolyte uptake of SPE. The most relevant properties of CNT are their high surface area, high electrical conductivity and excellent thermal and mechanical properties [26-27]. CNT/polymer composite membranes have been suggested for different purposes such as filtration [28] sensing and monitoring systems [29], among others. In the particular case of batteries, CNT have been mainly used for electrode fabrication [30-34] and recently for battery separators. For separator membranes, the CNT content must be below the electrical percolation threshold, due to the need to obtain electronically insulator membranes with suitable ionic conductivity [35]. A recent study [11] reports the preparation of composite polymer electrolytes based on PEO, α CNT, LiPF_6 and EC with an ionic conductivity in the order of 10^{-3} S/cm for 5 wt% content of α CNT, which corresponds to an increase of 5 orders of magnitude with respect to the values of the pristine polymer.

The successful use of fillers reported in previous works [19-20], reinforce the relevance of this study to investigate the suitability of multiwall carbon nanotube, MWCNT, for the preparation of porous membranes based on MWCNT/P(VDF-TrFE) with improved electrolyte uptake, thermomechanical and electrical properties. Further, SPE filled with CNT can also improve compatibility of the separator membrane with the battery electrodes due to the carbonaceous nature of some of them [36-37].

5.2. Results and discussion

5.2.1. MWCNT type and concentration

The choice of MWCNT was based on the characteristics (table 5.1) and electrical performance evaluated in previous works [38]. The MWCNT content in the samples was below the percolation threshold (figure 5.1) in order to ensure that membranes are electrically insulating.

Table 5.1: Characteristics of the MWCNT.

	Diameter (nm)	Length (μm)	Purity (%)
Baytubes [®] C 150 P (MWCNT_B)	13 – 16 (outer)	1 – > 10	> 95
NC 3100 Nanocyl [™] (MWCNT_N)	9.5	1.5	> 95

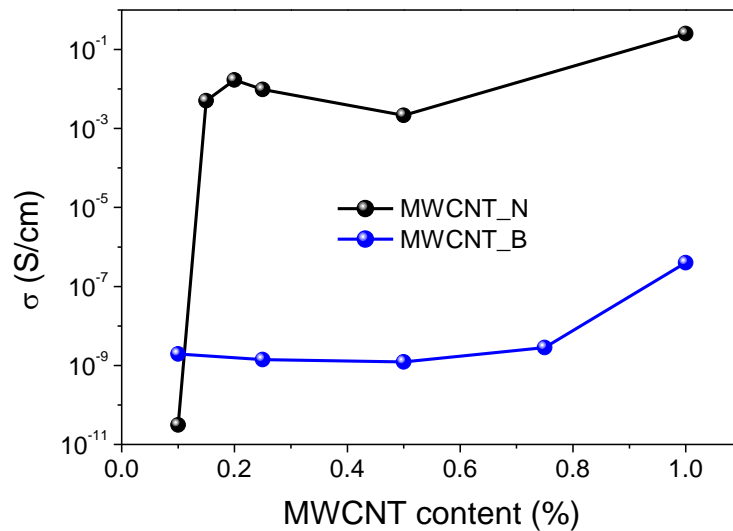


Figure 5.1: DC conductivity as function of filler amount for the different MWCNT used at room temperature.

Figure 5.1 shows the electrical conductivity of both MWCNT/PVDF composites as a function of the MWCNT content. The percolation threshold concentration of MWCNT_N is below 0.2 wt% whereas for MWCNT_B it is below 0.5 wt%. The different dimensions of the MWCNT (table 5.1) results in different overall aspect ratios, which influences the electrical properties of the composites [39], as observed in figure 5.1. The experimental trends in the composites of both types of MWCNT are similar and therefore the following sections will focus on the results obtained for the

MWCNT_B. A comparison of the performance of both MWCNT types will be provided in the final section.

5.2.2. Microstructural characteristics

It has been shown that pristine P(VDF-TrFE) membranes produced under suitable solvent evaporation conditions gives origin to porosity and pore configurations appropriate for lithium ion batteries applications [15]. This characteristic porous microstructure has been explained by the spinodal decomposition of the liquid-liquid phase separation followed by crystallization of the copolymer rich phase [40].

Figure 5.2 shows the cross section scanning electron microscopy (SEM) images of the MWCNT/P(VDF-TrFE) composites with different MWCNT contents and the histograms of the pore size diameter as obtained from the SEM images.

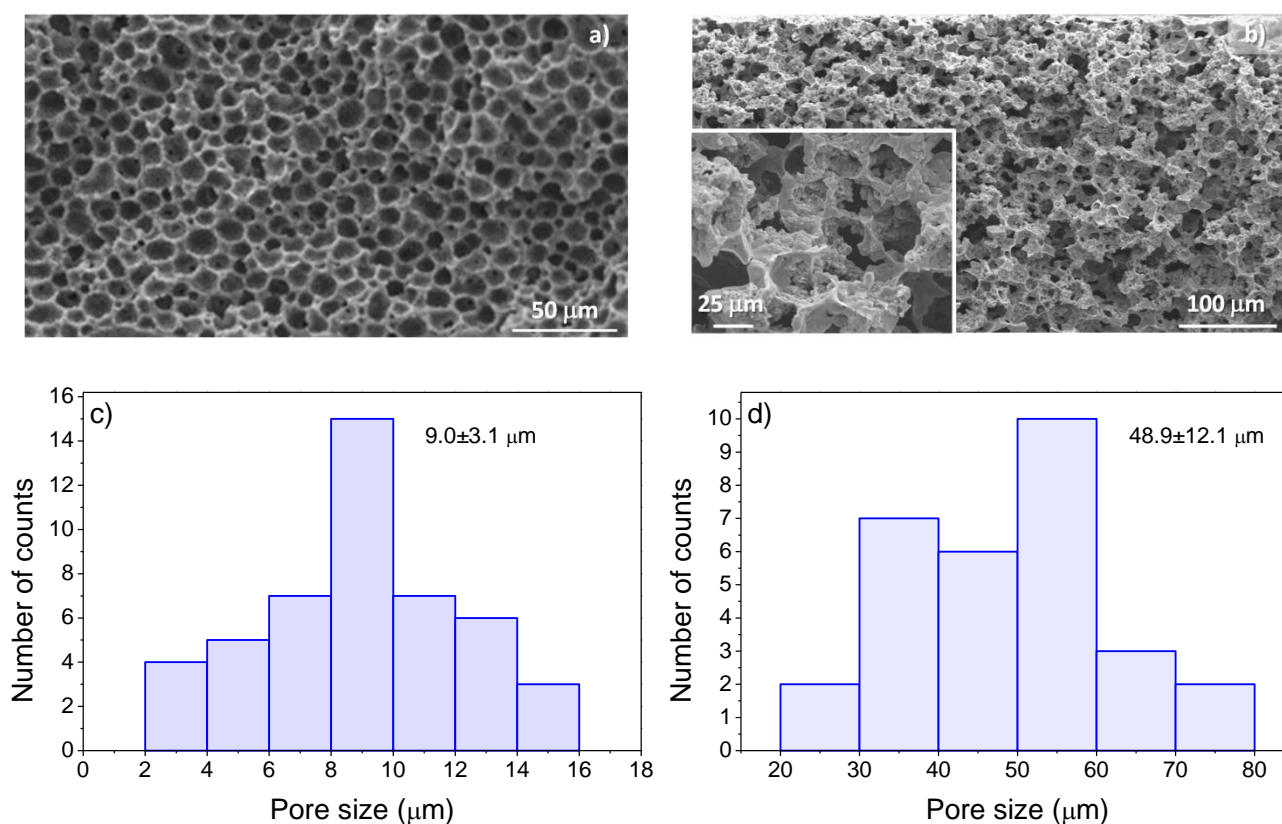


Figure 5.2: Cross section SEM images and histograms of pore size diameter of the MWCNT/P(VDF-TrFE) composites with different filler content: a) and c) 0.0 wt%, b) and d) 0.5 wt%.

The inclusion of MWCNT in the membranes does not affect the distribution of pores, the porous microstructure remaining homogeneous after the addition of fillers. The average pore diameter increases from ~9 to ~60 μm for 0.0 and 0.1 wt% content of

MWCNT, respectively, decreasing for higher filler contents, due to the filler effect on the bi-phase solvent-polymer phase diagram and therefore on the phase separation and solvent evaporation processes.

Figure 5.3 shows the porosity and electrolyte solution uptake as a function of MWCNT content.

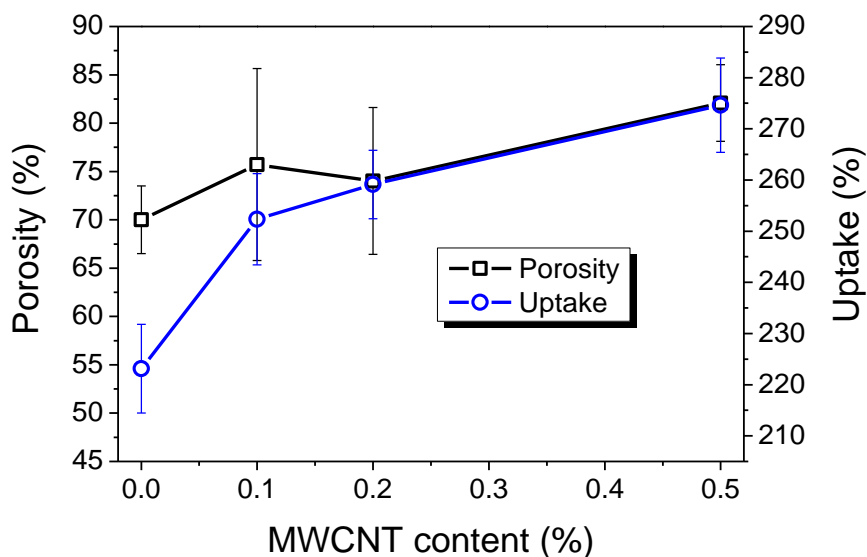


Figure 5.3: Porosity and electrolyte uptake as function of MWCNT content for membranes with different content of fillers.

The porosity and electrolyte solution uptake increase with increasing filler content but in different ways: whereas the porosity shows just a smaller increase from 70 to 80 % for increasing filler content from 0 to 0.5 wt%, the uptake shows a stronger increase from 55 up to 80 %, indicating a strong interaction of the MWCNT with the solution.

Figure 5.4 shows the Fourier transformed infrared spectroscopy (FTIR) spectra for membranes of the pristine copolymer and the composite with 0.5 wt% MWCNT without electrolyte solution uptake. The FTIR spectra of the membranes with 0.1 wt% and 0.2 wt% MWCNT filler contents are similar to the ones obtained for the membranes with 0.5 wt% MWCNT.

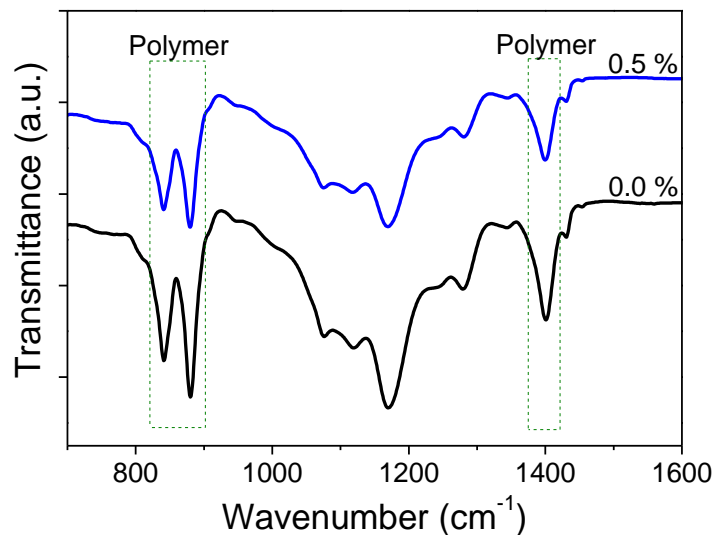


Figure 5.4: FTIR spectra of the MWCNT/P(VDF-TrFE) composites with different MWCNT content without electrolyte solution uptake.

The FTIR spectra show the characteristic vibration modes (851 cm⁻¹, 886 cm⁻¹ and 1402 cm⁻¹) of the polymer all-trans configuration [41] for all MWCNT contents. The presence of MWCNT does not affect the polymer characteristic bands, which means that polymer crystallizes in the same phase for all samples. Further, these bands are also unaffected by the presence of electrolyte solution [19-20].

Figure 5.5 shows the room temperature ionic conductivity (σ_i) and tortuosity (τ) of the membranes soaked with the electrolyte solution as function of MWCNT content, as calculated by equations 2.5 and 2.6, respectively.

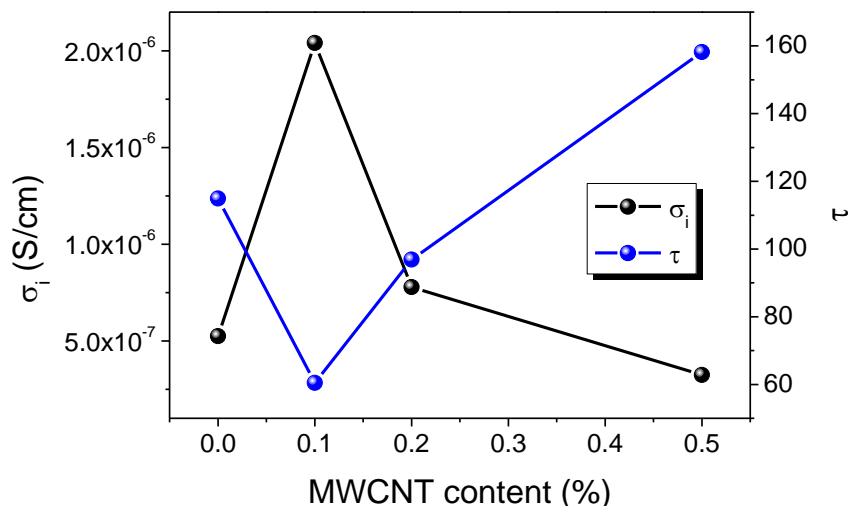


Figure 5.5: Room temperature ionic conductivity and tortuosity of membranes + 1 M $\text{LiClO}_4 \cdot 3\text{H}_2\text{O}$; σ_0 (S/cm) = 9.8 mS/cm at 25 °C.

The ionic conductivity (figure 5.5) increases with increasing MWCNT content up to 0.2 wt%, which is attributed to the increase in porosity and electrolyte uptake, as well as the increase of the amorphous phase fraction present in the polymer membrane as observed by differential scanning calorimetry (DSC) (figure 5.6 and table 5.2) [42]. The decrease of the conductivity for larger filler contributions is attributed to the increasing tortuosity which counteracts the increase in conductivity due to the presence of the conductive fillers.

The tortuosity (figure 5.5) is a property of a porous medium which describes the pore connectivity of a solid and is frequently determined through the effective conductivity [2]. The tortuosity of the membranes with 0.1 and 0.2 wt% filler content is lower than for the pure polymer, leading to an increase in the conductivity of the composites due to the presence of the fillers. For the membrane with 0.5 wt% of MWCNT the tortuosity is higher than that of the pristine one and the effective conductivity lower, indicating that pore blockage begins to occur at this concentration. Tortuosity ~ 1 describes an ideal porous body and higher values refer to more hindered systems leading to higher resistance [2, 43]. Regarding to the tortuosity, the ideal MWCNT concentration is thus between 0.1 and 0.2 wt%. The effective conductivity varies inversely of tortuosity, reaching its maximum for 0.2 wt% filler content.

5.2.3. Thermal and mechanical properties

Figure 5.6 illustrates the DSC thermograms of the membranes without electrolyte solution uptake.

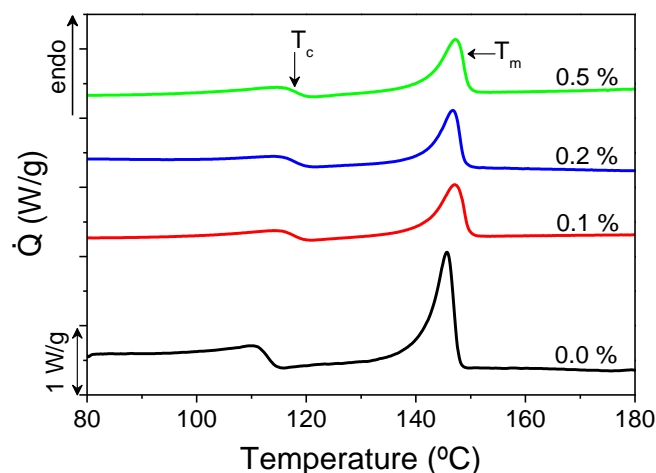


Figure 5.6: DSC thermograms of the MWCNT/P(VDF-TrFE) composites for the different filler contents without electrolyte solution uptake.

The DSC thermograms (figure 5.6) show the characteristic ferroelectric-paraelectric phase transition (lower temperature peak, T_c) around 117 °C and the melting temperature of the polymer (higher temperature peak, T_m) around 146 °C [44]. Thermograms show that the presence of MWCNT does not affect significantly the FE-PE transition and the melting temperature of the paraelectric phase. These parameters are also unaffected by the presence of the electrolyte solution as observed already with different fillers [19-20].

Table 5.2 shows the degree of crystallinity for the MWCNT/P(VDF-TrFE) membranes as a function of filler content.

Table 5.2: Degree of crystallinity of the membranes calculated by applying equation 2.1 to the melting peak of the samples

Sample	$\chi_c \pm 2$ (%)
0.0 %	28
0.1 %	31
0.2 %	22
0.5 %	23

The degree of crystallinity has a slight tendency to decrease with increasing filler content. The addition of MWCNT induces a defective crystallization of the polymer at

the contact zones with MWCNT, due to changes in the nucleation and growth kinetics [45].

The mechanical properties are essential for the safe handling and mechanical stability of the battery [7]. Figure 5.7 shows the stress-strain curves for the MWCNT/P(VDF-TrFE) membranes with different fillers content without (figure 5.7a) and with (figure 5.7b) electrolyte solution uptake.

The main mechanical characteristics of the composites are summarized in table 5.3 as obtained from the data of figure 5.7.

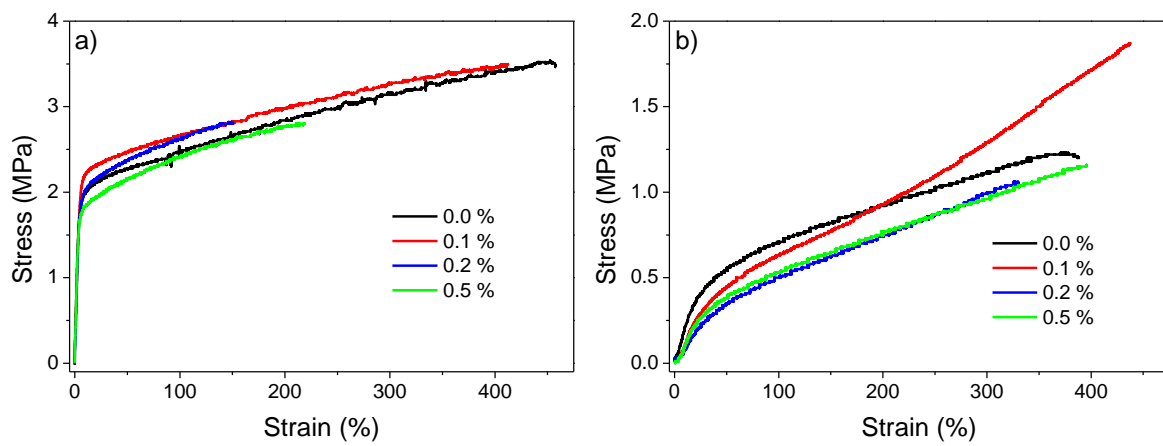


Figure 5.7: Stress-strain curves of the MWCNT/P(VDF-TrFE) composites with different filler contents: a) without electrolyte solution uptake; b) with electrolyte solution uptake.

Table 5.3: Mechanical properties of the MWCNT/P(VDF-TrFE) membranes with and without electrolyte solution uptake.

Sample	Without electrolyte uptake				With electrolyte uptake			
	0.0 %	0.1 %	0.2 %	0.5 %	0.0 %	0.1 %	0.2 %	0.5 %
Yield stress (MPa)	2.1	2.2	1.9	1.7	0.3	0.2	0.2	0.2
Elastic modulus (MPa)	40.0	40.2	41.2	41.6	1.9	1.5	1.0	1.4

Figure 5.7 and table 5.3 show that the addition of MWCNT does not affect significantly the overall mechanical properties of the membranes. The elastic modulus and the yield stress remain in the same value range after the inclusion of MWCNT, indicating that the mechanical properties are still determined by the microporous microstructure of the samples. However, there is a decrease in the yield stress and elastic modulus of the samples after electrolyte solution uptake, attributed to the larger uptake and swelling verified in all samples.

5.2.4. Electrical properties

Electrochemical impedance spectroscopy (EIS) was performed to evaluate the electrochemical properties of the samples after electrolyte solution uptake [46]. The results are shown through the Nyquist plots (imaginary impedance Z'' as function of real impedance Z') and Bode plots (impedance modulus $|Z|$ and phase angle as function of frequency). Figure 5.8 presents the Nyquist plots for all samples after electrolyte uptake at 25 °C (figure 5.8a) as well as the Bode plots (figure 5.8b and 5.8c).

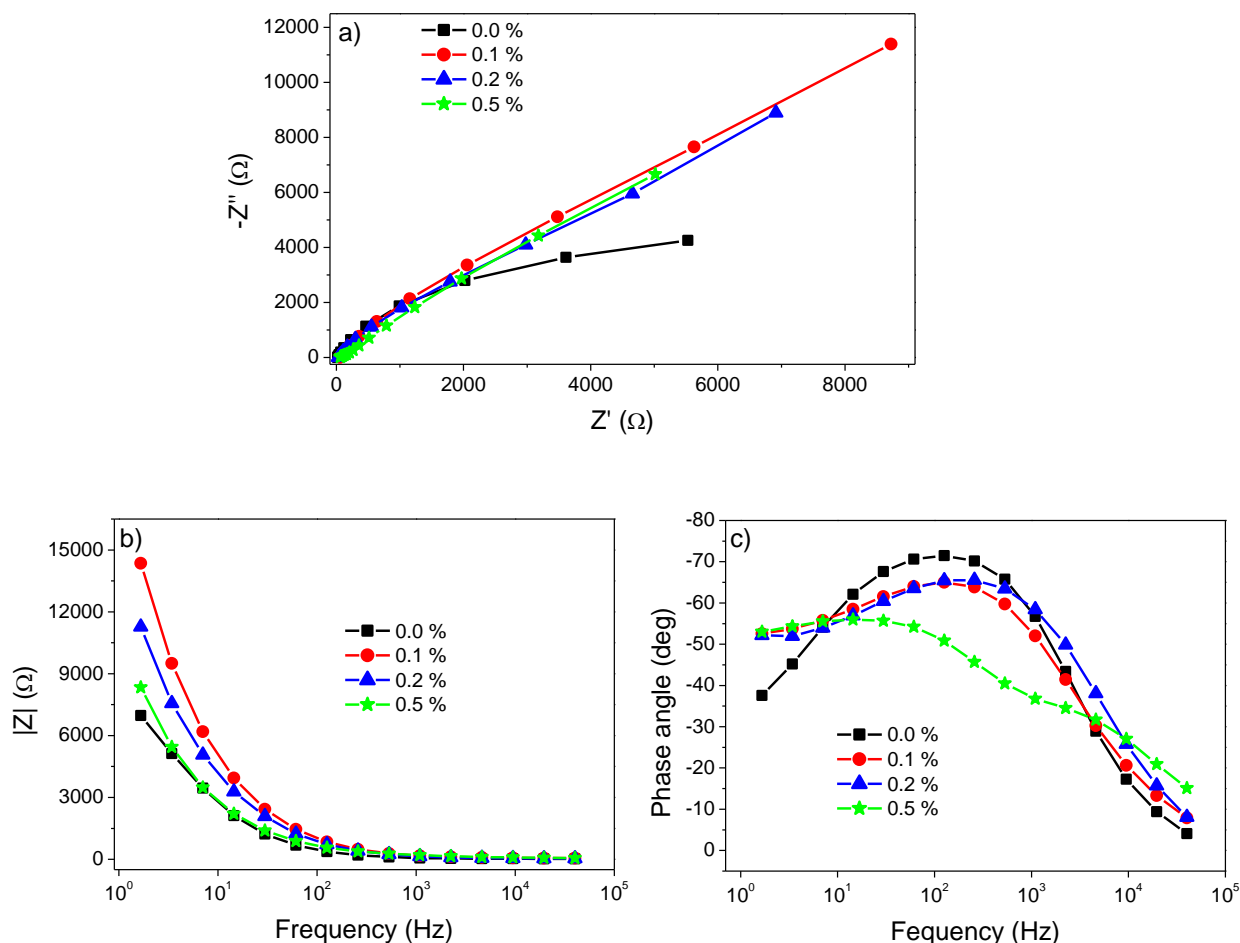


Figure 5.8: a) Nyquist plot and b-c) Bode diagram of the MWCNT/P(VDF-TrFE) composites for different filler content at 25 °C.

The Nyquist plot (figure 5.8a) shows that the inclusion of MWCNT attenuates the semicircle corresponding to the charge transfer process, indicating that the presence of the fillers facilitates the charge transfer process due to the increasing electrical conductivity [47].

The Bode diagram (figure 5.8b) shows that the impedance tends to decrease with increasing frequency for all samples, which indicates a restricted dynamics of ion mobility within the porous membranes.

Figure 5.8c shows a maximum phase angle between -55 and -70° for all samples which indicates that the membrane can be represented by a constant phase element (CPE) [48].

The EIS was analyzed by the equivalent electrical circuit, with ZView software, represented in figure 5.9. This circuit is similar to that used to describe gold [49-50] and bismuth [51] electrode processes. This circuit is used to describe electrode processes when both kinetics and diffusion processes can be relevant, such as in the composite polymer electrolytes.

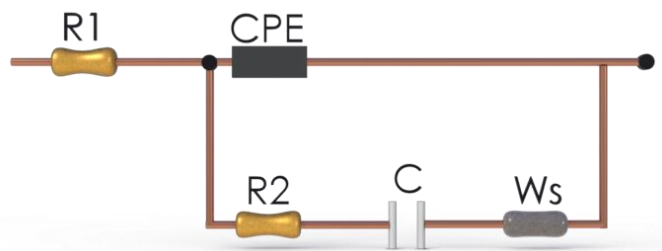


Figure 5.9: Equivalent circuit proposed for the impedance data measured in the different MWCNT/P(VDF-TrFE) membranes at different temperatures.

The equivalent circuit consists of a resistor R_1 connected in series to a constant phase element CPE connected in parallel to a resistor R_2 , a capacitor C and a Warburg impedance W_s . The resistor R_1 corresponds to the resistance of ionic migration of the electrolyte solution; the resistor R_2 and capacitor C are the charge transfer resistance and the double layer capacitance; the constant phase element CPE represents the interface between electrodes and membrane separator, i.e., the ion charges localized at the electrode interfaces; and the Warburg impedance W_s reflects the influence of the mass transport component of electroactive species on the total impedance of the electrochemical cell.

This equivalent circuit was fitted to the impedance results of all samples. The results for sample with 0.2 wt% filler content are presented in figure 5.10.

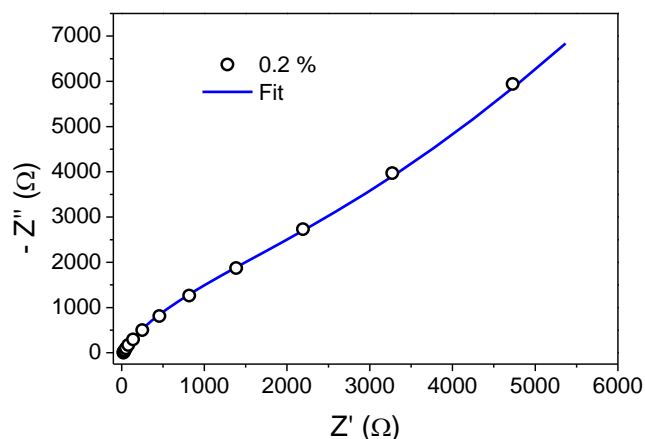


Figure 5.10: Nyquist plot for the experimental data and fitting for the equivalent circuit of figure 5.9 for membrane with 0.2 wt% of MWCNT at 50 °C.

The remaining composite membranes also present similar good fits for the equivalent circuit represented in figure 5.9. The best equivalent circuit fitted for the pristine polymer is the Randles circuit as reported in [52].

Table 5.4 shows the fitting parameters of the equivalent electrical circuit for all composite membranes with different MWCNT contents at 50 °C.

Table 5.4: Equivalent circuit parameters for MWCNT/P(VDF-TrFE) membranes at 50 °C.

	0.1 %	0.2 %	0.5 %
C ($\times 10^{-6}$ F)	49.80	55.40	1.09
R₁ (Ω)	40.63	22.23	31.45
R₂ (Ω)	3308.5	3362.7	336.18
W_S (Ω)	28194	17471	4208.4
CPE ($\times 10^{-6}$ F)	5.76	7.12	37.1
n₁	0.83	0.82	0.60

All fitted parameter values decrease with increasing filler content, except for the CPE element. The increase of the parameters C, R₁, R₂ and W_S is due to the increasing conductivity originated by the increasing filler content. The increase of the CPE value results from the increase of the interface charges between electrodes and composite membrane.

Figure 5.11 presents the ionic conductivity as a function of temperature with and without electrolyte solution uptake for all the membranes.

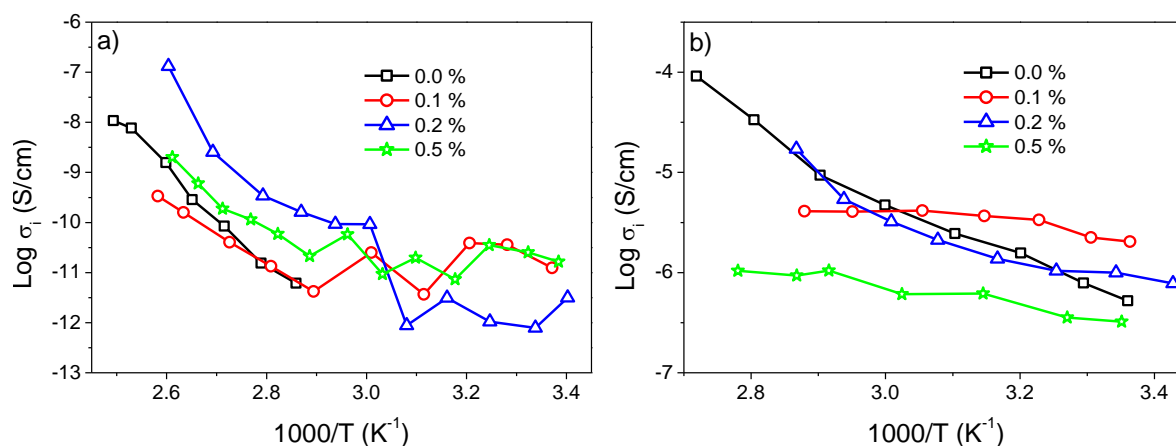


Figure 5.11: $\text{Log } \sigma_i$ as a function of $1000/T$ for MWCNT/P(VDF-TrFE) composites: a) without electrolyte solution uptake; b) with electrolyte solution uptake.

In figure 5.11a, the composite samples show higher ionic conductivity as compared to the pristine one, being about one order of magnitude higher for 0.2 wt% MWCNT filled composite. Membranes with electrolyte solution uptake (figure 5.11b) have an ionic conductivity about 4 orders of magnitude higher than that without electrolyte solution and are more stable as a function of temperature. This thermal stability is achieved for MWCNT contents significantly lower than the ones reported in [11]. The pure polymer shows higher ionic conductivity than the composites but is strongly dependent on temperature. The inclusion of CNT improves significantly the electrical properties of the membranes due of the low activation energy of conduction (table 5.5), almost eliminating the dependence of the conductivity with temperature, fact which is very convenient for battery applications. Further, the electrolyte solution does not affect the thermal stability of the polymer as determined by thermo gravimetric analysis TGA [15].

Table 5.5 shows the activation energy (E_a) for the ion transport, calculated by fitting with the Arrhenius equation (equation 2.7) to data of figure 5.11.

Table 5.5: Activation energies for all membranes with and without electrolyte solution uptake.

Samples	E_a without electrolyte solution (kJ/mol)	E_a with electrolyte solution (kJ/mol)
0.0 %	181	64
0.1 %	10	5
0.2 %	45	7
0.5 %	11	8

The activation energy shows a strong dependence with the MWCNT content and also with the electrolyte solution uptake. The addition of fillers and the electrolyte solution lead to a significant decrease of the E_a . The presence of fillers decreases significantly the energy required for the ionic conduction process, due to the decrease of the crystalline phase fraction and the increase of the free volume of the polymer, leading to higher ion mobility.

To evaluate the electrochemical stability and diffusion coefficients of the membranes, cyclic voltammetry over the potential range -2.0 to 6.0 V was carried out after electrolyte solution uptake. The wide voltage window of electrochemical stability of the membranes immersed in the electrolyte solution is observed in the figure 5.12.

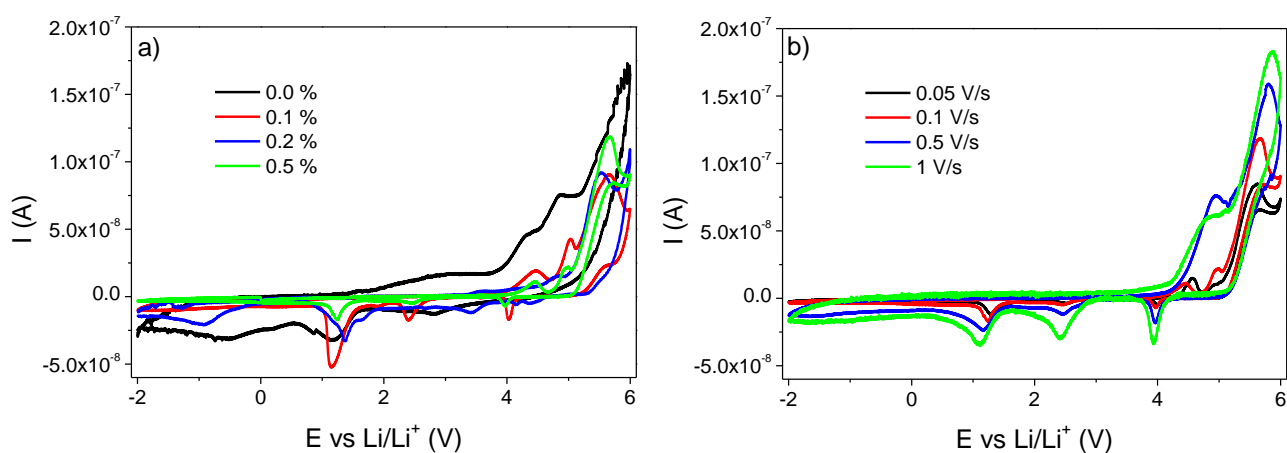


Figure 5.12: a) Voltammogram of MWCNT/P(VDF-TrFE) composites at 0.1 V/s; b) voltammogram of MWCNT/P(VDF-TrFE) with 0.5 wt% of MWCNT at different scanning rates.

The voltammogram of figure 5.12a shows that the membranes with MWCNT are more stable than the pure polymer. The operation window, between -2.0 and 4.0 V, is more stable for MWCNT/P(VDF-TrFE) membranes. In figure 5.12a it is observed a good electrochemical stability independently of MWCNT filler content, with anodic potentials higher than 4.0 V and oxidation peak around 1.0 V. The anodic current onset may be associated with the decomposition of the polymer electrolyte.

The electrochemical deposition of lithium salts is observed in the cathodic current onset at about 1.0 V in figure 5.12a.

For high scanning rates above 0.5 V/s it is detected the presence of multiples cathodic peaks starting from 4.0 V due to the electrodeposition of the cation on the lithium substrate (figure 5.12 b). On the other hand, figure 5.12b demonstrates that the scan rate does not affect significantly the electrochemical stability of the composite membranes, the stable operation window remaining in the same value range for all scanning rates; although the cathodic peaks tend to increase with increasing scan rate. From voltammograms can be inferred that the addition of MWCNT improves the electrochemical stability of the membranes; however the stable operation window is still essentially determined by the electrolyte solution. The diffusion coefficient, calculated from the voltammograms of figure 5.12 does not show dependence with filler content.

The pure polymer presents the lowest value of $3.45 \times 10^{-5} \text{ cm}^2/\text{s}$ and the membrane with 0.2 wt% of MWCNT presents the highest value of $3.84 \times 10^{-5} \text{ cm}^2/\text{s}$.

5.2.5. MWCNT type comparison

In order to evaluate the influence of the MWCNT type in the membranes performance, two filler concentrations were compared.

Figure 5.13 shows the mechanical (figure 5.13a) and electrical properties (impedance spectroscopy: figure 5.13b and c; cyclic voltammetry: figure 5.13d) of the membranes with different MWCNT types and contents.

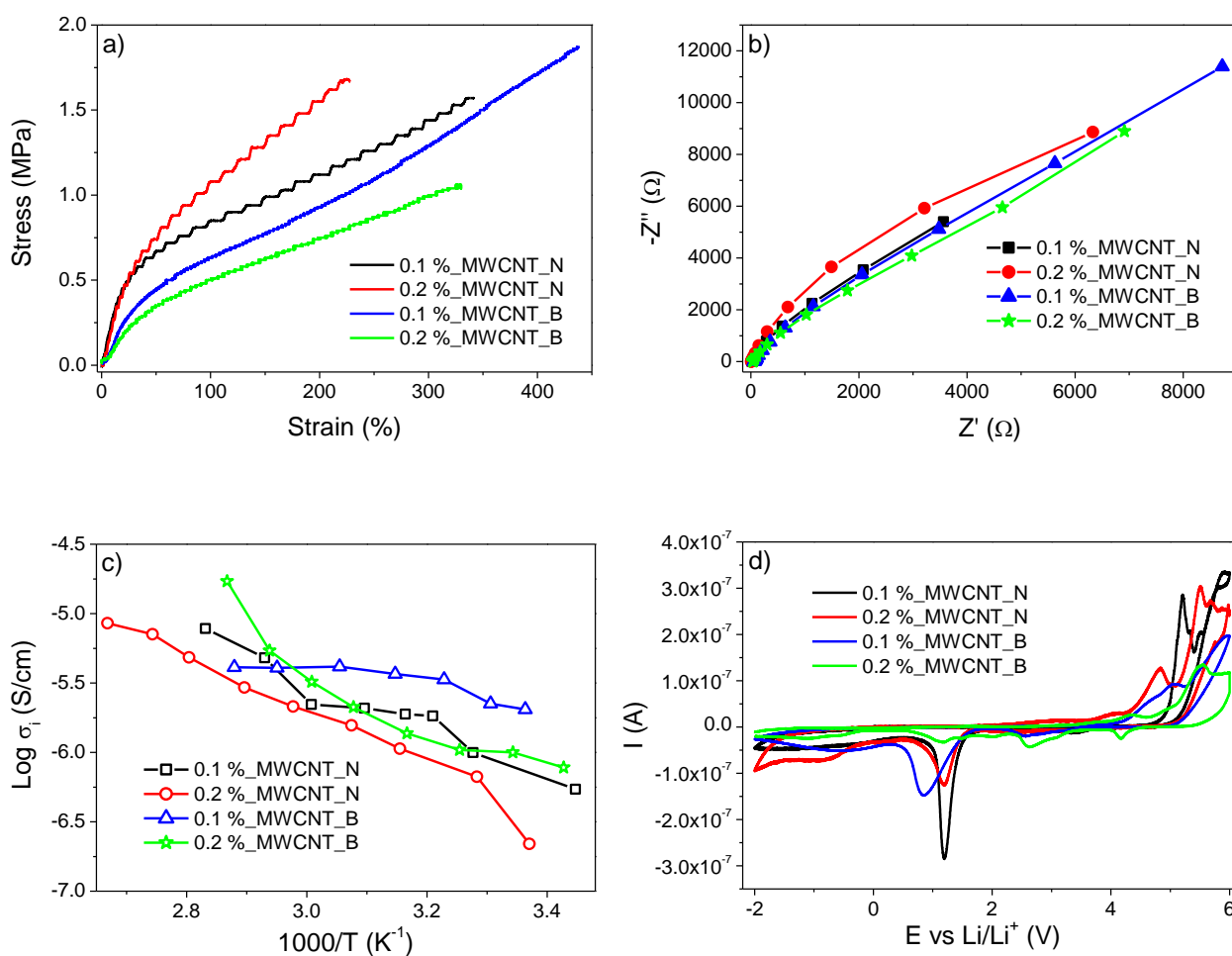


Figure 5.13: a) Stress-strain curves of the MWCNT/P(VDF-TrFE) membranes with electrolyte uptake; b) Nyquist plot of the MWCNT/P(VDF-TrFE) composites with electrolyte uptake at 25 °C; c) $\text{Log } \sigma_i$ as a function of $1000/T$ for MWCNT/P(VDF-TrFE) composites with electrolyte uptake; d) Voltammograms of the MWCNT/P(VDF-TrFE) membranes with electrolyte uptake at 0.5 V/s.

Figure 5.13a illustrates that the overall mechanical properties are similar for all samples. The MWCNT_N presents a slightly improvement in the elastic modulus and in the yield stress, which is not significant in the overall mechanical performance.

In the Nyquist plot of figure 5.13b it is shown that the impedance behaviour is similar for all composite membranes, the charge diffusion not depending on MWCNT type. The ionic conductivity (figure 5.13c) is also analogous for all samples, as well as the cyclic voltammetry (figure 5.13d). In the latter case, just the sample with 0.1 % filler content of MWCNT_N shows a more intense oxidation peak around 1.0 V.

From these graphs can be concluded that the type of MWCNT considered in this work does not affect significantly the overall performance of the membranes as battery separator.

5.4. Conclusion

MWCNT/P(VDF-TrFE) porous membranes with different contents of MWCNT were prepared by thermally induced phase separation (TIPS). The addition of MWCNT to the polymer matrix increases the average pore size, leading to an increase in the porosity up to ~82 % and electrolyte solution uptake up to ~275 % for 0.5 wt% MWCNT filler content membranes. The polymer crystallizes in the polar phase after the inclusion of MWCNT, and the ferroelectric to paraelectric transition and melting temperatures remain at similar values of pristine polymer. The degree of crystallinity decreases to 23 % for 0.5 wt% filler content composite. The tortuosity increases with increasing filler content up to 0.2 wt% of MWCNT. The overall membrane mechanical properties are not significantly affected by the presence of MWCNT. The ionic conductivity increases with increasing MWCNT content, from 5×10^{-7} to 2×10^{-6} S/cm for 0 and 0.1 wt%, respectively, and is more stable to temperature variations. The electrochemical stability evaluated by cyclic voltammetry revealed a stable operation window between -2.0 and 4.0 V, *versus* Li/Li⁺.

The mechanical properties, ionic conductivity and the thermal electrochemical and stabilities of the polymer membranes are independently of the type of the MWCNT used in this work.

The results show that MWCNT/P(VDF-TrFE) composite membranes have adequate morphological, thermal, mechanical and electrochemical properties for being used as separator membranes for lithium ion batteries.

5.5. References

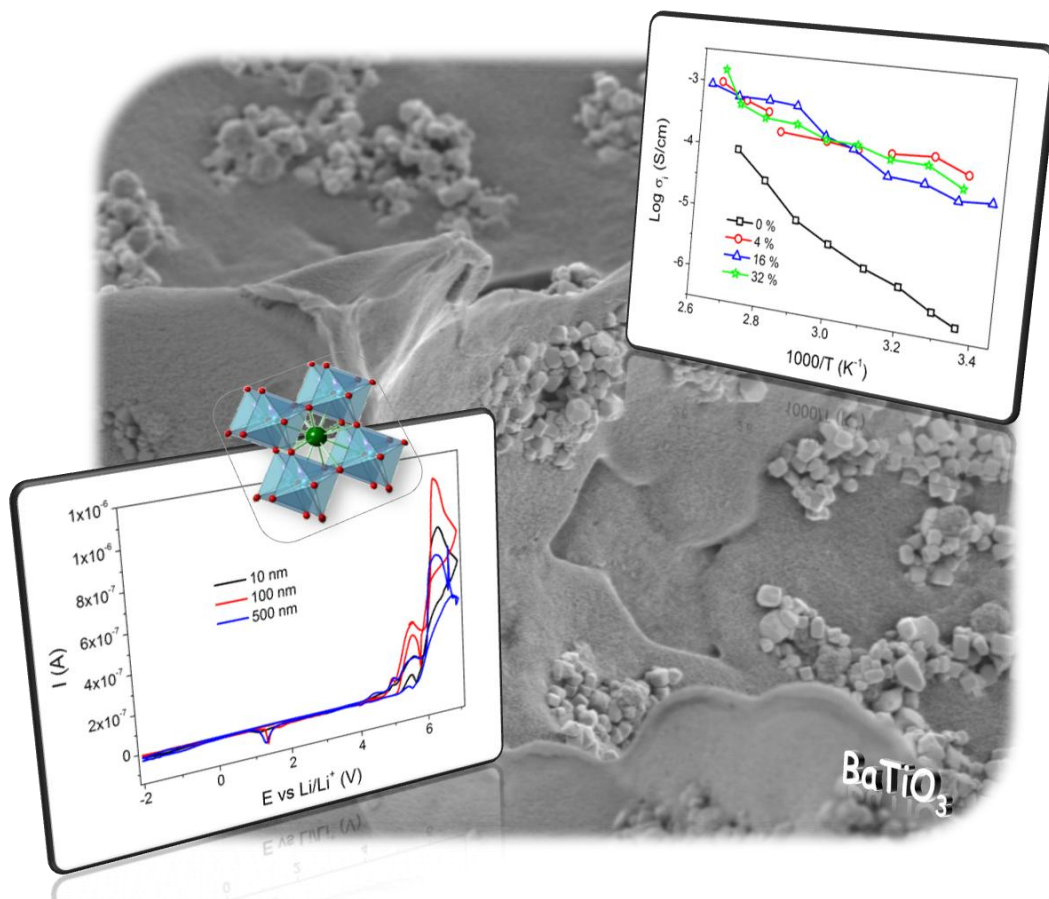
1. Tarascon, J.-M. *Key challenges in future Li-battery research*. Philosophical Transactions of the Royal Society A: Mathematical, Physical and Engineering Sciences, 2010. **368**(1923): p. 3227-3241.
2. Arora, P. and Z. Zhang. *Battery Separators*. Chemical Reviews, 2004. **35**(50): p. 4419-4462.
3. Whittingham, M.S. *Lithium Batteries and Cathode Materials*. Chemical Reviews, 2004. **104**(10): p. 4271-4302.
4. Tarascon, J.M. and M. Armand. *Issues and challenges facing rechargeable lithium batteries*. Nature, 2001. **414**(6861): p. 359-367.
5. Zhang, J. and J. Lee. *A review on prognostics and health monitoring of Li-ion battery*. Journal of Power Sources, 2011. **196**(15): p. 6007-6014.
6. Vincent, C.A. *Lithium batteries: a 50-year perspective, 1959–2009*. Solid State Ionics, 2000. **134**(1–2): p. 159-167.
7. Huang, X. *Separator technologies for lithium-ion batteries*. Journal of Solid State Electrochemistry, 2011. **15**(4): p. 649-662.
8. Kim, D.-W., J.-M. Ko, J.-H. Chun, S.-H. Kim, and J.-K. Park. *Electrochemical performances of lithium-ion cells prepared with polyethylene oxide-coated separators*. Electrochemistry Communications, 2001. **3**(10): p. 535-538.
9. Persi, L., F. Croce, B. Scrosati, E. Plichta, and M.A. Hendrickson. *Poly(ethylene oxide)-Based, Nanocomposite Electrolytes as Improved Separators for Rechargeable Lithium Polymer Batteries*. Journal of The Electrochemical Society, 2002. **149**(2): p. A212-A216.
10. Wang, C., Y. Wei, G.R. Ferment, W. Li, and T. Li. *Poly(ethylene oxide)–silica hybrid materials for lithium battery application*. Materials Letters, 1999. **39**(4): p. 206-210.
11. Ibrahim, S., S.M.M. Yasin, M.N. Ng, R. Ahmad, and M.R. Johan. *Impedance spectroscopy of carbon nanotube/solid polymer electrolyte composites*. Solid State Communications, 2011. **151**(23): p. 1828-1832.
12. Cho, T.H., T. Sakai, S. Tanase, K. Kimura, Y. Kondo, T. Terao, and M. Tanaka. *Electrochemical performances of polyacrylonitrile nanofiber-based nonwoven separator for lithium-ion battery*. Electrochemical and Solid State Letters, 2007. **10**(7): p. A159-A162.
13. Huai, Y., J. Gao, Z. Deng, and J. Suo. *Preparation and characterization of a special structural poly(acrylonitrile)-based microporous membrane for lithium-ion batteries*. Ionics, 2010. **16**(7): p. 603-611.

14. Cheng, C.L., C.C. Wan, and Y.Y. Wang. *Preparation of porous, chemically cross-linked, PVdF-based gel polymer electrolytes for rechargeable lithium batteries*. Journal of Power Sources, 2004. **134**(2): p. 202-210.
15. Costa, C.M., L.C. Rodrigues, V. Sencadas, M.M. Silva, J.G. Rocha, and S. Lanceros-Méndez. *Effect of degree of porosity on the properties of poly(vinylidene fluoride-trifluoroethylene) for Li-ion battery separators*. Journal of Membrane Science, 2012. **407–408**(0): p. 193-201.
16. Stephan, A.M., K.S. Nahm, M. Anbu Kulandainathan, G. Ravi, and J. Wilson. *Poly(vinylidene fluoride-hexafluoropropylene) (PVdF-HFP) based composite electrolytes for lithium batteries*. European Polymer Journal, 2006. **42**(8): p. 1728-1734.
17. Wachtler, M., D. Ostrovskii, P. Jacobsson, and B. Scrosati. *A study on PVdF-based SiO₂-containing composite gel-type polymer electrolytes for lithium batteries*. Electrochimica Acta, 2004. **50**(2–3): p. 357-361.
18. Djian, D., F. Alloin, S. Martinet, and H. Lignier. *Macroporous poly(vinylidene fluoride) membrane as a separator for lithium-ion batteries with high charge rate capacity*. Journal of Power Sources, 2009. **187**(2): p. 575-580.
19. Nunes-Pereira, J., A.C. Lopes, C.M. Costa, R. Leones, M.M. Silva, and S. Lanceros-Méndez. *Porous Membranes of Montmorillonite/Poly(vinylidene fluoride-trifluoroethylene) for Li-Ion Battery Separators*. Electroanalysis, 2012. **24**(11): p. 2147-2156.
20. Nunes-Pereira, J., A.C. Lopes, C.M. Costa, L.C. Rodrigues, M.M. Silva, and S. Lanceros-Méndez. *Microporous membranes of NaY zeolite/poly(vinylidene fluoride-trifluoroethylene) for Li-ion battery separators*. Journal of Electroanalytical Chemistry, 2013. **689**(0): p. 223-232.
21. Nalwa, H.S. *Ferroelectric polymers : chemistry, physics, and applications*. 1995, New York: Dekker.
22. Costa, C.M., A. California, V.F. Cardoso, V. Sencadas, L.C. Rodrigues, M.M. Silva, and S. Lanceros-Méndez. *Electroactive Poly(Vinylidene Fluoride-Trifluoroethylene) (PVDF-TrFE) Microporous Membranes for Lithium-Ion Battery Applications*. Ferroelectrics, 2012. **430**(1): p. 103-107.
23. Jung, S., D. Kim, S. Lee, M. Cheong, D. Nguyen, B. Cho, and H. Kim. *Fillers for Solid-State Polymer Electrolytes : Highlight*. Bull. Korean Chem. Soc., 2009. **30**(10): p. 2355-2361.
24. Hwang, H.-Y., D.-J. Kim, H.-J. Kim, Y.-T. Hong, and S.-Y. Nam. *Effect of nanoclay on properties of porous PVdF membranes*. Transactions of Nonferrous Metals Society of China, 2011. **21, Supplement 1**(0): p. s141-s147.

25. Koh, M.J., H.Y. Hwang, D.J. Kim, H.J. Kim, Y.T. Hong, and S.Y. Nam. *Preparation and Characterization of Porous PVdF-HFP/clay Nanocomposite Membranes*. Journal of Materials Science & Technology, 2010. **26**(7): p. 633-638.
26. Dalmas, F., J.-Y. Cavaillé, C. Gauthier, L. Chazeau, and R. Dendievel. *Viscoelastic behavior and electrical properties of flexible nanofiber filled polymer nanocomposites. Influence of processing conditions*. Composites Science and Technology, 2007. **67**(5): p. 829-839.
27. O'Connell, M. *Carbon nanotubes : properties and applications*. 2006, Boca Raton, FL: CRC/Taylor & Francis.
28. Ahn, C.H., Y. Baek, C. Lee, S.O. Kim, S. Kim, S. Lee, S.-H. Kim, S.S. Bae, J. Park, and J. Yoon. *Carbon nanotube-based membranes: Fabrication and application to desalination*. Journal of Industrial and Engineering Chemistry, 2012. **18**(5): p. 1551-1559.
29. de Lannoy, C.F., D. Jassby, D.D. Davis, and M.R. Wiesner. *A highly electrically conductive polymer–multiwalled carbon nanotube nanocomposite membrane*. Journal of Membrane Science, 2012. **415–416**(0): p. 718-724.
30. Hu, L., H. Wu, F. La Mantia, Y. Yang, and Y. Cui. *Thin, Flexible Secondary Li-Ion Paper Batteries*. ACS Nano, 2010. **4**(10): p. 5843-5848.
31. Goyal, A., A.L.M. Reddy, and P.M. Ajayan. *Flexible Carbon Nanotube–Cu₂O Hybrid Electrodes for Li-Ion Batteries*. Small, 2011. **7**(12): p. 1709-1713.
32. Lu, W., A. Goering, L. Qu, and L. Dai. *Lithium-ion batteries based on vertically-aligned carbon nanotube electrodes and ionic liquid electrolytes*. Physical Chemistry Chemical Physics, 2012. **14**(35): p. 12099-12104.
33. Liu, X.-M., Z.d. Huang, S.w. Oh, B. Zhang, P.-C. Ma, M.M.F. Yuen, and J.-K. Kim. *Carbon nanotube (CNT)-based composites as electrode material for rechargeable Li-ion batteries: A review*. Composites Science and Technology, 2012. **72**(2): p. 121-144.
34. Zou, M.-m., D.-j. Ai, and K.-y. Liu. *Template synthesis of MnO₂/CNT nanocomposite and its application in rechargeable lithium batteries*. Transactions of Nonferrous Metals Society of China, 2011. **21**(9): p. 2010-2014.
35. Ahn, J.-H., Y.-J. Kim, and G.X. Wang. *Electrochemical properties of carbon nanotube-dispersed PEO-LiX electrolytes*. Metals and Materials International, 2006. **12**(1): p. 69-73.
36. Guo, X., C. Wang, M. Chen, J. Wang, and J. Zheng. *Carbon coating of Li₄Ti₅O₁₂ using amphiphilic carbonaceous material for improvement of lithium-ion battery performance*. Journal of Power Sources, 2012. **214**(0): p. 107-112.

37. Sun, X., X. Wang, N. Feng, L. Qiao, X. Li, and D. He. *A new carbonaceous material derived from biomass source peels as an improved anode for lithium ion batteries*. *Journal of Analytical and Applied Pyrolysis*, 2013. **100**(0): p. 181-185.
38. Carabineiro, S.A.C., M.F.R. Pereira, J. Nunes-Pereira, J. Silva, C. Caparros, V. Sencadas, and S. Lanceros-Méndez. *The effect of nanotube surface oxidation on the electrical properties of multiwall carbon nanotube/poly(vinylidene fluoride) composites*. *Journal of Materials Science*, 2012. **47**(23): p. 8103-8111.
39. Shehzad, K., Z.-M. Dang, M.N. Ahmad, R.U.R. Sagar, S. Butt, M.U. Farooq, and T.-B. Wang. *Effects of carbon nanotubes aspect ratio on the qualitative and quantitative aspects of frequency response of electrical conductivity and dielectric permittivity in the carbon nanotube/polymer composites*. *Carbon*, 2013. **54**(0): p. 105-112.
40. Ferreira, A., J. Silva, V. Sencadas, J.L.G. Ribelles, and S. Lanceros-Méndez. *Poly[(vinylidene fluoride)-co-trifluoroethylene] Membranes Obtained by Isothermal Crystallization from Solution*. *Macromolecular Materials and Engineering*, 2010. **295**(6): p. 523-528.
41. Prabu, A.A., J.S. Lee, K.J. Kim, and H.S. Lee. *Infrared spectroscopic studies on crystallization and Curie transition behavior of ultrathin films of P(VDF/TrFE) (72/28)*. *Vibrational Spectroscopy*, 2006. **41**(1): p. 1-13.
42. Park, J.W., E.D. Jeong, M.-S. Won, and Y.-B. Shim. *Effect of organic acids and nano-sized ceramic doping on PEO-based solid polymer electrolytes*. *Journal of Power Sources*, 2006. **160**(1): p. 674-680.
43. Quartarone, E., P. Mustarelli, and A. Magistris. *Transport Properties of Porous PVDF Membranes*. *The Journal of Physical Chemistry B*, 2002. **106**(42): p. 10828-10833.
44. Sencadas, V., S. Lanceros-Méndez, and J.F. Mano. *Thermal characterization of a vinylidene fluoride-trifluoroethylene (75–25) (%mol) copolymer film*. *Journal of Non-Crystalline Solids*, 2006. **352**(50–51): p. 5376-5381.
45. Costa, C.M., S. Firmino Mendes, V. Sencadas, A. Ferreira, R. Gregorio Jr, J.L. Gómez Ribelles, and S. Lanceros-Méndez. *Influence of processing parameters on the polymer phase, microstructure and macroscopic properties of poly(vinylidene fluoride)/Pb(Zr_{0.53}Ti_{0.47})O₃ composites*. *Journal of Non-Crystalline Solids*, 2010. **356**(41–42): p. 2127-2133.
46. Brett, A.M.C.F.O. and C.M.A. Brett. *Electroquímica: princípios, métodos e aplicações*. 1996, Coimbra: Livraria Almedina.
47. Ulaganathan, M. and S. Rajendran. *Studies on MWCNT-Incorporated Composite Polymer Electrolytes for Electrochemical Applications*. *Soft Materials*, 2010. **8**(4): p. 358-369.

48. Cole, K. *Dispersion and Absorption in Dielectrics I. Alternating Current Characteristics*. J. Chem. Phys., 1941. **9**(4): p. 341.
49. Bondarenko, A.S., G.A. Ragoisha, N.P. Osipovich, and E.A. Streltsov. *Potentiodynamic electrochemical impedance spectroscopy of lead upd on polycrystalline gold and on selenium atomic underlayer*. Electrochemistry Communications, 2005. **7**(6): p. 631-636.
50. Kerner, Z. and T. Pajkossy. *Measurement of adsorption rates of anions on Au(111) electrodes by impedance spectroscopy*. Electrochimica Acta, 2002. **47**(13–14): p. 2055-2063.
51. Nurk, G., H. Kasuk, K. Lust, A. Jänes, and E. Lust. *Adsorption kinetics of dodecyl sulfate anions on the bismuth (011) plane*. Journal of Electroanalytical Chemistry, 2003. **553**(0): p. 1-19.
52. Costa, C.M., V. Sencadas, J.G. Rocha, M.M. Silva, and S. Lanceros-Méndez. *Evaluation of the main processing parameters influencing the performance of poly(vinylidene fluoride–trifluoroethylene) lithium-ion battery separators*. Journal of Solid State Electrochemistry, 2013. **17**(3): p. 861-870.



6 - Porous membranes of $BaTiO_3/P(VDF-TrFE)$

This chapter is based on the following publication:

Nunes-Pereira, J., C.M. Costa, R.E. Sousa, A.V. Machado, M.M. Silva, and S. Lanceros-Méndez. *Li-ion battery separator membranes based on barium titanate and poly(vinylidene fluoride-co-trifluoroethylene)* Submitted to *Electrochimica Acta* 2013.

6.1. Introduction

Current lifestyle and technological advances, in particular in the area of mobile communications, lead to an increased need and availability of stored energy [1-2]. Despite many emerging technologies, the most attractive way to store energy to provide electrical power is to convert chemical into electrical energy. In this sense, lithium ion secondary batteries are the systems with the best performance with higher working voltage and energy density (210 Wh/kg; 650 Wh/l), longer service life and higher flexibility design when compared to other systems such as lead-acid, nickel-cadmium (Ni-Cd) or nickel-metal hydride (Ni-MH) batteries [1-4].

Up to now, the development of lithium secondary batteries has been mostly focused on powering small electronic devices, but new developments are needed to meet the requirements of new market trends, such as green energy, recycling and flexibility, among others. One way to accomplish these requirements is the use of polymers or organic/inorganic composites [2].

A battery is a device that converts stored chemical energy into electricity within a closed system. Lithium ion batteries have three fundamental constituents, the negative electrode (anode), the positive electrode (cathode) and the electrolyte within a separator. Most Li-batteries use carbon as anode, metal oxides as cathode and organic solvents as electrolyte solutions [2, 5]. The separator is often a porous polymer or ceramic membrane placed between cathode and anode. It plays a key role in the battery performance and safety, providing electrical insulation between electrodes and a pathway for ionic conduction. An ideal separator should meet requirements such as being electronic insulator, ionic conductor, mechanically strong, dimensionally stable, readily wetted by electrolyte and chemically resistant to electrolyte and impurity degradation, among others [2, 5-6]. Many polymers meet these demands and therefore many studies have been developed for their use as separators: poly(ethylene oxide) (PEO) [7-10], poly(acrylonitrile) (PAN) [11-12], polyimide (PI) [13] and poly(vinylidene fluoride) (PVDF) and its copolymers [14-20].

PVDF and poly(vinylidene fluoride-*co*-trifluoroethylene) (P(VDF-TrFE)) have attracted interest as battery separator due to its large polarity, controllable porosity, suitable mechanical properties, wettability by organic solvents, chemical inertness, good electrode/electrolyte contact and stability in cathodic environment [14-15, 21-22].

In particular, P(VDF-TrFE) has high polarity and crystallizes in a polar phase from the melt or by solution casting and its ferroelectric to paraelectric (FE-PE) transition occurs at a Curie temperature (T_c) below the melting (T_m) [23].

Despite developments in polymer based separator membranes, there is large space for improvement. In this way, the incorporation of suitable fillers in polymer matrixes has become an interesting approach to improve mechanical, thermal and chemical stability and electrolyte uptake of the separators. The use of carbon nanotubes [24-25], zeolites [22], clays [21, 26], BaTiO₃ [27-29] and others have been recently reported. Ferroelectric ceramic fillers, as BaTiO₃, enhance lithium interface stability, facilitate the salt dissociation into charge species and improve the ionic conductivity, by increasing the amorphous phase content of the polymers and the number of charge carriers [28].

BaTiO₃ crystallizes in the perovskite structure [30] and has high dielectric response at room temperature ($\epsilon' = 1200$, $\text{\AA} = 10$ nm; $\epsilon' = 3417$, $\text{\AA} = 500$ nm) [31-32]. BaTiO₃ exhibits five crystalline phases, hexagonal, cubic, tetragonal, orthorhombic, monoclinic and rhombohedral depending on temperature [33].

Recent studies report on the use of polymeric composites with BaTiO₃ as separator membranes. The addition of this ceramic filler in a PEO/P(VDF-TrFE) polymer blend increases the ionic conductivity up to 1.2×10^{-4} S/cm and the stable operation window to a range of -2.3 to 2.4 V for 15 wt% of BaTiO₃ [27]. Composites of PEO with BaTiO₃ also show high ionic conductivity, 1.5×10^{-5} S/cm, at room temperature, and a stable operation window up to 4.1 V vs Li/Li⁺ at 80 °C for 10 wt% of fillers [29].

The successful use of the ferroelectric filler BaTiO₃ reinforce the relevance of this work, since besides the effect of filler content, the effect of filler size in the morphological, thermal, mechanical, electrochemical properties of the polymeric membranes is also considered. This fact is relevant and the BaTiO₃ particle properties and therefore their effect in a composite highly depend on particle size, the ferroelectricity disappearing below a certain grain size [34].

In this study particles of 10, 100 and 500 nm average size are evaluated table 6.1.

Table 6.1: Structural properties of the ceramic fillers [35].

	$\phi = 10$ nm	$\phi = 100$ nm	$\phi = 500$ nm
Purity (%)	99.8	99.9	99.9
Crystallographic form	cubic	cubic	tetragonal

6.2. Results and discussion

6.2.1. Microstructural characteristics

The effect of BaTiO₃ concentration in the polymer matrix was studied in the membranes with average particle size of 100 nm.

The morphology of the separator membrane is paramount for the battery performance as well as in their assembling and handling [5]. It has been shown that pristine P(VDF-TrFE) membranes produced under specific solvent evaporation conditions lead to porosity and pore distribution adequate for Li-ion batteries applications [14, 36].

Figure 6.1 shows the cross section scanning electron microscopy (SEM) pictures of P(VDF-TrFE) and ceramic/P(VDF-TrFE) composites, the average pore size distribution and electrolyte solution uptake for the sample with 16 wt% filler content.

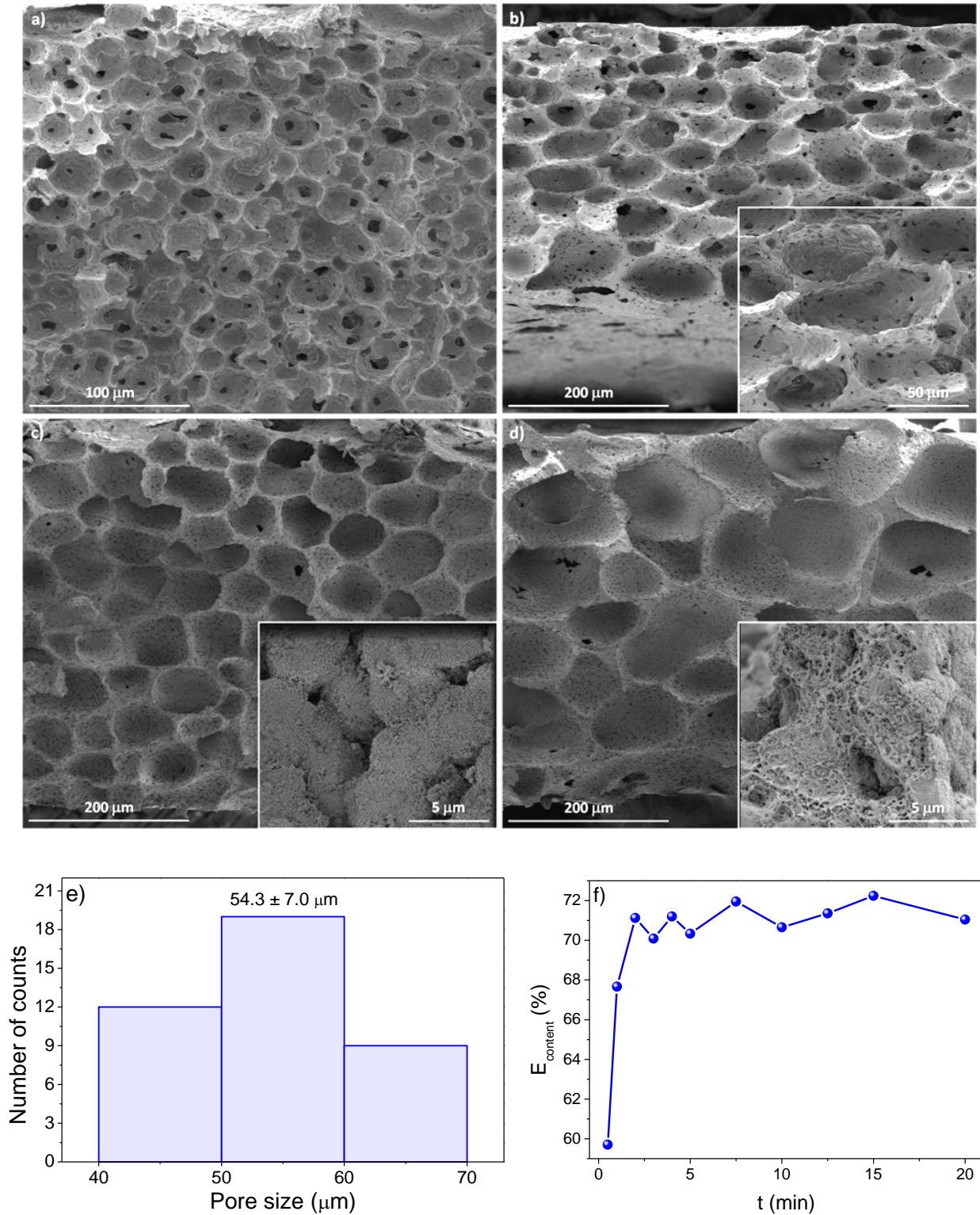


Figure 6.1: Cross section SEM images of the BaTiO₃/P(VDF-TrFE) composites with different filler contents: a) 0 wt%, b) 4 wt%, c) 16 wt% and d) 32 wt%; e) average pore size distribution and f) electrolyte content as function of time, for membrane with 16 wt% of BaTiO₃.

Figure 6.1a shows that the pristine copolymer is characterized by a homogeneous porous structure that remains after the addition of ceramic fillers (figures 6.1b, c and d). In the inset of figures 6.1c and d it is notorious that the BaTiO₃ nanoparticles decorate the internal walls of the polymer pores, the fillers being located in the pore cavities instead of being incorporated within the polymeric matrix.

Figure 6.1e represents the average pore size distribution of the sample with 16 wt% of fillers, all the pores have a diameter between 40 and 70 μm . The average pore size for all samples is represented in figure 6.2.

Figure 6.1f represents the electrolyte content as a function of time for the sample with 16 wt% of BaTiO₃ nanoparticles. The electrolyte content stabilizes about 2 minutes after the onset. After stabilizing, the electrolyte content varies about 2 %, which is within the experimental error. The behaviour is similar for the remaining samples.

Figure 6.2 shows the average pore size, porosity (figure 6.2a) and electrolyte content (figure 6.2b) of the different membranes.

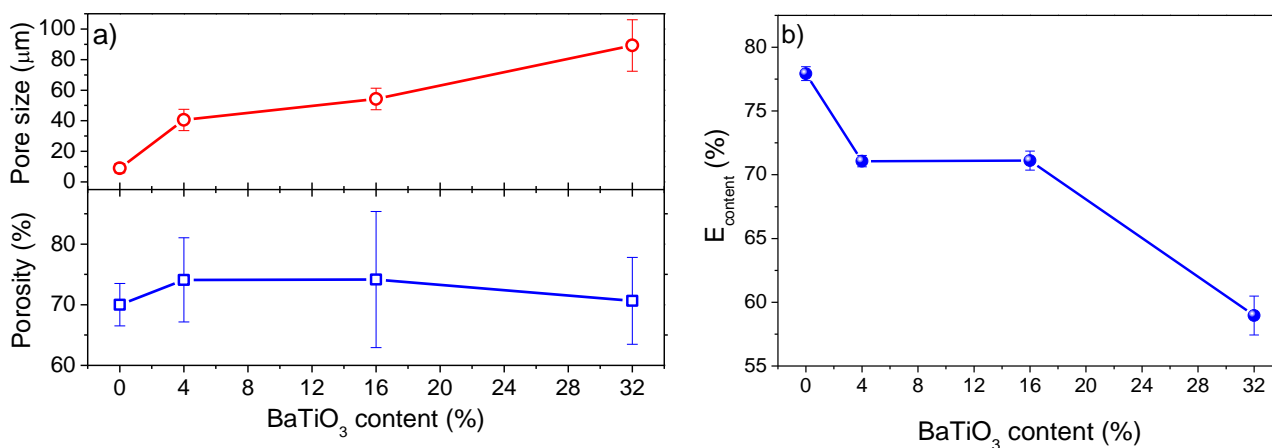


Figure 6.2: a) Average pore size and porosity and b) electrolyte content as function of BaTiO₃ content for all membrane.

Figure 6.2a shows that the pore size increases with increasing BaTiO₃ content, between a minimum of ~ 25 μm for the pure polymer to a maximum ~ 90 μm for the composite with 32 wt% of ceramic filler, which is to be ascribed to the filler effect on the bi-phase solvent-polymer phase diagram and therefore on the phase separation and solvent evaporation processes [37]. On the other hand, the porosity is not significantly affected, being the variations within experimental error.

Figure 6.2b shows that the electrolyte content decreases with increasing ceramic nanoparticles content, between approximately 76 and 59 %. Samples with higher

amounts of fillers have less free space in the pore cavities for the electrolyte liquid, resulting in lower electrolyte content. Further, larger pore sizes for a given degree of porosity leads to lower surface area for interaction between separator and electrolyte.

The results of the weight loss proved to be negligible. Losses over 60 min time do not show any significant variation due to the high evaporation temperature (242 °C) of the PC solvent of the electrolyte [38].

6.2.2. Polymer Phase and degree of crystallinity

Figure 6.3 shows the Fourier transformed infrared spectroscopy (FTIR) spectra and the differential scanning calorimetry (DSC) thermogram for membranes with different filler contents.

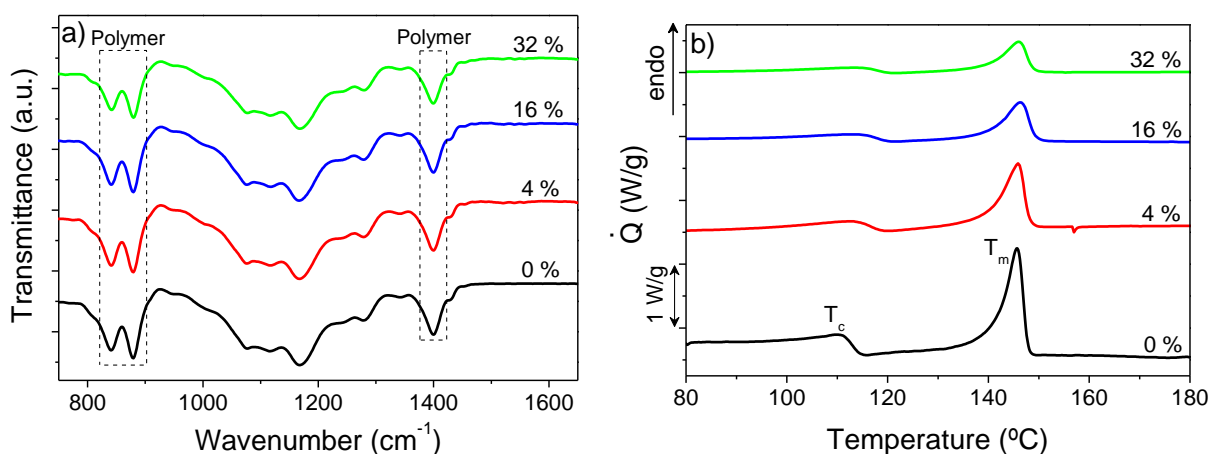


Figure 6.3: a) FTIR spectra of the BaTiO₃/P(VDF-TrFE) composites with different filler contents; b) DSC thermogram of membrane composites with different amounts of ceramic particles.

The infrared spectra shows that the presence of the fillers does not affect the characteristic vibration modes (851 cm⁻¹, 886 cm⁻¹ and 1402 cm⁻¹) of the all-trans configuration of the polymer matrix [39]. The polymer crystallizes therefore in the polar phase after the addition of BaTiO₃ ceramic particles. These characteristic vibration modes are also unaffected by the presence of electrolyte solution [21-22].

The thermograms of figure 6.3b show two endothermic peaks, the first around 117 °C, corresponding to the polymer ferroelectric to paraelectric transition (T_c) and the second around 146 °C corresponding to the polymer melting temperature (T_m) [40]. The addition of BaTiO₃ does not affect these reference temperatures of the polymer. In the

presence of electrolyte solution these parameters are also unaffected by the fillers [21-22].

Table 6.2 shows the degree of crystallinity of the composite membranes calculated by equation 2.1.

Table 6.2: Degree of crystallinity of the BaTiO₃/P(VDF-TrFE) membranes with different amounts of ceramic fillers.

Sample	$\chi_c \pm 2$ (%)
0 %	28
4 %	29
16 %	26
32 %	20

The table 6.2 shows that the degree of crystallinity of the composites membranes is lower than that of the pure polymer. The inclusion of fillers generally leads to an initial increase of the degree of crystallinity, as small filler contents can act as nucleation agents during the crystallization process. On the other hand, larger filler contents decrease the degree of crystallinity as ill crystallization of the polymer often occur in the presence of large content of ceramic fillers, that act as defects during the crystallization process [41].

6.2.3. Mechanical properties

Figure 6.4 shows the stress strain mechanical measurements for all the membranes after electrolyte solution uptake and the main parameters of the mechanical evaluation are summarized in table 6.3.

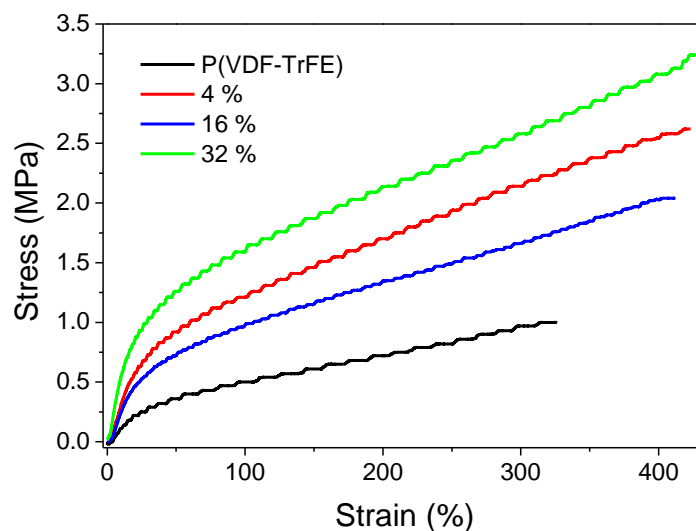


Figure 6.4: Stress-strain curves of the BaTiO₃/P(VDF-TrFE) composites with different ceramic nanoparticles contents after electrolyte solution uptake.

Table 6.3: Mechanical properties of the membranes with electrolyte solution uptake.

Sample	Yield Stress (MPa)	Elastic Modulus (MPa)	Stress at break (MPa)
0 %	0.3	1.9	1.0
4 %	0.9	3.0	2.6
16 %	0.7	2.8	2.0
32 %	1.3	5.4	3.2

The addition of BaTiO₃ to the polymer matrix affects the overall mechanical properties of the membranes. The yield stress, elastic modulus and stress at break show a slight increase in the composites membranes when compared to the pure polymer, indicating that ceramic particles mechanically reinforce the composite despite the decrease in crystallinity of the polymeric matrix [41-43]. In this sense the mechanical reinforcement effect by filler polymer interactions over impose any effect related to the variation in the degree of crystallinity. On the one hand, the proper wetting of the ceramic filler by the polymer, due to strong electrostatic interactions [41], lead to a mechanical reinforcement of the polymer within the composite, increasing the stress

values needed for a given deformation. On the other hand, the overall mechanical properties remain in same value range, being therefore determined by the microporous microstructure of the membranes.

6.2.4. Electrical response

Electrochemical impedance spectroscopy (EIS) was performed to evaluate the electrochemical properties of the membranes with electrolyte uptake. The results are presented through Nyquist plots (imaginary impedance Z'' versus real impedance Z' , figure 6.5a) and logarithmic ionic conductivity versus temperature (figure 6.5b).

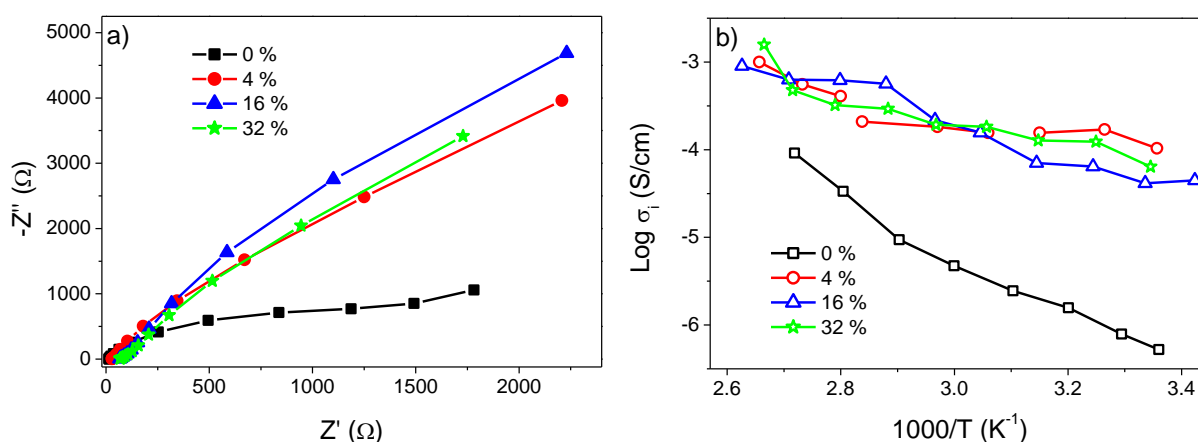


Figure 6.5: a) Nyquist plot for the BaTiO₃/P(VDF-TrFE) composites at 25 °C; b) $\text{Log } \sigma_i$ as a function of $1000/T$ for BaTiO₃/P(VDF-TrFE) composites with electrolyte solution uptake.

Table 6.4 shows the ionic conductivity (σ_i) and tortuosity (τ) at room temperature, obtained from equation 2.5 and 2.6 respectively.

Table 6.4: Room temperature ionic conductivity (σ_i) and tortuosity (τ) of the membranes filled with 1 M LiClO₄·3H₂O electrolyte solution; $\sigma_0 = 9.8$ mS/cm at 25 °C.

Sample	σ_i (S/cm)	τ
0 %	5.24×10^{-7}	114.9
4 %	1.04×10^{-4}	8.4
16 %	4.13×10^{-5}	13.4
32 %	6.40×10^{-5}	10.4

The Nyquist plot is characterized by three distinct regions: a semicircle at high frequencies corresponding to the charge transfer process, a straight line at low

frequencies related to the diffusion process and the transition between both [44-45]. In the Nyquist plot of figure 6.5a the high frequency semicircle appears only for the pristine polymer. It indicates that the fillers facilitate the charge transfer process due to the increase in ionic conductivity, as observed in figure 6.5b [46].

Figure 6.5b represents the ionic conductivity as function of temperature for the different membranes with electrolyte uptake. The ionic conductivity of the composite membranes is about two orders of magnitude higher than for the pure polymer (table 6.4), the ionic conduction is promoted by fillers through the increase of charge carriers and amorphous phase content in the composites (figure 6.3b and table 6.2). Furthermore, in the composite membranes the ionic conductivity is more stable in temperature [43].

Regarding tortuosity, composites present substantially lower values than the pure polymer. The tortuosity gives information about pore connectivity relating the mean actual path with direct sample thickness and it is often defined through the ionic conductivity [5]. Tortuosity of polymer composites is substantially lower than for the pure polymer, which indicates that the present of the fillers improve pore connectivity. The membrane with 4 wt% of BaTiO₃ shows the lower value of tortuosity, despite the differences between composite membranes being small, the obtained values suggest that for higher concentration pore blockage occurs as well as interface trapping of ions. An ideal porous body has tortuosity of ~ 1 , so the porous structure of composites is not far from the ideal value.

Table 6.5 represents the values of the activation energy of the conductive process.

Table 6.5: Activation energy (E_a) of the composite membranes with electrolyte solution uptake, determined after equation 2.7.

Samples	E_a (kJ/mol)
0 %	64
4 %	11
16 %	15
32 %	10

Table 6.5 shows that activation energy is lower and similar for all composite membranes, with respect to the pure polymer. The activation energy decreases substantially in composite membranes, which could be associated to the decrease of the

degree of crystallinity and the increase in the number of charge carriers, which leads to an increase of the ionic mobility.

The figure 6.6 presents the cyclic voltammetry for samples with different BaTiO₃ contents (figure 6.6a) and scan rates (figure 6.6b) used to evaluate the electrochemical stability of the membranes.

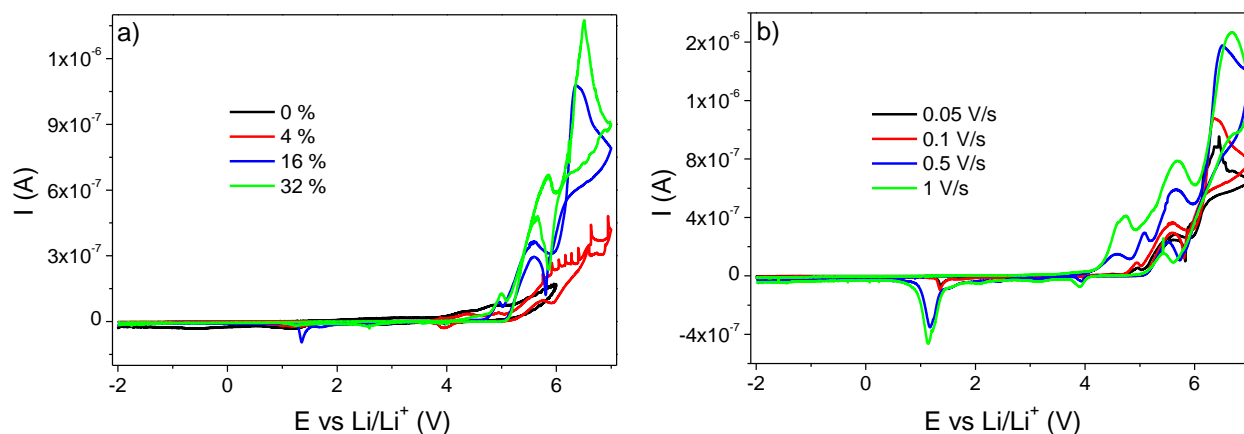


Figure 6.6: a) Voltammogram of BaTiO₃/P(VDF-TrFE) composites at 0.1 V/s with different filler contents; b) voltammogram of BaTiO₃/P(VDF-TrFE) with 16 wt% of ceramic particles with 100 nm in diameter at different scanning rates.

The voltammograms of fig 6.6a show stable operation windows between -2.0 and 4.0 V. The amount of fillers does not affect significantly the electrochemical stability, although composite membranes present a cathodic peak higher than the pure polymer around 6.0 V, probably due to charges accumulated at the interface between electrodes and sample [47]. The voltammograms of figure 6.6b also show stable operation windows between -2.0 and 4.0 V. For the higher scan rates, 0.5 and 1 V/s, an anodic peak appears around 1.0 V and the cathodic peaks around 6.0 V are higher than for lower speeds, since higher scan rates tends induce irreversible electrochemical processes [48]. Generally, the electrochemical stability of the membranes is determined by the electrolyte solution, so the presence of ceramic nanoparticles does not affect significantly the electrochemical behaviour. All membranes present a stable operation window at least 5.0 V amplitude, suitable for most common lithium-based couples, which have voltages of about 3.0 V [28]. The diffusion coefficient calculated by equation 2.8 through the maximum current value of the oxidative peak in the voltammograms of figure 6 shows an increase with increasing BaTiO₃ content. The

pristine polymer presents the lowest value of $2.85 \times 10^{-5} \text{ cm}^2/\text{s}$ and the membrane with 32 wt% of ceramic nanoparticles presents the highest value of $1.22 \times 10^{-4} \text{ cm}^2/\text{s}$, which is similar for the other composites; this effect is attributed to the increase of ionic charge carriers with the addition of fillers.

6.2.5. Particles size effect

In order to study the BaTiO₃ filler size effect in the membranes performance, membranes with 16 wt% filler content with 10, 100 and 500 nm average diameter were prepared. Figure 6.7 shows the SEM images for samples with different average filler size.

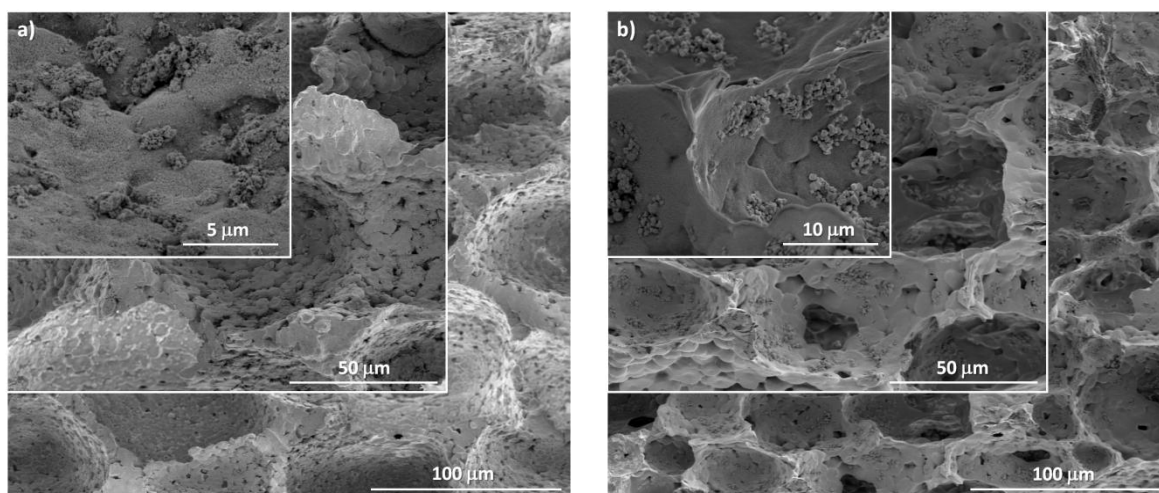


Figure 6.7: Cross section SEM images of BaTiO₃/P(VDF-TrFE) composites with 16 wt% of ceramic particles with filler sizes of a) 10 nm and b) 500 nm.

Figure 6.7 show that the different membranes present a homogeneous pore distribution unaffected by the size of the fillers. In all cases the fillers are lodged in the pore cavities, not being incorporated into the polymer matrix structure.

The influence of filler size in pore size, porosity and electrolyte content is presented in figure 6.8.

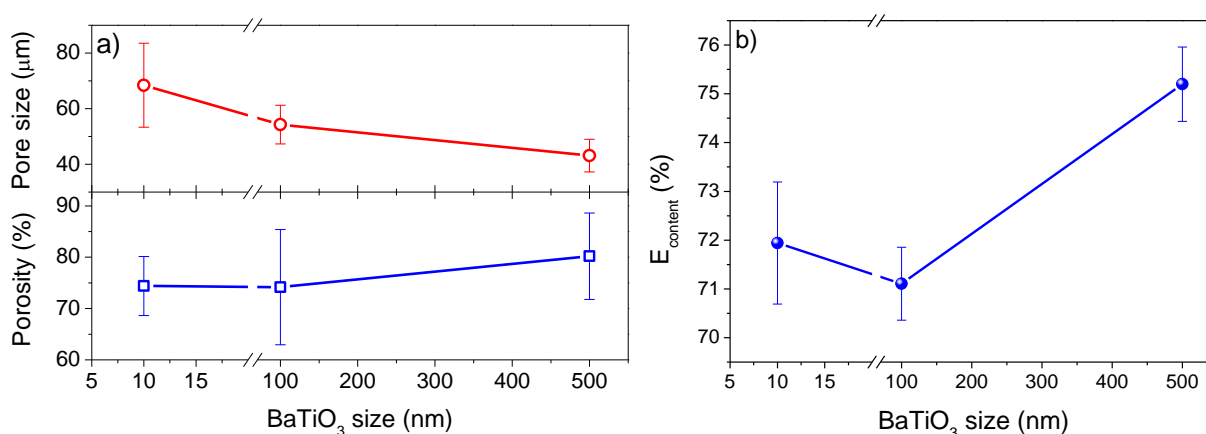


Figure 6.8: a) Average pore size and porosity and b) electrolyte content of membranes with 16 wt% of BaTiO₃ particles as a function of filler average diameter.

Concerning to the pore size (figure 6.8a), there is a decrease with increasing filler size, from a maximum of ~68 to a minimum of ~43 μm for 10 and 500 nm filler average diameter, respectively. During crystallization, the liquid-liquid phase separation of the composite membranes is influenced by ceramic particle size [49], the fillers with larger volume and lower surface area (100 and 500 nm) leading to a decrease of the average pore size.

The porosity (figure 6.8a) and electrolyte content (figure 6.8b), on the other hand, are affected by the size of the fillers. The porosity of the membranes increases and the pore size decreases with increasing ceramic size as shown in figure 6.8a. As the electrolyte content depends on the surface area-to-volume ratio and electrolyte-membrane interaction, the electrolyte content increases for increasing ceramic size.

In this sense the pore size, porosity and electrolyte uptake are affected by particle size and particle characteristic, such as crystalline phase (table 6.1).

Figure 6.9 presents information about the mechanical and electrical properties of the composite membranes: tensile stress strain, the impedance, ionic conductivity and the electrochemical behaviour.

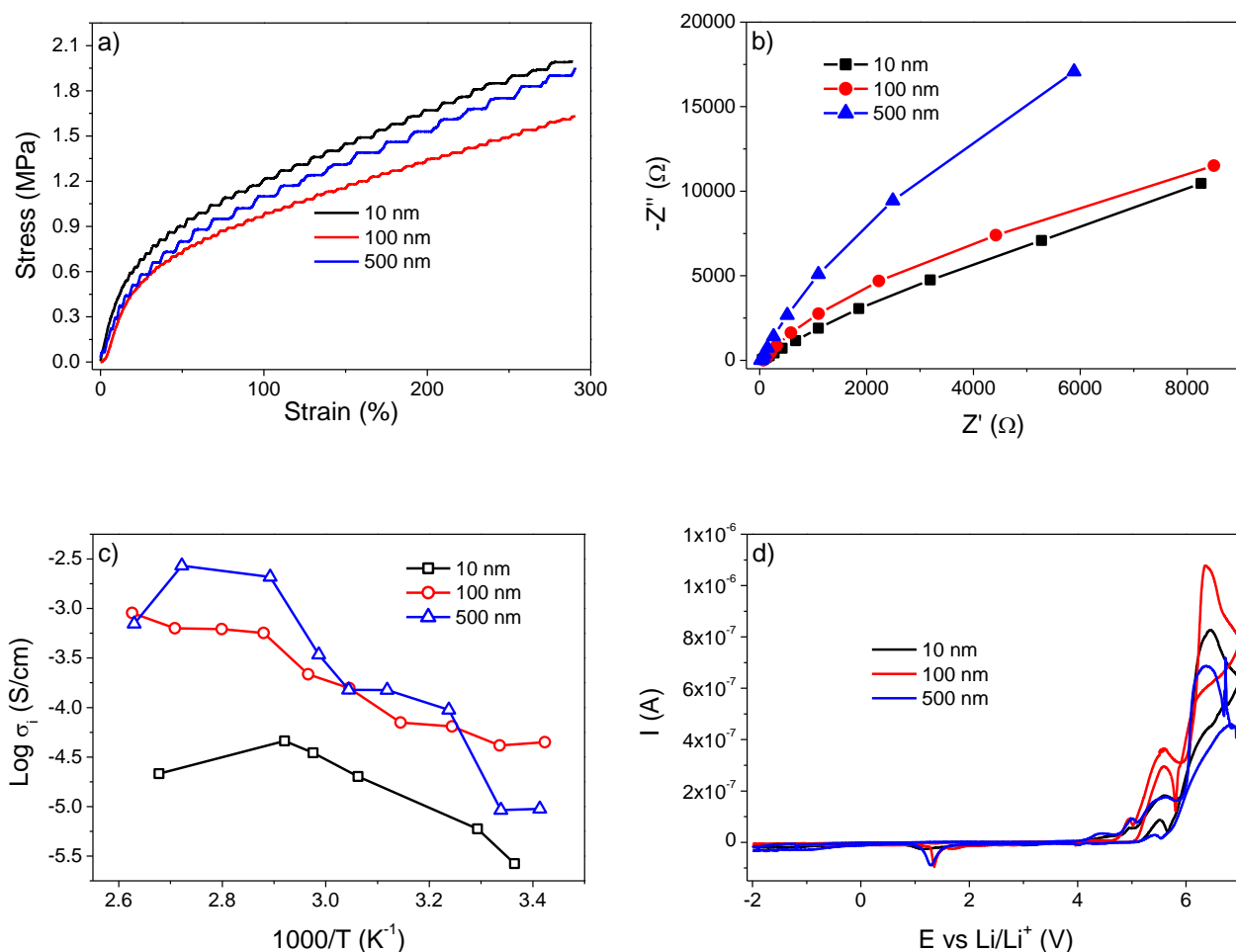


Figure 6.9: a) Tensile stress-strain measurements, b) Nyquist plot at 25 °C, c) $\text{Log } \sigma_i$ as a function of $1000/T$ and d) cyclic voltammetry, of BaTiO₃/P(VDF-TrFE) composites with 16 wt% filler content.

The figure 6.9a shows that the overall mechanical properties are very similar for all composites. The elastic modulus and yield stress are in the same value range for all membranes, 3-4 and 0.5 MPa respectively. Nevertheless, it is noted a dependence on ceramic size, due to better wetting and stronger electrostatic surface interactions of the polymer with the smaller ceramic particles, related to the larger surface to volume ratio (figure 6.9a).

In the Nyquist plot of figure 6.9b is notorious the absence of the high frequency semicircle, which also indicates higher ionic mobility for all ceramic size.

The ionic conductivity (figure 6.9c) is similar for the membranes with 500 and 100 nm average diameter fillers. This is an interesting fact as the 500 nm diameter filler presents ferroelectric properties due to the tetragonal crystallographic form, showing therefore a large polarity that could lead to larger interactions with the ions present in the electrolyte [50]. The lowest ionic conductivity is observed for the samples prepared with 10 nm fillers, so filler size appears to be the most relevant parameter influencing ionic conductivity due to increased filler surface area and, therefore, electrolyte-filler interaction.

The voltammograms presented in figure 6.9d show that all composite membranes have a stable operation window between -2.0 and 4.0 V, with a small reduction peak for all samples around 1.0 V.

Overall, it can be concluded that filler size, as well as filler content, is relevant and affects the performance of the membranes for Li-ion battery applications.

6.3. Conclusion

BaTiO₃/P(VDF-TrFE) porous membranes with different filler contents and sizes were prepared by thermally induced phase separation (TIPS). Filler inclusion leads to an increase in the pore size up to ~90 μm and in the porosity up to ~74 %. The inclusion of the fillers does not influence the phase of the polymer and the T_c and T_m remain unaltered with respect to the values found in the pristine polymer. The main effects of the fillers are a decrease of the degree of crystallinity to 20 %, a slight enhancement of the mechanical properties and an increase of the ionic conductivity from 5.24×10⁻⁷ to 1.04×10⁻⁴ S/cm for pristine polymer and 4 wt% filler content, respectively. The cyclic voltammetry reveals a stable operation window between -2.0 and 4.0 V vs Li/Li⁺ for all membranes. Filler size, on the other hand show relevant effects on membrane performance (ionic conductivity) despite a slight increase of pore size for the smaller particles. It can be concluded that BaTiO₃/P(VDF-TrFE) composite membranes show adequate morphological, thermal, mechanical and electrochemical properties for being used as separators in lithium ion batteries. Furthermore, the addition of Ø = 500 nm BaTiO₃ ceramic particles up to 4 % enhances the mechanical properties and increases

significantly the ionic conductivity without affecting the stable operation window of the membrane separators.

6.4. References

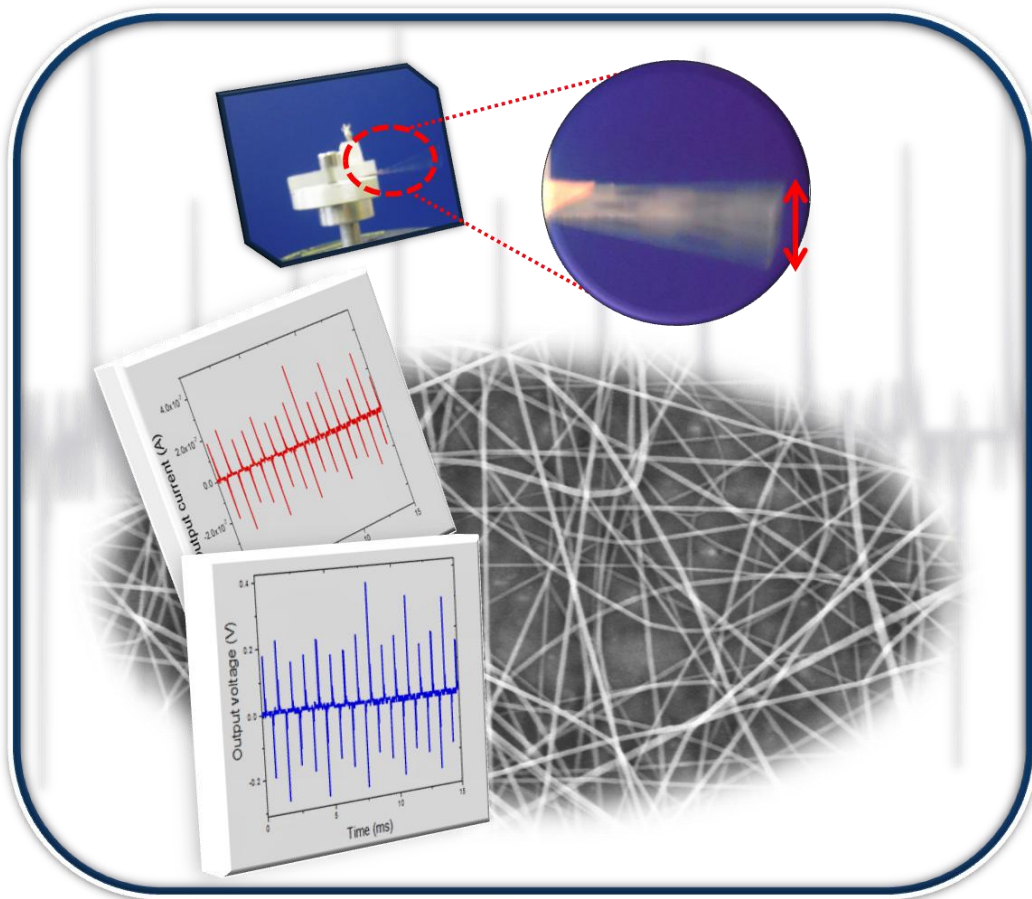
1. Tarascon, J.-M. *Key challenges in future Li-battery research*. Philosophical Transactions of the Royal Society A: Mathematical, Physical and Engineering Sciences, 2010. **368**(1923): p. 3227-3241.
2. Park, J.-K. *Principles and applications of lithium secondary batteries*. 2012, Weinheim: Wiley-VCH.
3. Tarascon, J.M. and M. Armand. *Issues and challenges facing rechargeable lithium batteries*. Nature, 2001. **414**(6861): p. 359-367.
4. Linden, D. and T.B. Reddy. *Handbook of batteries*. 2002, New York: McGraw-Hill.
5. Huang, X. *Separator technologies for lithium-ion batteries*. Journal of Solid State Electrochemistry, 2011. **15**(4): p. 649-662.
6. Arora, P. and Z. Zhang. *Battery Separators*. Chemical Reviews, 2004. **35**(50): p. 4419-4462.
7. Costa, C.M., J. Nunes-Pereira, L.C. Rodrigues, M.M. Silva, J.L.G. Ribelles, and S.Lanceros-Méndez. *Novel poly(vinylidene fluoride-trifluoroethylene)/poly(ethylene oxide) blends for battery separators in lithium-ion applications*. Electrochimica Acta, 2013. **88**(0): p. 473-476.
8. Ibrahim, S., S.M.M. Yasin, M.N. Ng, R. Ahmad, and M.R. Johan. *Impedance spectroscopy of carbon nanotube/solid polymer electrolyte composites*. Solid State Communications, 2011. **151**(23): p. 1828-1832.
9. Persi, L., F. Croce, B. Scrosati, E. Plichta, and M.A. Hendrickson. *Poly(ethylene oxide)-Based, Nanocomposite Electrolytes as Improved Separators for Rechargeable Lithium Polymer Batteries*. Journal of The Electrochemical Society, 2002. **149**(2): p. A212-A216.
10. Angulakshmi, N., K.S. Nahm, J.R. Nair, C. Gerbaldi, R. Bongiovanni, N. Penazzi, and A.M. Stephan. *Cycling profile of MgAl₂O₄-incorporated composite electrolytes composed of PEO and LiPF₆ for lithium polymer batteries*. Electrochimica Acta, 2013. **90**(0): p. 179-185.
11. Huai, Y., J. Gao, Z. Deng, and J. Suo. *Preparation and characterization of a special structural poly(acrylonitrile)-based microporous membrane for lithium-ion batteries*. Ionics, 2010. **16**(7): p. 603-611.
12. Liang, Y., Z. Lin, Y. Qiu, and X. Zhang. *Fabrication and characterization of LATP/PAN composite fiber-based lithium-ion battery separators*. Electrochimica Acta, 2011. **56**(18): p. 6474-6480.

13. Miao, Y.-E., G.-N. Zhu, H. Hou, Y.-Y. Xia, and T. Liu. *Electrospun polyimide nanofiber-based nonwoven separators for lithium-ion batteries*. Journal of Power Sources, 2013. **226**(0): p. 82-86.
14. Costa, C.M., L.C. Rodrigues, V. Sencadas, M.M. Silva, J.G. Rocha, and S. Lanceros-Méndez. *Effect of degree of porosity on the properties of poly(vinylidene fluoride–trifluoroethylene) for Li-ion battery separators*. Journal of Membrane Science, 2012. **407–408**(0): p. 193-201.
15. Costa, C.M., V. Sencadas, J.G. Rocha, M.M. Silva, and S. Lanceros-Méndez. *Evaluation of the main processing parameters influencing the performance of poly(vinylidene fluoride–trifluoroethylene) lithium-ion battery separators*. Journal of Solid State Electrochemistry, 2013. **17**(3): p. 861-870.
16. Costa, C.M., M.M. Silva, and S. Lanceros-Mendez. *Battery separators based on vinylidene fluoride (VDF) polymers and copolymers for lithium ion battery applications*. RSC Advances, 2013. **3**(29): p. 11404-11417.
17. Djian, D., F. Alloin, S. Martinet, and H. Lignier. *Macroporous poly(vinylidene fluoride) membrane as a separator for lithium-ion batteries with high charge rate capacity*. Journal of Power Sources, 2009. **187**(2): p. 575-580.
18. Huang, X. *Cellular porous polyvinylidene fluoride composite membranes for lithium-ion batteries*. Journal of Solid State Electrochemistry, 2013. **17**(3): p. 591-597.
19. Liu, J., W. Li, X. Zuo, S. Liu, and Z. Li. *Polyethylene-supported polyvinylidene fluoride–cellulose acetate butyrate blended polymer electrolyte for lithium ion battery*. Journal of Power Sources, 2013. **226**(0): p. 101-106.
20. Xiao, W., X. Li, H. Guo, Z. Wang, Y. Zhang, and X. Zhang. *Preparation of core–shell structural single ionic conductor SiO₂@Li⁺ and its application in PVDF–HFP-based composite polymer electrolyte*. Electrochimica Acta, 2012. **85**(0): p. 612-621.
21. Nunes-Pereira, J., A.C. Lopes, C.M. Costa, R. Leones, M.M. Silva, and S. Lanceros-Méndez. *Porous Membranes of Montmorillonite/Poly(vinylidene fluoride-trifluoroethylene) for Li-Ion Battery Separators*. Electroanalysis, 2012. **24**(11): p. 2147-2156.
22. Nunes-Pereira, J., A.C. Lopes, C.M. Costa, L.C. Rodrigues, M.M. Silva, and S. Lanceros-Méndez. *Microporous membranes of NaY zeolite/poly(vinylidene fluoride–trifluoroethylene) for Li-ion battery separators*. Journal of Electroanalytical Chemistry, 2013. **689**(0): p. 223-232.
23. Nalwa, H.S. *Ferroelectric polymers : chemistry, physics, and applications*. 1995, New York: Dekker.

24. Jung, S., D. Kim, S. Lee, M. Cheong, D. Nguyen, B. Cho, and H. Kim. *Fillers for Solid-State Polymer Electrolytes : Highlight*. Bull. Korean Chem. Soc., 2009. **30**(10): p. 2355-2361.
25. Nunes-Pereira, J., C.M. Costa, R. Leones, M.M. Silva, and S. Lanceros-Méndez. *Li-ion battery separator membranes based on poly(vinylidene fluoride-trifluoroethylene)/carbon nanotube composites*. Solid State Ionics, 2013. **249–250**(0): p. 63-71.
26. Moreno, M., R. Quijada, M.A. Santa Ana, E. Benavente, P. Gomez-Romero, and G. González. *Electrical and mechanical properties of poly(ethylene oxide)/intercalated clay polymer electrolyte*. Electrochimica Acta, 2011. **58**(0): p. 112-118.
27. Lee, L., S.-J. Park, and S. Kim. *Effect of nano-sized barium titanate addition on PEO/PVDF blend-based composite polymer electrolytes*. Solid State Ionics, 2013. **234**(0): p. 19-24.
28. Sun, H.Y., H.J. Sohn, O. Yamamoto, Y. Takeda, and N. Imanishi. *Enhanced Lithium-Ion Transport in PEO-Based Composite Polymer Electrolytes with Ferroelectric BaTiO₃*. Journal of The Electrochemical Society, 1999. **146**(5): p. 1672-1676.
29. Li, Q., N. Imanishi, Y. Takeda, A. Hirano, and O. Yamamoto. *PEO-based composite lithium polymer electrolyte, PEO-BaTiO₃-Li(C₂F₅SO₂)₂N*. Ionics, 2002. **8**(1-2): p. 79-84.
30. Cross, L.E. *Ferroelectric materials for electromechanical transducer applications*. Materials Chemistry and Physics, 1996. **43**(2): p. 108-115.
31. Roberts, S. *Dielectric and Piezoelectric Properties of Barium Titanate*. Physical Review, 1947. **71**(12): p. 890-895.
32. Damjanovic, D., F. Brem, and N. Setter. *Crystal orientation dependence of the piezoelectric d₃₃ coefficient in tetragonal BaTiO₃ as a function of temperature*. Applied Physics Letters, 2002. **80**(4): p. 652-654.
33. Mostaghaci, H. and R.J. Brook. *Microstructure development and dielectric properties of fast-fired BaTiO₃ ceramics*. Journal of Materials Science, 1986. **21**(10): p. 3575-3580.
34. Chao, F. and C. Liangyan. *Domain structure of nano BaTiO₃ ceramic described by a second-order transition model*. in *Computer Science and Automation Engineering (CSAE), 2012 IEEE International Conference on*. 2012.
35. Nanoamor[®]. *Nanostructured & Amorphous Materials, Inc.* 2001 [cited 2013; Available from: <http://www.nanoamor-europe.com/catalogsearch/result/?q=barium+titanate>].

36. California, A., V.F. Cardoso, C.M. Costa, V. Sencadas, G. Botelho, J.L. Gómez-Ribelles, and S. Lanceros-Méndez. *Tailoring porous structure of ferroelectric poly(vinylidene fluoride-trifluoroethylene) by controlling solvent/polymer ratio and solvent evaporation rate*. European Polymer Journal, 2011. **47**(12): p. 2442-2450.
37. Ferreira, A., J. Silva, V. Sencadas, J.L.G. Ribelles, and S. Lanceros-Méndez. *Poly[(vinylidene fluoride)-co-trifluoroethylene] Membranes Obtained by Isothermal Crystallization from Solution*. Macromolecular Materials and Engineering, 2010. **295**(6): p. 523-528.
38. Xu, K. *Nonaqueous Liquid Electrolytes for Lithium-Based Rechargeable Batteries*. Chemical Reviews, 2004. **104**(10): p. 4303-4418.
39. Prabu, A.A., J.S. Lee, K.J. Kim, and H.S. Lee. *Infrared spectroscopic studies on crystallization and Curie transition behavior of ultrathin films of P(VDF/TrFE) (72/28)*. Vibrational Spectroscopy, 2006. **41**(1): p. 1-13.
40. Sencadas, V., S. Lanceros-Méndez, and J.F. Mano. *Thermal characterization of a vinylidene fluoride-trifluoroethylene (75–25) (%mol) copolymer film*. Journal of Non-Crystalline Solids, 2006. **352**(50–51): p. 5376-5381.
41. Costa, C.M., S. Firmino Mendes, V. Sencadas, A. Ferreira, R. Gregorio Jr, J.L. Gómez Ribelles, and S. Lanceros-Méndez. *Influence of processing parameters on the polymer phase, microstructure and macroscopic properties of poly(vinylidene fluoride)/Pb(Zr_{0.53}Ti_{0.47})O₃ composites*. Journal of Non-Crystalline Solids, 2010. **356**(41–42): p. 2127-2133.
42. Vacche, S., F. Oliveira, Y. Leterrier, V. Michaud, D. Damjanovic, and J.-A. Manson. *The effect of processing conditions on the morphology, thermomechanical, dielectric, and piezoelectric properties of P(VDF-TrFE)/BaTiO₃ composites*. Journal of Materials Science, 2012. **47**(11): p. 4763-4774.
43. Ulaganathan, M., R. Nithya, and S. Rajendran. *Surface Analysis Studies on Polymer Electrolyte Membranes Using Scanning Electron Microscope and Atomic Force Microscope*, in *Scanning Electron Microscopy*. 2012.
44. Chang, B.-Y. and S.-M. Park. *Electrochemical Impedance Spectroscopy*. Annual Review of Analytical Chemistry, 2010. **3**(1): p. 207-229.
45. Park, M., X. Zhang, M. Chung, G.B. Less, and A.M. Sastry. *A review of conduction phenomena in Li-ion batteries*. Journal of Power Sources, 2010. **195**(24): p. 7904-7929.
46. Ulaganathan, M. and S. Rajendran. *Studies on MWCNT-Incorporated Composite Polymer Electrolytes for Electrochemical Applications*. Soft Materials, 2010. **8**(4): p. 358-369.

47. Nissen, D.A. *A Study of the Anode-Electrolyte Interface in a Thermal Battery*. Journal of The Electrochemical Society, 1979. **126**(2): p. 176-180.
48. Brett, A.M.C.F.O. and C.M.A. Brett. *Electroquímica : princípios, métodos e aplicações*. 1996, Coimbra: Almedina.
49. Nakanishi, K. and N. Soga. *Phase Separation in Gelling Silica–Organic Polymer Solution: Systems Containing Poly(sodium styrenesulfonate)*. Journal of the American Ceramic Society, 1991. **74**(10): p. 2518-2530.
50. Hsiang, H.-I. and F.-S. Yen. *Effect of Crystallite Size on the Ferroelectric Domain Growth of Ultrafine BaTiO₃ Powders*. Journal of the American Ceramic Society, 1996. **79**(4): p. 1053-1060.



7 - Energy harvesting performance of PVDF based electrospun fibers

This chapter is based on the following publication:

Nunes-Pereira, J., V. Sencadas, V. Correia, J.G. Rocha, and S. Lanceros-Méndez. *Energy harvesting performance of piezoelectric electrospun polymer fibers and polymer/ceramic composites*. *Sensors and Actuators A: Physical*, 2013. **196**: p. 55-62.

7.1. Introduction

Energy harvesting from mechanical vibrations has become increasingly important over the last years [1-3] mainly due to low power requirement of small electronic components, such as wireless sensor networks used in monitoring applications. Powering small electronics using the vibrational energy available in their environment could reduce the requirement of external power sources, like batteries, and thus avoiding the associated maintenance costs [1-3].

There are three basic vibration-to-electrical conversion mechanisms: electromagnetic, electrostatic and piezoelectric transductions [3-4]. Piezoelectric transduction has received the largest attention when compared to the other transductions systems due to its main advantages, such as large power density, easy application (piezoelectric devices could be fabricated both in macro and micro scale due to well established production techniques), and that the output voltage is obtained directly from piezoelectric material itself, that suppresses the requirement of an external voltage input [1].

The energy conversion in piezoelectric materials is based on variations in the dipolar moment when a strain is applied and therefore the formation of a potential difference that can be used to power devices [3].

In recent years a large efforts has been developed focused in improving the efficiency of piezoelectric power harvesting systems. The most common type of piezoelectrics used for power harvesting are ceramics like lead zirconate titanate (PZT) or BaTiO_3 [3]. Nevertheless, piezoceramics are susceptible to fatigue crack when subjected to high frequency cyclic loading, which created the need to search for alternatives as poly(vinylidene fluoride) (PVDF), a piezoelectric polymer with high flexibility when compared with ceramics materials [5-7].

PVDF and poly(vinylidene fluoride-*co*-trifluoroethylene) (P(VDF-TrFE)) copolymer have attracted scientific and technological interest due to their chemical resistance, good mechanical properties and excellent electroactive properties. P(VDF-TrFE) has a ferroelectric to paraelectric (FE-PE) phase transition at a Curie temperature (T_c) that occurs in the bulk material at temperatures melting temperature (T_m), and has a large electromechanical coupling coefficient at room temperature [8-9].

PVDF and VDF copolymers crystalline structures in the ferroelectric phase are packed in an “all-trans”, TTT, planar zigzag polymer chain configuration [8]. In (VDF-TrFE), the paraelectric crystalline structure above T_c is hexagonal, essentially consisting in a statistical configuration of TT, TG and TG' rotational isomers [10]. The FE-PE transition temperature is highly dependent upon VDF content, but other factors such as heat treatments, electrical poling and processing history can also affect the transition [11-13].

New research fields are emerging based on the exploration of the nanoscale properties of such materials improving the possibilities of piezoelectric materials become a real choice for energy harvesting devices [14]. In this sense, it was reported a nanogenerator, based on PZT aligned nanofibers on a silicon substrate with interdigitated electrodes, which reaches an output voltage peak of 1.63 V and a power generation of 0.03 μ W [15] and another piezoelectric nanogenerator based on BaTiO₃ on plastic substrate connected by interdigitated electrodes [16] with an output voltage up to 1.0 V and a power density of ~ 7 mW/cm³. This later nanogenerator needs extra poling treatment after processing in order to enhance the piezoelectric properties of the materials. Output voltages of nearly 40 V after poling has been reported for micropower harvesters based on PZT/PVDF and PZT/PP, [17] but the generated power was not reported.

Polymer nanofibers offer the possibility to tailor materials properties and increase performance for a number of applications, including energy generation and storage. Micro and nanofibers can be produced by several techniques such as drawing, template synthesis, phase separation self-assembly and electrospinning, [18] the latter is the most straightforward, convenient and scalable technique for nanomaterials production, [18-19] allowing the production of continuum fibers with diameters of a hundreds of nanometers up to few micrometers [20]. Electrospinning is process for producing nanofibers by forcing a viscous solution through a spinneret subjected to an electric field. Crossing the spinneret the solution drips and the high applied voltage leads the drop into an elongated cone; with appropriated viscosity and surface tension a stable solution jet erupts from the solution droplet. The process makes use of fluid applied charges to provide a stretching force to a collector where is a potential gradient. This mechanism ensures the fibers polarization [18, 21].

Several parameters have influence in electrospun fibers morphology and properties and can be divided in three main groups: initial polymer solution, jet formation and finally the collection procedure [18].

Electrospun piezoelectric nanofibers offers excellent flexibility and improved strength, so it is expected their exploitation in a wide variety of applications [22]. Generators based on randomly electrospun PVDF fibers have been developed [23] that when submitted to periodic oscillations between 1 and 10 Hz achieved output voltages between 0.43 and 6.3 V. The reported current, around 5 μA , seems to be too high for an insulating material such as PVDF. Even so, the output power generated was around 0.03 μW [24].

PZT and BaTiO_3 are known to be excellent piezoelectric materials, with high dielectric and piezoelectric values [25-26]. It seems interesting in this way to explore the possibility to prepare electrospun composite fibers of PVDF and P(VDF-TrFE) with BaTiO_3 on top of an interdigitated circuit in a single step process (no poling of the fibers is further needed) in order to study the influence of the ceramic filler in the energy harvesting efficiency of the polymer. In this way, both the influence of the processing parameters on the fiber characteristics and the nanogenerator performances will be addressed.

7.2. Results and discussion

7.2.1. Morphology

The influence of the electrospun processing parameters on average PVDF [27] and P(VDF-TrFE) [28] fibers size and characteristics such as electroactive phase content and degree of crystallinity have been study previously, and this section will focus on the composite fibers. The influence of the applied electric field in the $\text{BaTiO}_3/\text{P(VDF-TrFE)}$ electrospun fibers nanocomposites has been evaluated keeping constant the needle inner diameter of 0.5 mm and the flow rate of 0.5 mL/h.

Generally, BaTiO₃/P(VDF-TrFE) electrospun membranes show a random distribution and smooth, and bead free fibers with average diameter of 450 ± 100 nm (figure 7.1).

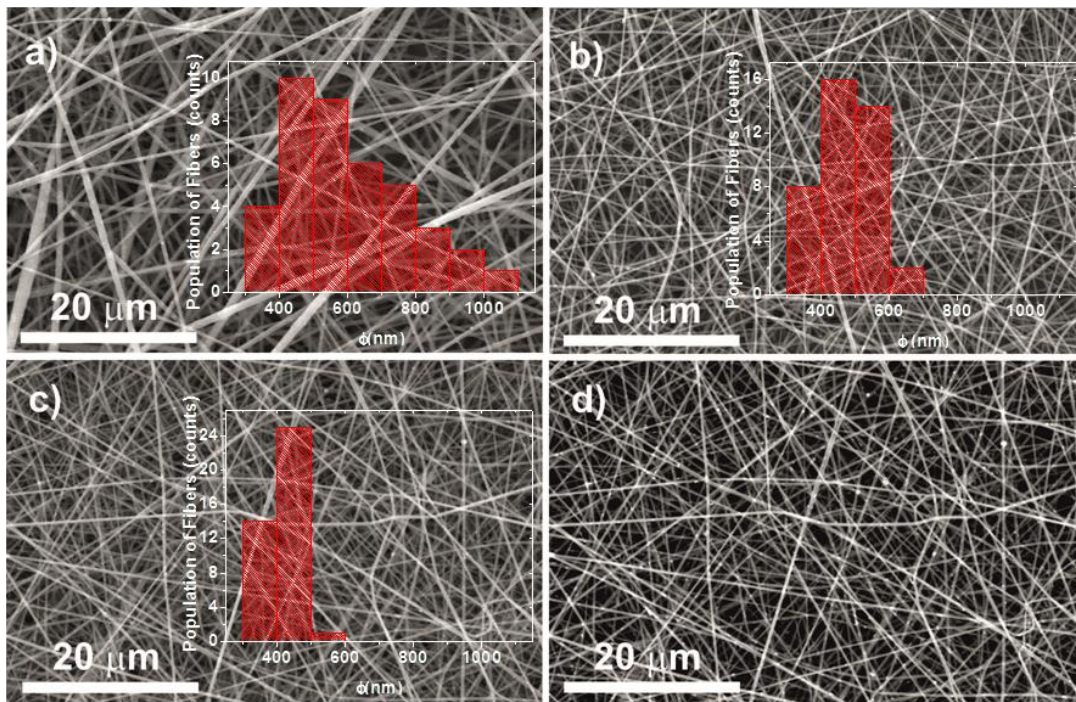


Figure 7.1: BaTiO₃/P(VDF-TrFE) electrospun membrane obtained at 15/85 polymer/solution and with 5 % BaTiO₃ nanoparticles with particle size of $\phi = 100$ nm: a) 20 kV, b) 35 kV, c) 25 kV and d) backscattering image of sample obtained at 25 kV (image b). Traveling distance of 20 cm, needle inner diameter of 0.5 mm and flow rate of 0.5 mL/h.

A histogram of the fiber diameter distribution was obtained through scanning electron microscopy (SEM) images and the fiber average diameter was obtained from 40 measurements of the nanofibers present in each image.

Following a similar procedure, from the systematic variation of the other main parameters affecting the electrospinning process their influence on the average fiber diameter has been obtained (figure 7.2).

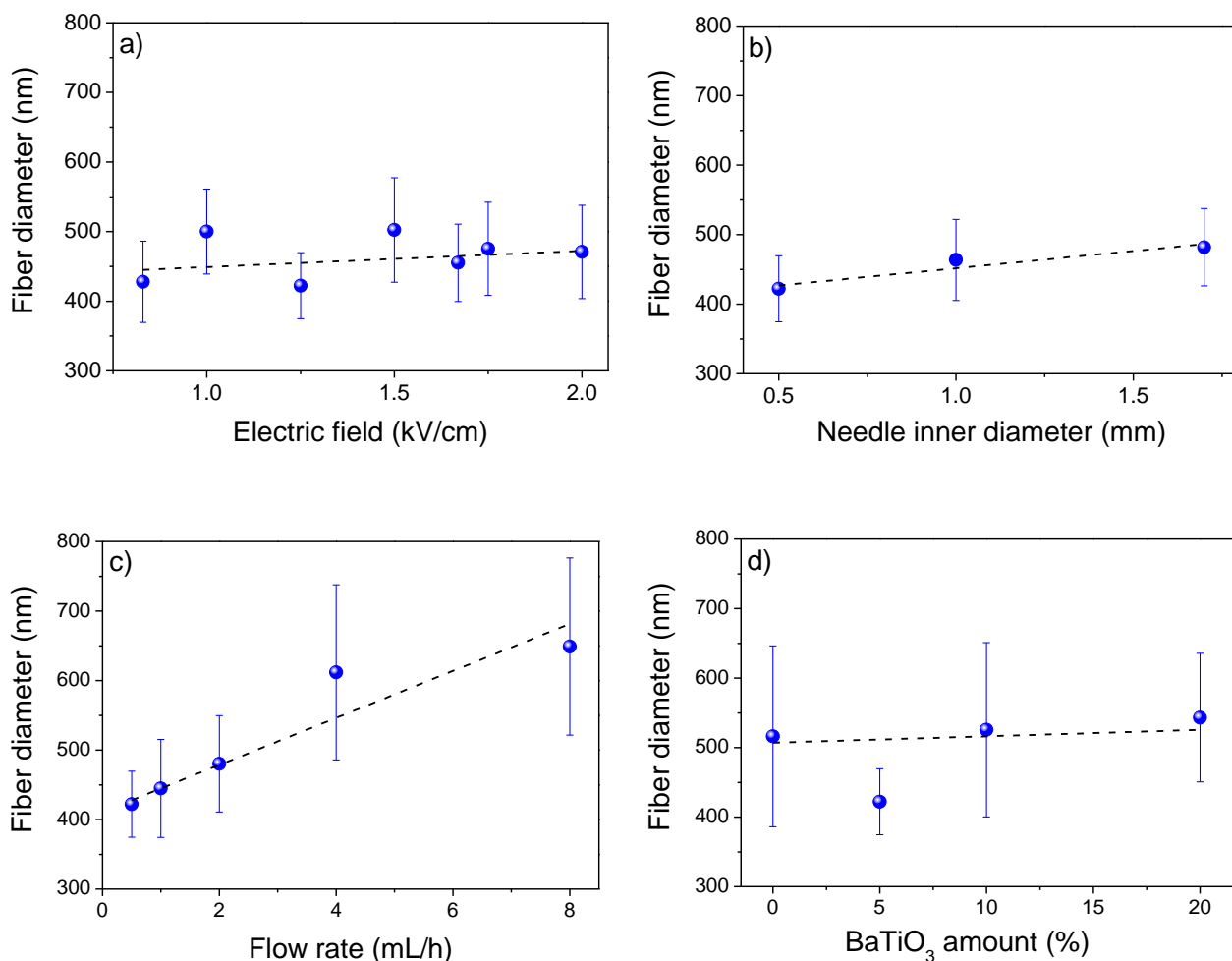


Figure 7.2: a) Influence of applied electric field on the mean diameter of the electrospun BaTiO₃/P(VDF-TrFE) fibers, the flow rate was 0.5 mL/h and needle inner diameter of 0.5 mm; b) Influence of tip inner diameter on the mean diameter of the electrospun BaTiO₃/P(VDF-TrFE) fibers, the flow rate was 0.5 mL/h and applied electric field of 1.25 kV/cm; c) Influence of flow rate on the mean diameter of the electrospun BaTiO₃/P(VDF-TrFE) fibers, the tip inner diameter was 0.5 mm and the applied electric field of 1.25 kV/cm; d) Influence of BaTiO₃ content on the fiber mean diameter for the electrospun BaTiO₃/P(VDF-TrFE) membrane, the tip inner diameter was 0.5 mm, applied electric field of 1.25 kV/cm and a flow rate of 0.5 mL/h. Average filler size: $\varnothing = 100$ nm; filler concentration in a), b) and c) 5 %.

It was observed that the applied electric field does have no influence on the fiber diameter and distribution (figure 7.2a). On other hand, for a constant applied electric field, flow rate and for the same polymer/ceramic concentration, an increase of the average fiber diameter was observed with the increase of the needle inner diameter (figure 7.2b).

Fiber average diameter and its distribution are strongly affected by the flow rate, demonstrated by an increase of the mean fiber diameter from 422 ± 27 nm to 649 ± 127 nm by increasing the flow rate from 0.5 mL/h to 8 mL/h (figure 7.2c). Feed rate determines the amount of solution available at the needle tip for electrospinning. When feed rate increases, there is a corresponding increase on the fiber diameter due to the larger volume of solution that is drawn away from the needle tip [18].

It was interesting to note that the inclusion of ceramic BaTiO₃ nanoparticles in the polymer solution does not influence the fiber average diameter and distribution (figure 7.2d).

The effect of BaTiO₃ particle average diameter in the fiber size and distribution was characterized for ceramic particles with 10, 100 and 500 nm (figure 7.3) for the fibers with 20 % BaTiO₃ volume content. All membranes show no polymer beads, however some particle clusters were identified as result of the large ceramic content for the given fiber average diameter.

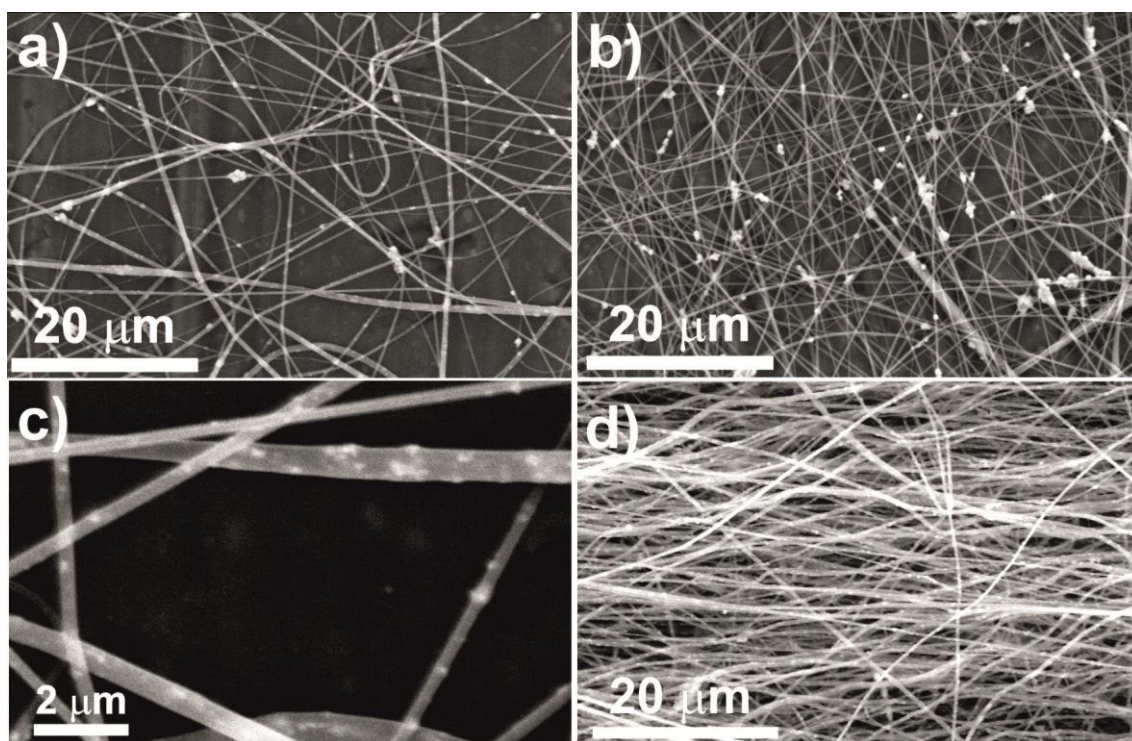


Figure 7.3: Influence of BaTiO₃ particle average size in the composite fiber diameter: a) 10 nm, b) 500 nm, c) backscattering image of electrospun fibers with 20 % BaTiO₃ ($\phi = 100$ nm) and d) electrospun BaTiO₃/P(VDF-TrFE) (20 % BaTiO₃ and $\phi = 100$ nm) membrane obtained at 750 rpm. For all samples, tip inner diameter was 0.5 mm, applied electric field of 1.25 kV/cm and a flow rate of 0.5 mL/h.

With respect to the particle average size, particles with a mean diameter lower than 100 nm are trapped inside the fiber (figure 7.3a and d), but the particles with an

average diameter of 500 nm are randomly dispersed out and inside the fibers due to the fact that the fiber average diameter is smaller than the BaTiO₃ single particles and clusters (figure 7.3b). The average fiber diameter for the BaTiO₃/P(VDF-TrFE) composites with 10 nm particles diameter is 469 ± 136 nm, for the composite with 100 nm particles is 543 ± 92 nm and for the membrane with 500 nm particles size shows an mean diameter of 377 ± 70 nm, which is smaller than the particles itself making impossible entrapment of the filler inside the polymer fiber (figure 7.3).

The sample obtained in the drum collector (figure 7.3d) presents a preferential fiber orientation with an average fiber diameter of 525 ± 126 nm and with a compact structure. For randomly and aligned fibers, it was noted that composites fibers are uniformly filled with discontinuous ceramic particles that are essentially inside of the fibers giving origin to a self-assemble BaTiO₃ fiber morphology (figure 7.3c and d). This preferential arrangement of electroactive ceramic particles is probably due to the difference of specific density between the polymer matrix and the filler.

7.2.2. Polymer phase and crystallinity

The nature of the polymer crystalline phase present in the electrospun BaTiO₃/P(VDF-TrFE) fibers can be identified by Fourier transformed infrared spectroscopy (FTIR) (figure 7.4a) and by differential scanning calorimetry (DSC) (figure 7.4b).

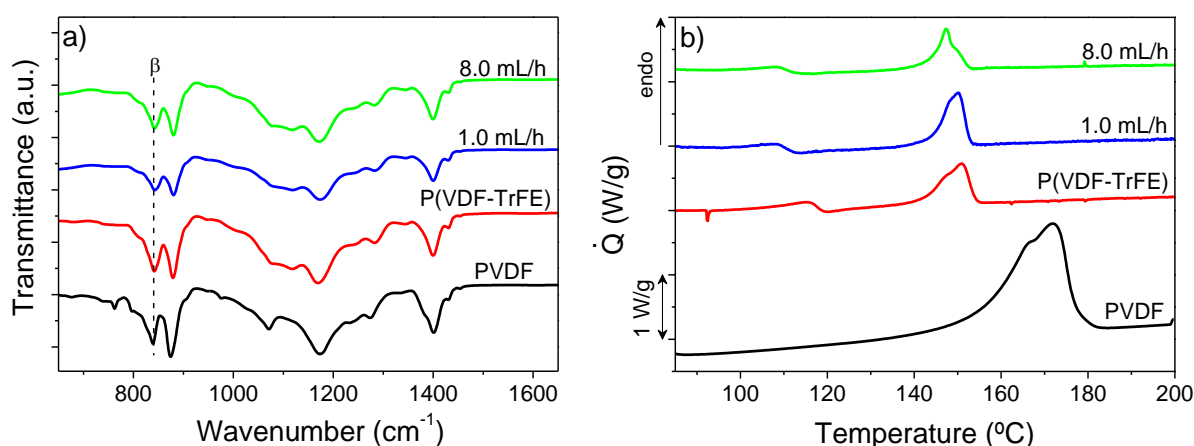


Figure 7.4: a) Infrared measurements for the PVDF and BaTiO₃/P(VDF-TrFE) electrospun membranes with a tip inner diameter of 0.5 mm, applied voltage of 25 kV, distance between tip and collector of 20 cm and a flow rate of 1.0 and 8.0 mL/h; b) DSC results for the PVDF and BaTiO₃/P(VDF-TrFE) electrospun membranes with a tip inner diameter of 0.5 mm, applied voltage of 25 kV and a distance between tip and collector of 20 cm and a flow rate of 1.0 and 8.0 mL/h.

FTIR spectra showed that nanocomposite crystallization occurs in the polymer ferroelectric phase due to the presence of the characteristic absorption band at 840 cm^{-1} [27] (figure 7.4a). It was observed that changes in electrospinning processing conditions do not affect polymer crystallization, because any suppression of polymer absorption bands was noted.

Poly(vinylidene-fluoride) DSC thermogram shows a peak around $160\text{ }^{\circ}\text{C}$ which corresponds to the melting temperature of the polymer (figure 7.4b). The DSC thermogram of the P(VDF-TrFE) shows two characteristic peaks: the one at lower temperatures corresponds to the ferroelectric-paraelectric transition and occurs around $117\text{ }^{\circ}\text{C}$, the second peak correspond to the melting of the paraelectric phase and is located around $145\text{ }^{\circ}\text{C}$ (figure 7.4b). The DSC thermograms of $\text{BaTiO}_3/\text{P(VDF-TrFE)}$ composites show the same two peaks, located at the same temperatures, which confirms that changes in the electrospinning conditions does not change the ferroelectric polymer phase. The inclusion of different filler contents also does not affect the polymer polar phase, as has been demonstrated in previous works [29].

7.2.3. Energy harvesting response

Piezoelectric properties are being used for sensors and actuators as well as for energy harvesting applications, taking advantage of nanoscale materials such as nanowires, nanorods and nanofibers from PZT, BaTiO_3 or ZnO [15-16, 22].

It has been demonstrated the capability of PVDF film, [17] PZT [15] and BaTiO_3 [16] fibers as energy harvesters once the materials have been processed and poled. It was also demonstrated that the electrospinning process results in electrically poled fibers in a single step production process due to the high electric field involved during the processing stage [28].

$\text{BaTiO}_3/\text{P(VDF-TrFE)}$ composite fiber as well as pure PVDF and P(VDF-TrFE) electrospun fibers were directly spun into a interdigitated array (figure 7.4b) at an electric field of 1.25 kV/cm , a needle inner diameter of 0.5 mm and a flow rate of 1

mL/h. It was observed previously by Sencadas *et al.* that the PVDF electrospun fibers are poled when the fiber travel from the needle to the collector [28], and is unnecessary to perform an extra poling procedure after fiber processing. Electrospun samples were submitted to a periodic bending oscillation at different frequencies. The energy harvesting device was then submitted to mechanical excitations in the frequency range between 1 Hz to 1 kHz using an electromechanical vibration generator (figure 2.3c), in which the polymer and polymer/ceramic fibers are working in longitudinal mode with the alternating pressure results in surface charge variations in the fibers due to their combined tensile and bending stresses. A voltage difference between two adjacent electrodes is thereby induced; interdigitated electrodes enhance the power output of the generator as the piezoelectric fibers between each pair of adjacent electrodes results in a power generating unit connected in parallel to other units.

In order to align the fibers, the interdigitated electrodes were grounded on two terminals in a process similar to the one suggested by Ramakrishna *et al.* [18]. The distance between the anode and the cathode was about 0.5, 0.2 and 0.1 mm as showed in figure 2.3b.

The piezoelectric fiber generators were tested under two different conditions. In the first one, the output voltage of the PVDF, P(VDF-TrFE) and BaTiO₃/P(VDF-TrFE) (20 % ceramic loading at the different filler average sizes) electrospun fibers was measured by applying a periodic deformation at different frequencies.

As presented in figure 7.5, the generated voltage induced by piezopotential reached ~ 150 mV for the PVDF fibers. On the other hand, P(VDF-TrFE) fibers showed a maximum piezopotential around 110 mV and the electrical output voltage measured for the BaTiO₃/P(VDF-TrFE) electrospun fibers decreases with increasing ceramic particle average diameter for a fixed fiber loading. An average piezopotential of ~ 100 mV was found for the fibers with BaTiO₃ particles of ~ 10 nm, which is higher to the one found for the pure polymer matrix, the piezopotential strongly decreases with increasing filler size (figure 7.5c).

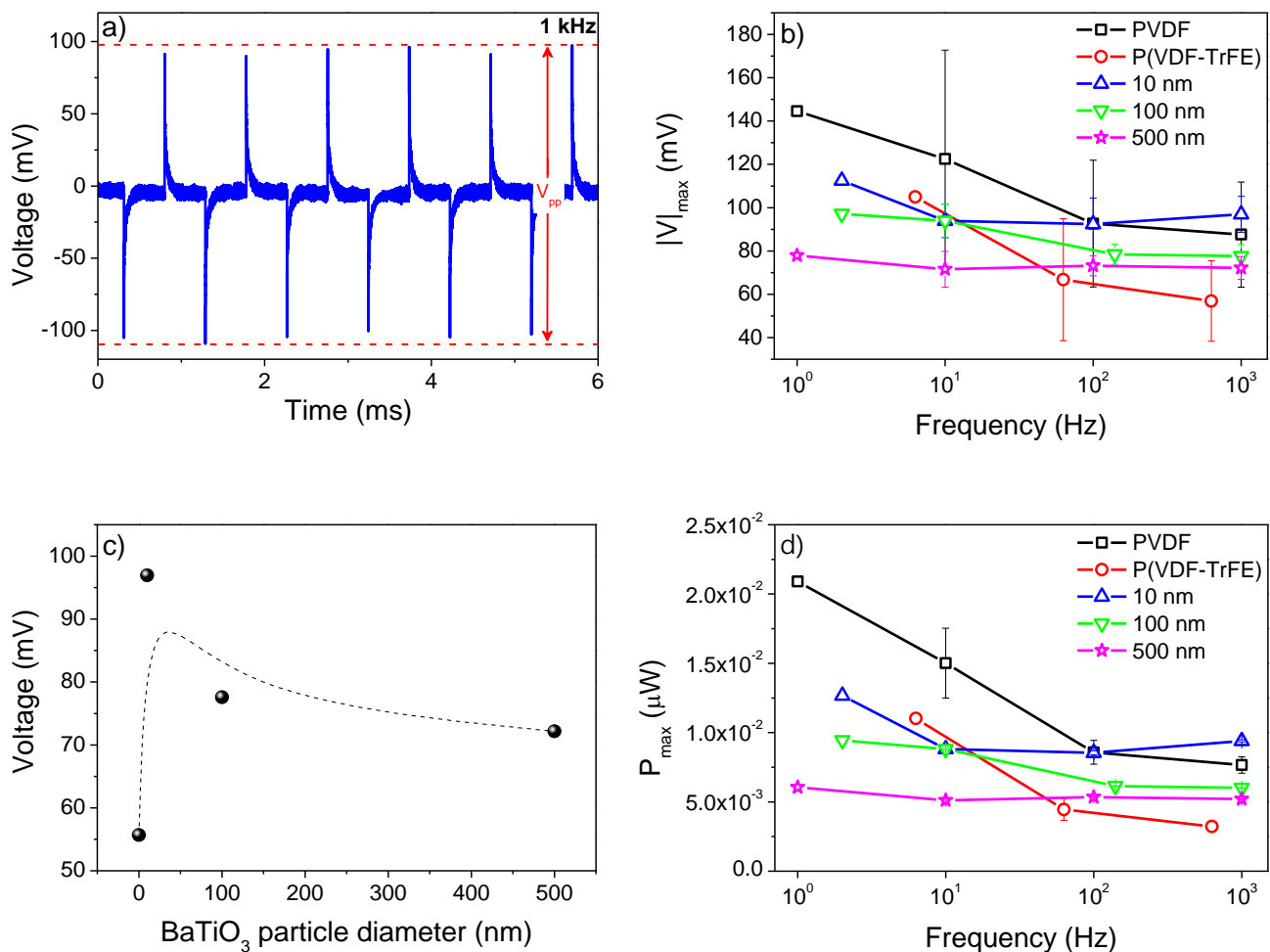


Figure 7.5: Voltage generated during 6 ms at a frequency of 1 kHz, of an electrospun sample of BaTiO₃/P(VDF-TrFE) with 20 % of ceramic 10 nm; b) maximum voltage generated at different frequencies for all type of samples produced; c) piezopotential obtained at 1 kHz for P(VDF-TrFE) and BaTiO₃/P(VDF-TrFE) with 20 % ceramic filler and d) maximum power generated by the electrospun membranes as a function of frequency.

The negative voltage signal observed in figure 7.5a is generated by reverse flowing carriers when the external load is removed and the piezopotential vanishes. The

fibers generated power promoted by the periodic harmonic vibration can be calculated through equation 2.9.

In this setup, where the fibers are attached to each pair of adjacent electrodes, the piezoelectric coefficient that mostly contributes for the electrical output voltage is the one along the fiber longitudinal direction, commonly denominated as d_{31} , where the polymer chains are stretched along the fiber and the output electrical signal is measured in the thickness direction.

Goldfard and Jones [30] investigated the efficiency of a piezoelectric material in a stack configuration for converting mechanical harmonic excitation into electric energy. In general, the conversion efficiency can be improved with a larger coupling coefficient and smaller damping. Table 7.1 shows the characteristic electroactive properties of PVDF, P(VDF-TrE) and BaTiO₃.

Table 7.1: Characteristic physical properties of electroactive PVDF, P(VDF-TrFE) and BaTiO₃ [26, 31].

	PVDF	P(VDF-TrFE)	BaTiO ₃
d_{31} (pC/N)	8 - 22	12	-34
d_{33} (pC/N)	-24 to -34	-38	125
k_{33}	0.20	0.29	12.6
ϵ'	6 - 12	18	1700

Table 7.1 shows that piezoelectric coefficients of the ceramic filler and its electromechanical coupling coefficient are larger than pure polymer and therefore will tend to increase electromechanical conversion and power output. On the other hand, the electromechanical system can be modeled by a coupled spring-mass-damper system, [32] and in the case of the BaTiO₃/P(VDF-TrFE) the ceramic nanoparticles acts as defects in fibers (figure 7.3), contributing for the increase of the damping of the composite fibers and consequently for the decrease of the mechanical to electrical energy conversion. As observed in figure 7.5, the reduction of the electromechanical conversion due to increased damping is larger than positive contribution of the larger coupling coefficient of the fillers, resulting in an overall decrease of the power output. It should be noted that, despite the larger electromechanical coupling coefficient, the output power for P(VDF-TrFE) fibers is also lower due to lower piezoelectric coefficient and larger damping, related to the increase of stiffness with respect to the pure polymer. Additional contributions to the decrease of the output power in the composites can arise from the random orientation of the BaTiO₃ electroactive domains,

leading to an overall reduction of the effective dipolar moment of the electroactive composite fibers when compared to the single polymer. The piezoelectric coefficients of organic and inorganic phases are opposed, which can lead to counteract effects [33-34]. It's important to notice that among all the used ceramic particles only the particles with 500 nm are tetragonal and therefore piezoelectric (table 7.2), the particles with 10 and 100 nm are cubic and then non-piezoelectric, contributing to an increase of the dielectric constant but without direct piezoelectric contribution to the final composite response.

Table 7.2: Structural properties of the BaTiO₃ ceramic particles [35].

	$\phi = 10 \text{ nm}$	$\phi = 100 \text{ nm}$	$\phi = 500 \text{ nm}$
Purity (%)	99.8	99.9	99.9
Crystallographic form	cubic	Cubic	tetragonal

Consequently, the maximum output power is obtained for the PVDF fibers ($\sim 0.02 \mu\text{W}$) and a decrease of the generated power was observed for the P(VDF-TrFE) and for the BaTiO₃/P(VDF-TrFE) fibers (figure 7.5d). It is interesting to notice that the output power is nearly frequency independent in the 100 Hz to 1 kHz frequency range under study, which is interesting for a broad range of applications.

In order to study the effect of larger deformations on the output voltage of the electroactive polymer fibers and fiber composites, the finger (protected by an insulator glove to prevent interferences from human bioelectricity) was used to apply a periodic dynamic loading on the top of the generator by simple tapping during which, the positive and the negative output voltage was measured (figure 7.6).

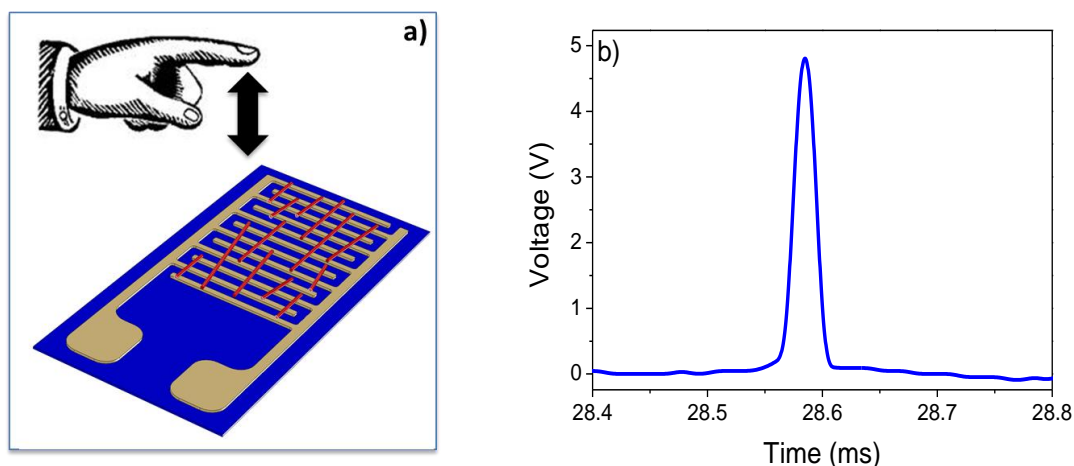


Figure 7.6: a) Diagram of a bending test performed with a finger; b) Positive output voltage generated during a test performed with finger deformation for the PVDF electrospun fibers.

The highest output voltage record during the finger experiment was 5.02 V, allowing concluding that amplitude of the voltage output depends on the amount of the strain imposed to the surface generator, being higher for higher mechanical deformations (figure 7.6b) as larger strains provide more mechanical energy available for conversion into electrical energy. The maximum output power generated for higher strains was 25 μW , which confers large interest to these piezoelectric vibration-to-electricity converters for micromechanical memory devices [36] and bioapplications in order to harvest human motion to power in-body biosensors.

Chen *et al.* [15] studied the characteristics of a piezoelectric nanowires of only PZT on top of interdigitated electrodes and obtained a power generation of $\sim 0.03 \mu\text{W}$ for higher deformations. In another work, the same amount of power was generated with poled BaTiO_3 , Park *et al.* [16] obtained by magnetron sputtering on top of a flexible interdigitated electrodes substrate an under higher mechanical deformation.

7.3. Conclusion

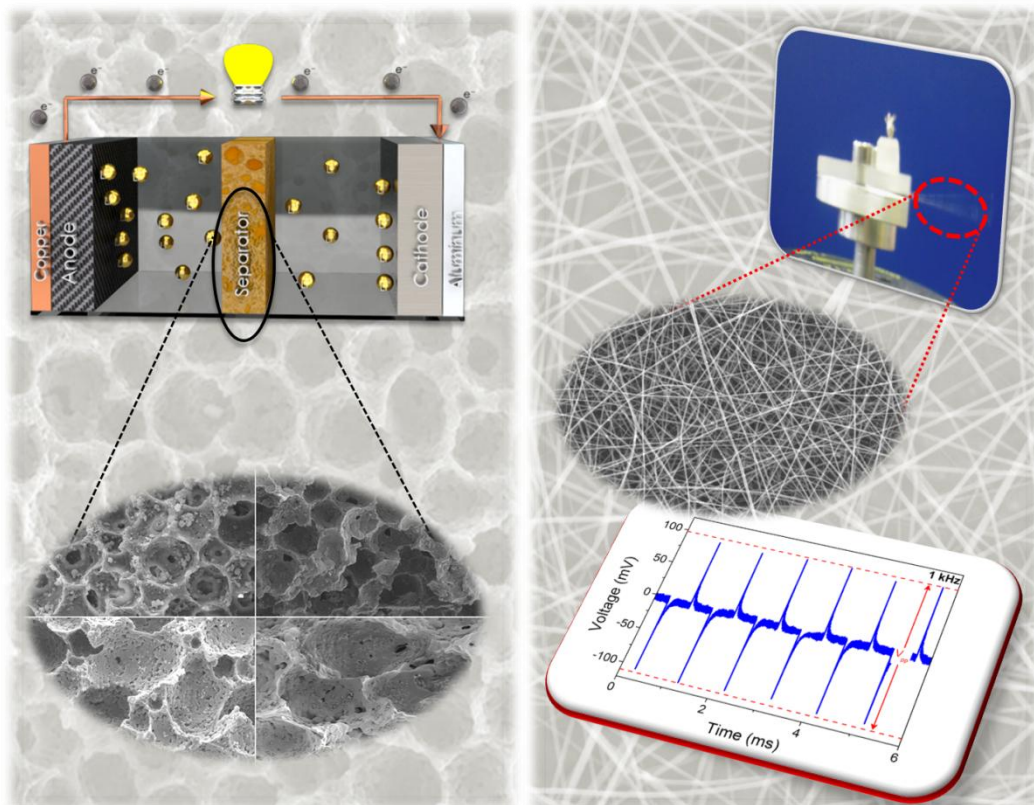
As a conclusion, the largest energy harvesting efficiency is obtained for the pure poly(vinylidene fluoride) fibers, with power outputs up to 0.02 μW and 25 μW under low and high mechanical deformation. The copolymer and the polymer/ceramic composites show reduced power output due to increased mechanical stiffness. The obtained values, among the largest found in the literature, the easy processing and the low cost and robustness of the polymer, demonstrate the applicability of the developed system.

7.4. References

1. Alper Erturk and D.J. Inman. *Introduction to Piezoelectric Energy Harvesting*, in *Piezoelectric Energy Harvesting*, Alper Erturk and D.J. Inman, Editors. 2011, John Wiley & Sons, Ltd: Chichester, UK. p. 1-14.
2. Hyunuk Kim, Yonas Tadesse, and S. Priya. *Piezoelectric Energy Harvesting*, in *Energy Harvesting Technologies*, Shashank Priya and D.J. Inman, Editors. 2009, Springer: New York, USA. p. 3-36.
3. Anton, S.R. and H.A. Sodano. *A review of power harvesting using piezoelectric materials (2003–2006)*. *Smart Materials and Structures*, 2007. **16**(3): p. R1.
4. Williams, C.B. and R.B. Yates. *Analysis of a micro-electric generator for microsystems*. *Sensors and Actuators A: Physical*, 1996. **52**(1–3): p. 8-11.
5. Rocha, J.G., L.M. Goncalves, P.F. Rocha, M.P. Silva, and S. Lanceros-Mendez. *Energy Harvesting From Piezoelectric Materials Fully Integrated in Footwear*. *Industrial Electronics, IEEE Transactions on*, 2010. **57**(3): p. 813-819.
6. Lee, C.S., J. Joo, S. Han, and S.K. Koh. *Multifunctional transducer using poly (vinylidene fluoride) active layer and highly conducting poly (3,4-ethylenedioxythiophene) electrode: Actuator and generator*. *Applied Physics Letters*, 2004. **85**(10): p. 1841-1843.
7. Lee, C.S., J. Joo, S. Han, J.H. Lee, and S.K. Koh. *Poly (vinylidene fluoride) transducers with highly conducting poly (3,4-ethylenedioxythiophene) electrodes*. *Synthetic Metals*, 2005. **152**(1–3): p. 49-52.
8. Tashiro, K. *Crystal Structure and Phase Transition of PVDF and Related Copolymers in Ferroelectric Polymers: chemistry, physics, and applications*, H.S. Nalwa, Editor. 1995, Marcel Dekker, Inc: New York, USA. p. 63-.
9. Brown, L.F. *Design considerations for piezoelectric polymer ultrasound transducers*. *Ultrasonics, Ferroelectrics and Frequency Control, IEEE Transactions on*, 2000. **47**(6): p. 1377-1396.
10. Sencadas, V., S. Lanceros-Méndez, and J.F. Mano. *Effect of the mechanical stretching on the ferroelectric properties of a (VDF/TrFE) (75/25) copolymer film*. *Solid State Communications*, 2004. **129**(1): p. 5-8.
11. Kap Jin, K. and K. Gwan Bum. *Curie transition, ferroelectric crystal structure and ferroelectricity of a VDF/TrFE (⁷⁵/₂₅) copolymer: 2. The effect of poling on Curie transition and ferroelectric crystal structure*. *Polymer*, 1997. **38**(19): p. 4881-4889.
12. Sencadas, V., S. Lanceros-Méndez, and J.F. Mano. *Thermal characterization of a vinylidene fluoride-trifluorethylene (75–25) (%mol) copolymer film*. *Journal of Non-Crystalline Solids*, 2006. **352**(50-51): p. 5376-5381.

13. Tanaka, R., K. Tashiro, and M. Kobayashi. *Annealing effect on the ferroelectric phase transition behavior and domain structure of vinylidene fluoride (VDF)–trifluoroethylene copolymers: a comparison between uniaxially oriented VDF 73 and 65% copolymers*. *Polymer*, 1999. **40**(13): p. 3855-3865.
14. Wang, Z.L. and J. Song. *Piezoelectric Nanogenerators Based on Zinc Oxide Nanowire Arrays*. *Science*, 2006. **312**(5771): p. 242-246.
15. Chen, X., S. Xu, N. Yao, and Y. Shi. *1.6 V Nanogenerator for Mechanical Energy Harvesting Using PZT Nanofibers*. *Nano Letters*, 2010. **10**(6): p. 2133-2137.
16. Park, K.-I., S. Xu, Y. Liu, G.-T. Hwang, S.-J.L. Kang, Z.L. Wang, and K.J. Lee. *Piezoelectric BaTiO₃ Thin Film Nanogenerator on Plastic Substrates*. *Nano Letters*, 2010. **10**(12): p. 4939-4943.
17. Patel, I., E. Siores, and T. Shah. *Utilisation of smart polymers and ceramic based piezoelectric materials for scavenging wasted energy*. *Sensors and Actuators A: Physical*, 2010. **159**(2): p. 213-218.
18. S. Ramakrishna, K. Fujihara, W. Teo, T. Lim, and Z. Ma. *Introduction*, in *An Introduction to Electrospinning and Nanofibers*, S. Ramakrishna, K. Fujihara, W. Teo, T. Lim, and Z. Ma, Editors. 2005, World Scientific Printers Co. Pte. Ltd.: Singapore. p. 1-18.
19. Andrady, A.L. *Introduction*, in *Science and Technology of Polymer Nanofibers* A.L. Andrady, Editor. 2008, Jonh Wiley & Sons, Inc.: New Jersey, USA. p. 1-26.
20. Greiner, A. and J.H. Wendorff. *Electrospinning: A Fascinating Method for the Preparation of Ultrathin Fibers*. *Angewandte Chemie International Edition*, 2007. **46**(30): p. 5670-5703.
21. He, J.-H. *Electrospun Nanofibres and Their Applications*. 2008, Shawbury, Shrewsbury, Shropshire, U.K.: iSmithers.
22. Dong, Z., S.J. Kennedy, and Y. Wu. *Electrospinning materials for energy-related applications and devices*. *Journal of Power Sources*, 2011. **196**(11): p. 4886-4904.
23. Fang, J., X. Wang, and T. Lin. *Electrical power generator from randomly oriented electrospun poly(vinylidene fluoride) nanofibre membranes*. *Journal of Materials Chemistry*, 2011. **21**(30): p. 11088-11091.
24. Vullers, R.J.M., R. van Schaijk, I. Doms, C. Van Hoof, and R. Mertens. *Micropower energy harvesting*. *Solid-State Electronics*, 2009. **53**(7): p. 684-693.
25. Chao-Nan, X., M. Akiyama, K. Nonaka, and T. Watanabe. *Electrical power generation characteristics of PZT piezoelectric ceramics*. *Ultrasonics*,

- Ferroelectrics and Frequency Control, IEEE Transactions on, 1998. **45**(4): p. 1065-1070.
26. Liu, D. and J. Li. *The enhanced and optimal piezoelectric coefficients in single crystalline barium titanate with engineered domain configurations*. Applied Physics Letters, 2003. **83**(6): p. 1193-1195.
 27. Ribeiro, C., V. Sencadas, J.L.G. Ribelles, and S. Lanceros-Méndez. *Influence of Processing Conditions on Polymorphism and Nanofiber Morphology of Electroactive Poly(vinylidene fluoride) Electrospun Membranes*. Soft Materials, 2010. **8**(3): p. 274-287.
 28. Sencadas, V., C. Ribeiro, I.K. Bdikin, A.L. Kholkin, and S. Lanceros-Mendez. *Local piezoelectric response of single poly(vinylidene fluoride) electrospun fibers*. physica status solidi (a), 2012. **209**(12): p. 2605-2609.
 29. Mendes, S.F., C.M. Costa, C. Caparros, V. Sencadas, and S. Lanceros-Méndez. *Effect of filler size and concentration on the structure and properties of poly(vinylidene fluoride)/BaTiO₃ nanocomposites*. Journal of Materials Science, 2012. **47**(3): p. 1378-1388.
 30. Goldfarb, M. and L.D. Jones. *On the Efficiency of Electric Power Generation With Piezoelectric Ceramic*. Journal of Dynamic Systems, Measurement, and Control, 1999. **121**(3): p. 566-571.
 31. Martins, P., A.C. Lopes, and S. Lanceros-Mendez. *Electroactive phases of poly(vinylidene fluoride): Determination, processing and applications*. Progress in Polymer Science, (0).
 32. Erturk, A. and D.J. Inman. *Issues in mathematical modeling of piezoelectric energy harvesters*. Smart Materials and Structures, 2008. **17**(6): p. 065016.
 33. Lam, K.H. and H.L.W. Chan. *Piezoelectric and pyroelectric properties of 65PMN-35PT/P(VDF-TrFE) 0-3 composites*. Composites Science and Technology, 2005. **65**(7-8): p. 1107-1111.
 34. Chan, H.L.W., M.C. Cheung, and C.L. Choy. *Study on BaTiO₃/P(VDF-TrFE) 0-3 composites*. Ferroelectrics, 1999. **224**(1): p. 113-120.
 35. Nanoamor[®]. *Nanostructured & Amorphous Materials, Inc.* 2001 [cited 2013; Available from: <http://www.nanoamor-europe.com/catalogsearch/result/?q=barium+titanate>].
 36. Shu, Y.C. and I.C. Lien. *Efficiency of energy conversion for a piezoelectric power harvesting system*. Journal of Micromechanics and Microengineering, 2006. **16**(11): p. 2429.



8 - Final remarks, conclusions and future work

In this chapter some final remarks are presented comparing the characteristics of the different porous composite membranes prepared in this work for battery applications. The main conclusions of this study and some possibilities for the future work are also presented.

8.1. Final remarks

A battery separator should meet some requirements, such as being ionic conductor, electronic insulator, to show mechanical and dimensional stability, physically strength to allow easily handling, to be readily wetted by electrolyte solutions, to show resistant to chemical and thermal degradation, uniform thickness and structure, among others [1-3].

In this sense, among all prepared composites the 16 wt% NaY/P(VDF-TrFE), 4 wt% MMT/P(VDF-TrFE), 0.1 wt% MWCNT/P(VDF-TrFE) and 16 wt% BaTiO₃/P(VDF-TrFE) ($\varnothing = 500$ nm) were the ones with the best overall results [4-7] for each filler type, so their results are presented and compared below.

All tested composites present a uniform and homogenous porous structure, as shown in figure 8.1.

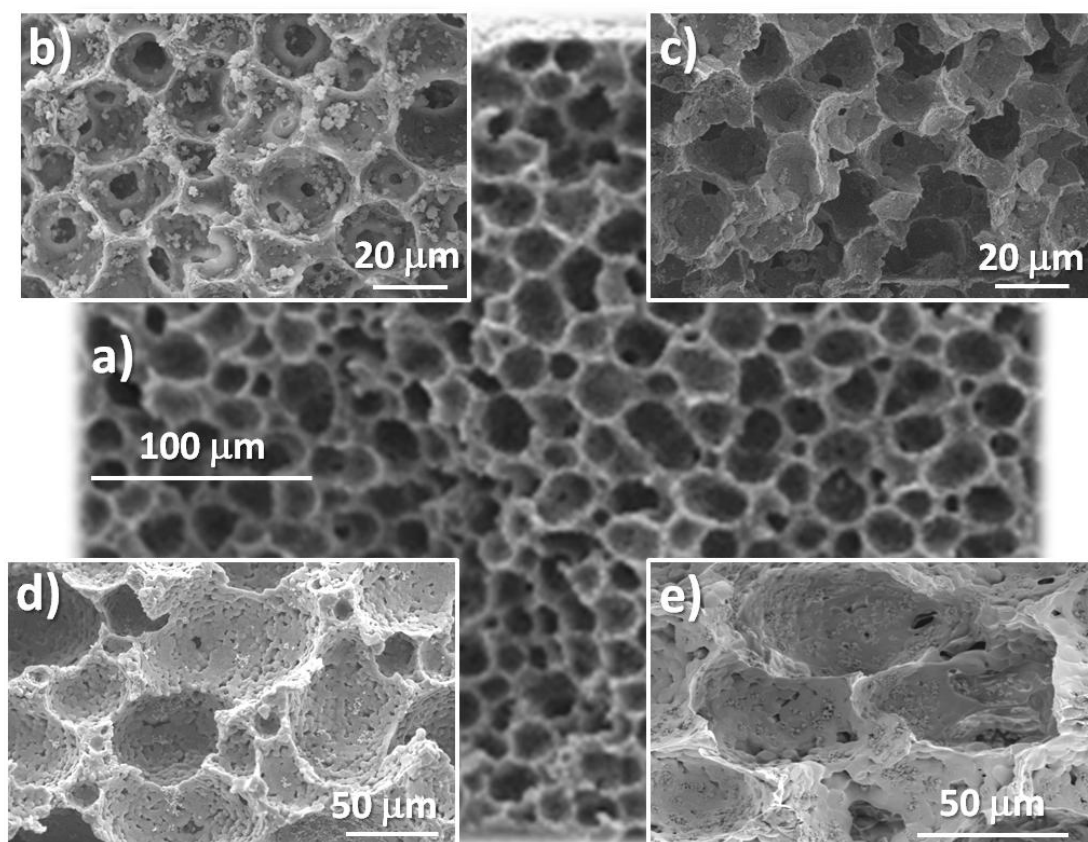


Figure 8.1: Cross section images of: a) pristine P(VDF-TrFE), b) 16 wt% NaY/P(VDF-TrFE), c) 4 wt% MMT/ P(VDF-TrFE), d) 0.1 wt% MWCNT/ P(VDF-TrFE) and e) 16 wt% BaTiO₃/ P(VDF-TrFE) membranes.

The inclusion of the different fillers into the P(VDF-TrFE) polymer matrix does not affect the homogeneity of the polymer porous structure.

The pore size and porosity largely affects the permeability and the electrolyte uptake of the separator [1]. Table 8.1 and figure 8.2 show the pore size, porosity and electrolyte solution uptake of the composite membranes.

Table 8.1: Average pore size, porosity and electrolyte uptake of the membranes.

Sample	Average pore size (μm)	Porosity (%)	Uptake (%)
P(VDF-TrFE)	7.9 ± 2.7	70.0 ± 3.5	223.1 ± 8.7
16 wt% NaY/P(VDF-TrFE)	20.6 ± 4.2	36.0 ± 1.8	232.8 ± 14.3
4 wt% MMT/P(VDF-TrFE)	11.3 ± 6.4	82.8 ± 4.1	327.4 ± 16.4
0.1 wt% MWCNT/P(VDF-TrFE)	59.8 ± 14.9	75.7 ± 9.9	252.3 ± 8.9
16 wt% BaTiO ₃ /P(VDF-TrFE)	43.1 ± 5.9	80.2 ± 8.4	303.5 ± 13.0

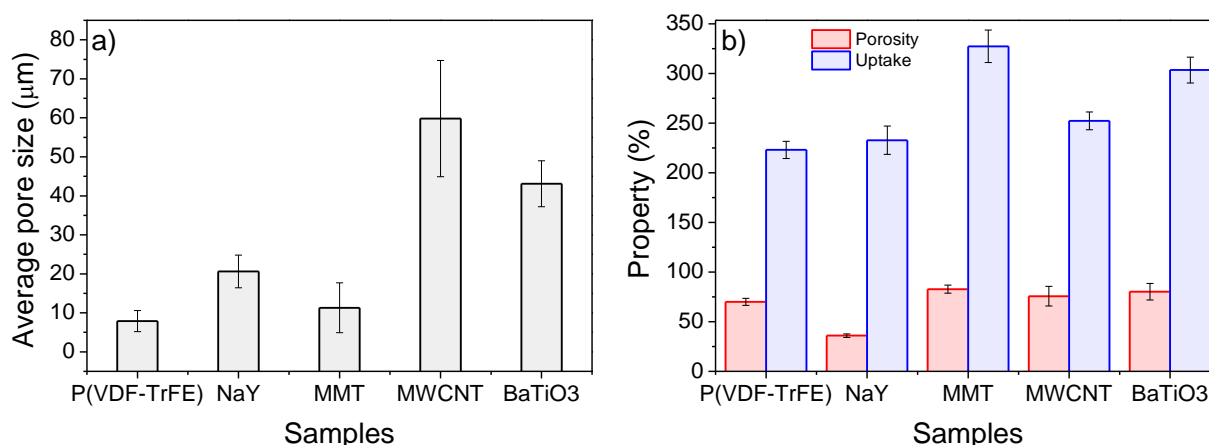


Figure 8.2: a) Average pore size and b) porosity and uptake for the P(VDF-TrFE), 16 wt% NaY/P(VDF-TrFE), 4 wt% MMT/P(VDF-TrFE), 0.1 wt% MWCNT/P(VDF-TrFE) and 16 wt% BaTiO₃/P(VDF-TrFE) membranes.

The pore size tends to be higher for the composite membranes, when compared to the pure copolymer, being markedly larger for MWCNT and BaTiO₃ composite membranes. The only exception is NaY composite membranes. This increase is reflected in the electrolyte solution uptake which is higher for MMT, MWCNT and BaTiO₃ membranes, and just slightly higher in NaY membrane, when compared to the pure co-polymer. This can be taken as an advantage of the NaY membranes, since too large uptakes can affect mechanical and thermal stabilities [8].

The electrochemical behaviour of the separator is crucial for the battery performance, as it affects the charge/discharge capacities [2-3]. The ionic conductivity

strongly depends on electrolyte uptake, which in turn depends on porosity and pore size [9].

Table 8.2 and figure 8.3 shows the ionic conductivity (σ_i), tortuosity (τ) and activation energy (E_a) of the composites, obtained from equation 2.5, 2.6 and 2.7 respectively.

Table 8.2: Room temperature ionic conductivity (σ_i), tortuosity (τ) and activation energy (E_a) of the membranes filled with 1 M $\text{LiClO}_4 \cdot 3\text{H}_2\text{O}$ electrolyte solution; $\sigma_0 = 9.8 \text{ S/cm}$ at 25 °C.

Sample	σ_i (S/cm)	τ	E_a (kJ/mol)
P(VDF-TrFE)	5.24×10^{-7}	115	64
16 wt% NaY/P(VDF-TrFE)	2.33×10^{-6}	39	44
4 wt% MMT/P(VDF-TrFE)	1.61×10^{-6}	117	10
0.1 wt% MWCNT/P(VDF-TrFE)	2.04×10^{-6}	61	5
16 wt% BaTiO_3 /P(VDF-TrFE)	9.22×10^{-6}	29	32

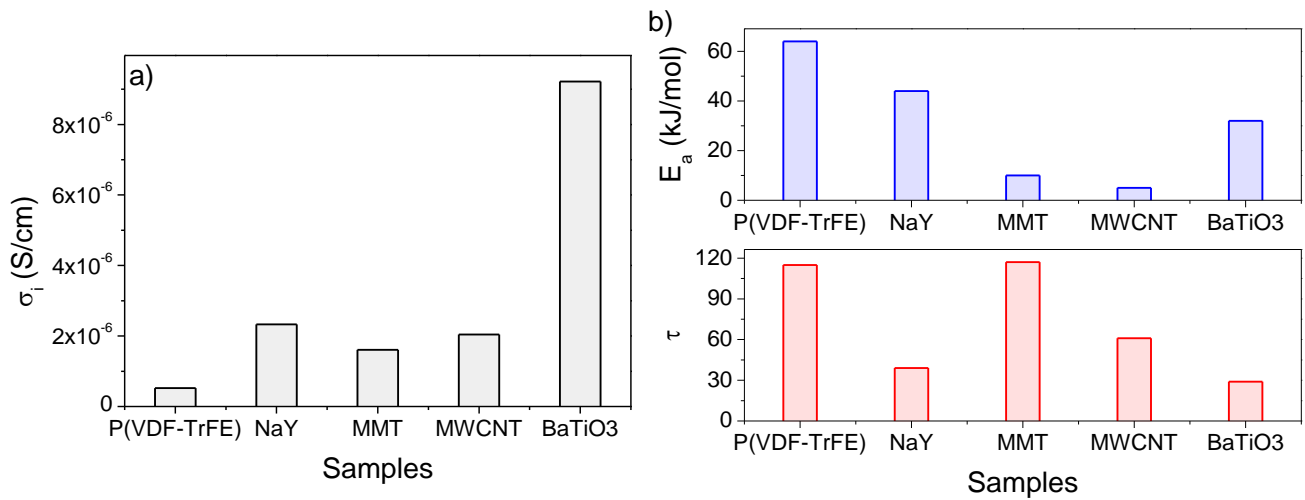


Figure 8.3: Room temperature a) ionic conductivity; b) tortuosity and activation energy for the P(VDF-TrFE), 16 wt% NaY/P(VDF-TrFE), 4 wt% MMT/P(VDF-TrFE), 0.1 wt% MWCNT/P(VDF-TrFE) and 16 wt% BaTiO_3 /P(VDF-TrFE) membranes.

The room temperature ionic conductivity of the composite membranes is about one order of magnitude higher than for the pure polymer, indicating that fillers inclusion benefits the ionic conduction process, which is confirmed by the decrease of the activation energy and tortuosity of almost all composite membranes.

The temperature stability of the ionic conductivity is important for the temperature range operation of a battery. The temperature dependence of the ionic conductivity is shown in figure 8.4.

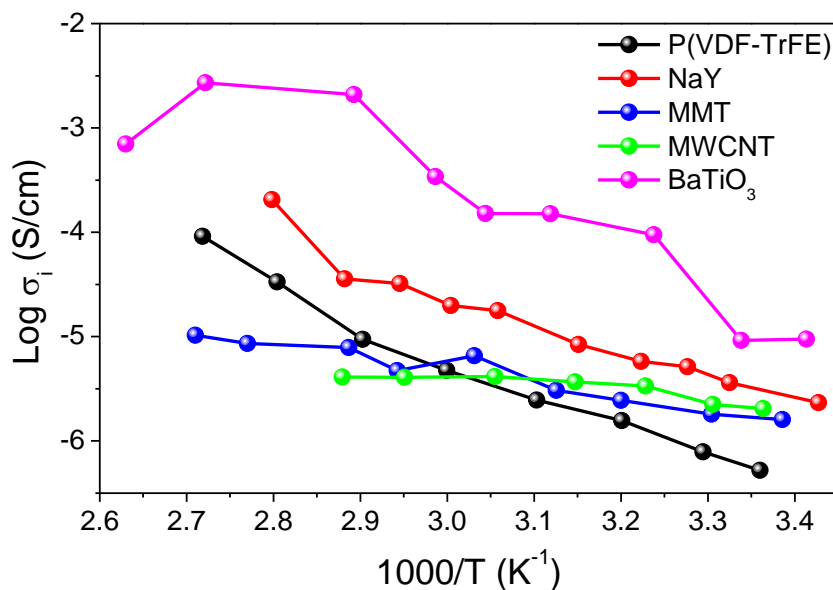


Figure 8.4: Log σ_i as function of $1000/T$ of (VDF-TrFE), 16 wt% NaY/P(VDF-TrFE), 4 wt% MMT/P(VDF-TrFE), 0.1 wt% MWCNT/P(VDF-TrFE) and 16 wt% BaTiO₃/P(VDF-TrFE) membranes.

All fillers contribute to diminish ionic conductivity variations with temperature, namely MMT and MWCNT.

In general, all fillers have specific improvements in the overall membranes performance, although NaY is the best choice for this application due to the high ionic conductivity (2.33×10^{-6} S/cm) in a large temperature range, suitable porosity and electrolyte uptake (36.0 and 232.8 %).

8.2. Conclusions

The need to develop efficient energy generation and storage devices was the main motivation for the present work. In this sense, the combined use of polymer-based materials (poly(vinylidene fluoride) (PVDF) and its copolymers) with different types of fillers (zeolites, clays, carbonaceous and ceramics fillers) proved to be a viable and promising route to improve the performance of these devices.

The thermally induced phase separation technique proved to be adequate to prepare polymer composite porous membranes based on poly(vinylidene fluoride-*co*-trifluoroethylene) (P(VDF-TrFE)) with NaY, montmorillonite (MMT), multiwalled-carbon nanotubes (MWCNT) and BaTiO₃ fillers with suitable properties for batteries separators applications.

The diverse nature of each filler results in different effects on the properties of the composite with respect to the pristine polymer. The presence of fillers in the polymeric matrix tends to increase the average pore size, from 7.9 μm for pristine polymer to higher values of 43.1 and ~60 μm for BaTiO₃ and MWCNT membranes, respectively.

The porosity of the composites also tends to be higher than that of the pristine polymer, increasing from 70.0 % for P(VDF-TrFE) to a maximum of 83 % for MMT, with the exception of NaY membrane which presents the lower value of 36.0 %. The membranes with higher porosities, MMT, MWCNT and BaTiO₃, also present higher electrolyte uptakes, 327, 252 and 304 % respectively, compared to the 223 % of the pristine polymer. The NaY membrane, despite the lower porosity, also presents a slight increase in the electrolyte uptake up to 238 %.

The tortuosity and activation energy show a strong decrease for almost all composites, when compared to the pristine polymer. The tortuosity of 115 is strongly decreased to 61, 39 and 29 for MWCNT, NaY and BaTiO₃ membranes respectively. The activation energy decreases markedly from 64 kJ/mol for P(VDF-TrFE) to 10 and 5 kJ/mol for MMT and MWCNT composites, respectively.

The inclusion of fillers leads to an increase in the room temperature ionic conductivity of the pristine polymer (5.24×10^{-7} S/cm), up to 2.33×10^{-6} S/cm for the composite with NaY, 1.61×10^{-6} S/cm for the MMT composite, 2.04×10^{-6} S/cm for the one with MWCNT and a maximum of 9.22×10^{-6} S/cm for the BaTiO₃ composite. The ionic conductivity variation with temperature is also diminished in the presence of

fillers, namely for MMT and MWCNT membranes. All the composite membranes showed a stable operation window of at least 6.0 V, suitable for applications.

In short, all fillers result in improved properties of the polymeric matrix, however the NaY particles are the best choice for these applications due to the suitable porosity (36.0 %), moderate electrolyte uptake (232.8 %) and high ionic conductivity in all temperature range. Furthermore, the increase in the ionic conductivity of the NaY membranes is related to the slight reduction in crystallinity from 28 % to 23 % for pristine polymer and NaY/P(VDF-TrFE) respectively, and not to higher porosity and electrolyte uptake which would affect the thermal and mechanical stability.

Regarding energy harvesting performance, electrospinning proved to be a suitable technique for the preparation of polymeric based fibres for energy harvesting systems. PVDF is more effective than P(VDF-TrFE) and BaTiO₃/P(VDF-TrFE) mainly due to mechanical damping fillers as well as a lower piezoelectric response of the composites. The generated output powers of 0.02 μ W and 25 μ W, under low and high mechanical deformation respectively, for PVDF fibers are suitable for micromechanical devices and biosensor applications.

It is concluded that main objectives of this study were successfully achieved and the work represents an effective contribution to the development of novel polymer-based materials for energy applications.

8.3. Future work

The obtained results of this study allow opening new lines of research and works for the future.

The incorporation of individualized specific fillers, in proper amounts, into polymer matrices has shown to be advantageous in producing porous membranes for battery applications. In this sense, the combined use of different fillers would be interesting and promising to tune specific characteristics of the polymeric matrix to improve its performance in Li-ion batteries separator applications. Further investigation in different functionalizations of the polymer matrix and/or fillers is also a path to follow for optimizing these systems. The obtained results also raise the possibility of upscaling these materials for use in the production of lithium batteries, therefore the

best composites should be tested as separators membranes in batteries, evaluating the cycling performance and rate capabilities.

The energy harvesting system proposed can be effectively improved by optimizing the interface between the interdigitated electrodes and fibers, e.g. encapsulating the fibers, as well as improving the energy collection circuit. These improvements could make the system able to be upscaled for energy generation systems.

8.4. References

1. Costa, C.M., M.M. Silva, and S. Lanceros-Mendez. *Battery separators based on vinylidene fluoride (VDF) polymers and copolymers for lithium ion battery applications*. RSC Advances, 2013. **3**(29): p. 11404-11417.
2. Arora, P. and Z. Zhang. *Battery Separators*. Chemical Reviews, 2004. **35**(50): p. 4419-4462.
3. Park, J.-K. *Principles and applications of lithium secondary batteries*. 2012, Weinheim: Wiley-VCH.
4. Nunes-Pereira, J., A.C. Lopes, C.M. Costa, L.C. Rodrigues, M.M. Silva, and S. Lanceros-Méndez. *Microporous membranes of NaY zeolite/poly(vinylidene fluoride-trifluoroethylene) for Li-ion battery separators*. Journal of Electroanalytical Chemistry, 2013. **689**(0): p. 223-232.
5. Nunes-Pereira, J., A.C. Lopes, C.M. Costa, R. Leones, M.M. Silva, and S. Lanceros-Méndez. *Porous Membranes of Montmorillonite/Poly(vinylidene fluoride-trifluoroethylene) for Li-Ion Battery Separators*. Electroanalysis, 2012. **24**(11): p. 2147-2156.
6. Nunes-Pereira, J., C.M. Costa, R. Leones, M.M. Silva, and S. Lanceros-Méndez. *Li-ion battery separator membranes based on poly(vinylidene fluoride-trifluoroethylene)/carbon nanotube composites*. Solid State Ionics, 2013. **249–250**(0): p. 63-71.
7. Nunes-Pereira, J., C.M. Costa, R.E. Sousa, A.V. Machado, M.M. Silva, and S. Lanceros-Méndez. *Li-ion battery separator membranes based on barium titanate and poly(vinylidene fluoride-co-trifluoroethylene)* Submitted to Electrochimica Acta (under revision).
8. Saunier, J., F. Alloin, J.Y. Sanchez, and L. Maniguet. *Plasticized microporous poly(vinylidene fluoride) separators for lithium-ion batteries. III. Gel properties and irreversible modifications of poly(vinylidene fluoride) membranes under swelling in liquid electrolytes*. Journal of Polymer Science Part B: Polymer Physics, 2004. **42**(12): p. 2308-2317.
9. Saito, Y., H. Kataoka, E. Quartarone, and P. Mustarelli. *Carrier Migration Mechanism of Physically Cross-Linked Polymer Gel Electrolytes Based on PVDF Membranes*. The Journal of Physical Chemistry B, 2002. **106**(29): p. 7200-7204.